Extreme precipitation and physical model-based estimates for return values and PMP in Norway

Karianne Ødemark

Department of Geosciences
Faculty of Mathematics and Natural Sciences

Series of dissertations submitted to the
Faculty of Mathematics and Natural Sciences, University of Oslo
No. 2668

ISSN 1501-7710

Cover: UiO.
Print production: Graphic center, University of Oslo.

Abstract

The occurrence of extreme precipitation events causing surface water excess and flooding is becoming a significant societal expense due to the rise in precipitation levels. The study of extreme precipitation is crucial due to its potential impact on various aspects of society, such as infrastructure, agriculture, and human safety. It is therefore essential to understand extreme precipitation events, predict their likelihood and frequency, and estimate robust design values for critical infrastructure. Extreme precipitation statistics and return value estimates are important for planning and designing infrastructure. Dams and nuclear power facilities, which pose a significant threat to society if destroyed, require risk assessment with sufficiently long return periods for the design values. The methodology for estimating design values is subject to ongoing research, and there are various methods being used across the field.

To secure water resource infrastructure, the concept of "probable maximum precipitation" (PMP) is used as a design value. PMP represents the greatest possible precipitation depth for a given duration, storm size, location, and time of year. Different hydrometeorological and statistical methods are employed to estimate PMP. WMO has recommended, if possible, to use physical-based approaches for estimating PMP in areas where orographic enhancement of precipitation is considerable, and the methodology for PMP estimation is currently under scrutiny.

The concept of PMP has been criticized by hydrologists as it assumes a physical upper bound of precipitation amounts possible. At the same time, extreme value theory indicates that this bound does not necessarily exist. Today's methodology for estimating PMP in Norway is the approach developed at NERC and standardized to fit Norwegian conditions. This approach is highly sensitive to available observation data and in addition influenced by which data points are included, which is a choice made subjectively. The method was developed in the 1970's and has not been revised since. Therefore, in addition to WMO's recommendation, a reconsideration of the PMP methodology is due.

This thesis focuses on extreme precipitation in Norway and explores alternative methods for PMP estimation. The result is a proposal to

combine a physical model-based prediction system with existing gridded observation data to obtain return values with robust estimates for long return periods.

Sammendrag

Kunnskap om ekstremnedbør er viktig for flere ulike samfunnsområder, som bl.a infrastruktur, landbruk og sikring av menneskers liv og verdier. Det er derfor nødvendig å forstå ekstreme nedbørshendelser for å kunne forutsi deres sannsynlighet og frekvens og videre gi et pålitelig dimensjoneringsgrunnlag.

Ekstremnedbør-statistikk og returverdier er viktig for både planlegging og utforming av infrastruktur. Infrastruktur som utgjør en betydelig trussel for samfunnet hvis de ødelegges, krever en risikovurdering med tilstrekkelig lange returperioder for dimensjonering. Det forskes stadig på metodikk for å beregne returverdier, og det finnes flere ulike metoder som blir brukt innen feltet. For å sikre damanlegg brukes begrepet "påregnelig maksimal nedbør" (PMP) som en dimensjonerende verdi. PMP representerer den største mulige nedbørdybden for en gitt varighet, storm-størrelse, sted og tidspunkt på året. Det finnes også forskjellige metoder for å estimere PMP, både hydrometeorologiske og statistiske. WMO har anbefalt å bruke fysiske baserte tilnærminger for å estimere PMP, særlig der orografisk forsterkning av nedbør er betydelig. Metodikken for å estimere PMP blir derfor for tiden gransket.

Konseptet PMP er nylig blitt kritisert av hydrologer, siden det antar en fysisk øvre grense for mulige nedbørsmengder, mens ekstremverditeori indikerer at denne grensen ikke nødvendigvis eksisterer. Dagens metode for å estimere PMP i Norge er basert på metoden utviklet av NERC og standardisert for norske forhold. Denne metoden er svært avhengig av tilgjengelige observasjonsdata, og i tillegg vil estimatet påvirkes av hvilke datapunkter som inkluderes i analysen, noe som velges subjektivt. Metoden ble utviklet på 1970-tallet og har ikke blitt revidert siden. Derfor, i tillegg til anbefalingen fra WMO, er det nødvendig å se nærmere på metodikken for å beregne PMP.

Hovedfokuset i denne avhandlingen er på ekstremnedbør i Norge, og på å utforske alternative metoder for å estimere PMP. Som resultat foreslås det å kombinere et fysisk modellbasert sesongvarslings-system med eksisterende gridda observasjonsdata for å oppnå pålitelige returverdier, også når det gjelder returverdiene med lange returperioder.

Contents

List of Figures

Preface

This synthesis and collection of papers are submitted for the degree of pilosophiae doctor (PhD) in atmospheric physics and chemistry at the Section for Meteorology and Oceanography (MetOs), Department of Geosciences, University of Oslo. The work has been carried out at the Norwegian Meteorological Institute (MET) and supervised by Malte Müller (MET and MetOs), Ole Einar Tveito (MET), Morten Køltzow (MET), Terje Berntsen (MetOs) and Richard Moore. The project was funded by the Norwegian Research Council through the project FlomQ (NFR – 235710/E20) and from the Norwegian Meteorological Institute. The thesis is divided into an introductory part and a part consisting of the following three papers:

Paper I **Karianne Ødemark**, Malte Müller and Ole Einar Tveito (2021), "Changing Lateral Boundary Conditions for Probable Maximum Precipitation Studies: A Physically Consistent Approach", In *Journal of Hydrometeorology*, doi:10.1175/JHM-D-20-0070.1

Paper II **Karianne Ødemark**, Malte Müller, Cyril Parlerme and Ole Einar Tveito (2023) "Recent changes in circulation patterns and their opposing impact on extreme precipitation at the west coast of Norway", In *Weather and Climate Extremes*, doi:10.1016/j.wace.2022.100530

Paper III **Karianne Ødemark**, Malte Müller, Ole Einar Tveito and Thordis L. Thorarinsdottir, "Towards a new framework for PMP estimates in Norway by combining an ensemble data set and gridded observations", Submitted to *Advances in Statistical Climatology, Meteorology and Oceanography*, 2023

Other publications from the PhD period that are not included in the thesis:

I Imme Benedict, **Karianne Ødemark**, Thomas Nipen and Richard Moore (2019), "Large-scale flow patterns associated with extreme precipitation and atmospheric rivers over Norway", In *Monthly Weather Review*, doi:10.1175/MWR-D-18-0362.1

Acknowledgements

I want to express my heartfelt gratitude to my supervisors, Malte Müller and Ole Einar Ellingbø Tveito, for their invaluable guidance, support, and encouragement throughout my PhD journey. Their expertise, patience, and commitment to my research have been instrumental in shaping my academic development and helping me achieve this important milestone. I am especially grateful for the countless hours they spent discussing, reading my drafts, providing insightful feedback, and helping me stay focused and motivated. I would not have been able to complete this thesis without their dedicated mentorship. Thank you from the bottom of my heart.

I also want to thank MET Norway and especially Hans Olav Hygen, for giving me the opportunity to keep working on this project, and my dear colleagues at MET for good discussions and coffee breaks, especially Helga Therese, Reidun, and Elin.

I would also like to thank my friends, who have been a source of comfort and inspiration. Their encouragement and support have been invaluable in helping me stay focused and motivated. Thank you for always being there for me and for making this journey so much more enjoyable.

Finally, I would like to express my sincerest thanks to my family, Sigmund, Vilde and Selma, for their unwavering love and support throughout these years. Their patience, understanding, and encouragement have been a constant source of strength and motivation. I am grateful for the sacrifices they made to help me pursue my dreams and for the endless love they have shown me.

Oslo, June 2023
Karianne Ødemark

Part I

Thesis

Chapter 1

Introduction

1.1 Motivation

The study of extreme precipitation is crucial due to its potential impact on various aspects of society, such as infrastructure, agriculture, and human safety. Norway's geography, with its mountainous regions and fjords, makes it particularly vulnerable to flash floods, landslides, and other weather-related hazards. As an example, the flood induced by an extreme precipitation event in October 2014 (Schaller et al. (2020)) led to severe consequences for the towns embedded in the complex terrain near the west coast of Norway. Accurately estimating design values for infrastructure such as bridges, roads, and buildings, is a challenge due to the uncertainty connected to extreme precipitation. Especially for return values with long return periods, the uncertainty of the estimate is large. The conventional method for calculating design values is based on a long-term statistical analysis of point-based precipitation data, which may not accurately reflect the rapidly spatial changing and highly variable nature of extreme precipitation events related to complex terrain and/or convective precipitation.

The uncertainty in design values can lead to under-designed or over-designed infrastructure, both of which can have significant consequences for the safety and sustainability of the built environment. The need for more robust and reliable design values that account for the uncertainty of extreme precipitation is crucial to ensure the safety and reliability of critical infrastructure in Norway. As such, the study of extreme precipitation can help to inform the development of more effective design methodologies, which can ultimately benefit communities and the environment.

When designing structures such as dams, reservoirs, and levees, as well as in the design of infrastructure such as roads and bridges "probable maximum precipitation" (PMP) is often used. PMP is a design value that estimates the maximum precipitation that can be expected to occur at a given point during the lifetime of a project or structure. PMP is defined as "... the greatest depth of precipitation for a given duration meteorologically possible for a given size storm area at a particular location at a particular time of year, with no allowance made for

long-time climatic trends" (WMO (2009)). By considering the PMP, engineers can ensure that their designs can withstand the most extreme precipitation events and provide long-term protection against the impacts of extreme weather.

There are several methods for estimating PMP including different hydrometeorological methods (WMO (2009) and Salas et al. (2014)) and the statistical method by Hershfield (Hershfield (1961)) (see sections 2.4.2 and 2.4.3). At MET Norway, a standardized statistical approach based on the NERC method is used to estimate PMP (NERC (1975) and Førland (1992a)). This approach is vulnerable to data availability that can strongly affect the PMP estimates. A large challenge when estimating design values, in general, is the dependence on historical point observation data that may not fully capture the complexity and variability of extreme weather events. In some areas, precipitation extremes might even be unprecedented (Kelder et al. (2020)).

In the latest manual for PMP methodology, The World Meteorological Organization (WMO) recommends applying physically based atmospheric models for PMP estimates, especially for areas where orographic precipitation is significant (WMO (2009)). Several studies have investigated the use of numerical weather prediction models (NWPs) for PMP estimation (Ohara et al. (2011), Ishida et al. (2015b) and Ishida et al. (2015a)). Ohara et al. (2011) studied PMP for a catchment in California and applied a regional scale NWP model. Other studies have also applied NWP-based methods to estimate PMP, where the approach is based on the physical maximization of a historical extreme rainstorm. Ishida et al. (2015b) alter boundary and initial conditions to maximize precipitation over targeted catchments. X. Chen and Hossain (2018) pointed out that there seems to have emerged a consensus that using a physical numerical model is the way forward for a new PMP methodology, but that there is missing a consensus on how to physically "maximize" the historical storms within numerical models for PMP estimation. Maximizing relative humidity is often applied, though the question is how large an effect this will have when the humidity in an extreme precipitation case is very high already. Toride et al. (2019) point out that systematic saturation of all boundaries of the NWP model potentially introduces disturbances to the fields beyond what is realistic. In addition, a sudden change at the boundaries of the model domain can induce physical and dynamical inconsistencies.

X. Chen and Hossain (2018) found that different dominant parameters control the storms at different locations across the continental United States. This study found that in some regions moisture availability together with vertical wind are the factors controlling the precipitation outcome, while in other regions instability controls the magnitude of the storm. The most successful approach for maximizing precipitation is by altering the parameters that will lead to the largest effect on precipitation values. A necessity is thus to know what type of atmospheric conditions lead to extreme precipitation in the area of interest.

The focus of this thesis is to improve our understanding of extreme precipitation

in Norway and to analyze new methods for determining design values with long return periods. The scope has been to investigate whether a NWP model approach can be utilized to estimate PMP for Norway in a physical and dynamically consistent way. Further, by using a large ensemble data set, aspects of large-scale circulation patterns related to extreme precipitation events have been analyzed, to better understand the characteristics and causes of extreme precipitation. The study of extreme precipitation in Norway provides an opportunity to improve the accuracy of existing design values so that policymakers and resource managers can make informed decisions to mitigate and prepare for future events. An important part of the thesis is to suggest a framework for estimating robust design values with a decreased uncertainty compared to current estimates.

1.2 Objectives

As described above, there is a need to consider a new methodology for estimating PMP values at MET Norway. The current study was therefore initiated to explore viable ways of using NWP models to strengthen the estimation of design values, especially with long return periods. The objectives have been to better understand:

- What are plausible ways of using an NWP framework for maximizing precipitation amounts in a targeted area
- What processes control extreme precipitation in Norway
- Can a modeling system be exploited to assemble a data set with a large enough sample size to produce more robust return values

More specific research questions and their relation to the papers of this thesis are as follows:

1. Is it possible to alter initial- and boundary conditions in an NWP framework in a physically and dynamically consistent way to maximize precipitation amounts in a targeted area (Paper I)?
2. Can large data sets be utilized to yield more insight about extreme precipitation in Norway (Paper II)?
3. Can the same large data set be utilized to derive extreme value analysis beyond what current observational records can (Paper III)?

The remainder of the thesis is structured as follows: Section 2 provides a general introduction to precipitation in Norway and its connection to atmospheric large-scale circulation, followed by a general overview of extreme value statistics as a tool for estimating design values, and existing methods for determining PMP. Section 3 describes data sets and models used in this thesis. A short presentation of the main objectives and findings of each of the three journal papers is given in Section 4, while a discussion and a future outlook are given in Section 5.

Chapter 2

Scientific Background

This chapter covers the basic scientific background necessary to elucidate the work carried out and the results presented in this thesis.

2.1 Precipitation in Norway

The distribution of precipitation in Norway is strongly dependent on the large-scale atmospheric circulation that will guide the path of frontal systems. Norway's complex topography and mountain range parallel to the coast serve as a barrier for the frontal systems, and dependent on the direction of the airflow, different parts of the country will be in the rain shadow or be exposed to heavy precipitation. The prevailing direction of frontal systems is westerly and the west coast of Norway is subject to the largest precipitation amounts in the country. Annual precipitation amounts for Norway are shown in Figure 2.1, where the areas that receive the most precipitation have annual values of around 6000 mm, which are among the highest amounts in Europe. There are however large differences across short distances, in the rain shadow on the lee-side of the mountain range, areas with annual precipitation values of 300 mm are found. North of the wettest areas the amounts decrease northward along the coast, with values up to 2000 mm, and less than 1000 mm in the northernmost part of the country.

The highest precipitation amounts are associated with large-scale precipitation connected to frontal systems that are generated over the Atlantic Ocean before reaching the coast of Norway. These systems occur most frequently during the fall and winter seasons. Precipitation caused by frontal and orographic processes covers widespread areas and can in some cases span over several days. Such events can lead to flooding and problematic excess water in urban areas. Urban area flooding can also be caused by precipitation with high intensity from convective systems. These flash-flood events are mainly found during summer, and while intense, the duration is normally on the scale of minutes to a few hours, and the horizontal scale on the order of a few kilometers. This thesis focuses on the former type of processes, with precipitation events having a temporal scale of days, and further on extreme events, which are by definition rare. Nevertheless, their impacts on both human society and environmental systems can be severe.

2.2 Atmospheric Large-Scale Circulation

The North-Atlantic region is characterized by a large natural variability, however, there can be recurrent patterns of atmospheric circulation, known as weather regimes or circulation patterns. D. Chen and Y. Chen (2003) defines atmospheric circulation patterns as insistent, recurring, and large-scale modes of pressure anomalies revealing long-term variability in natural occurrence of chaotic behavior in regional climatic conditions. Each weather regime is characterized by a specific large-scale atmospheric circulation pattern, with impacts on regional weather and extremes over Europe (Fabiano et al. (2020)). Circulation type classification is a common tool in order to organize the various states of atmospheric circulation into distinct types. There are several different classification methods (Philipp et al. (2010)), which fall into two main categories: subjective and objective meth-

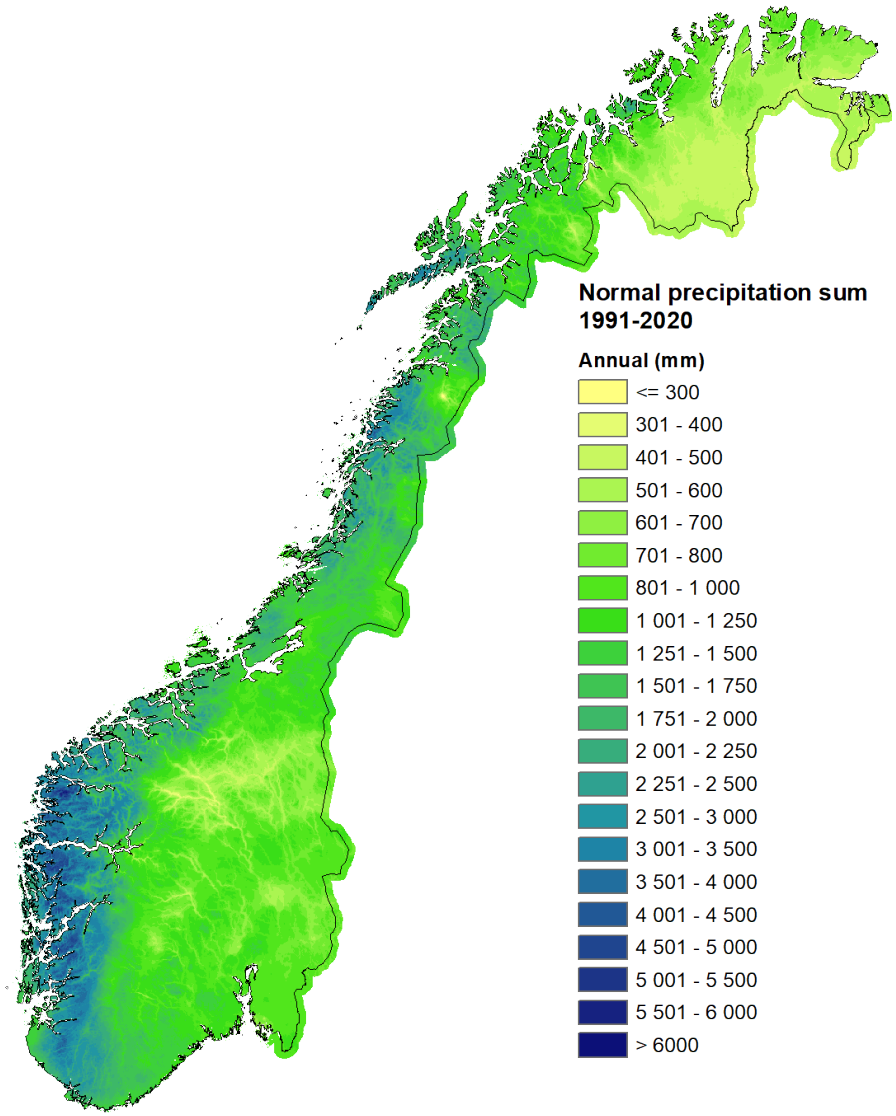

Figure 2.1: *Annual precipitation for the standard reference period 1991-2020. Figure from Tveito (2021).*

ods. The Hess–Brezowski Grosswetterlagen (Hess and Brezowsky (1952)), and the Lamb weather types (Lamb (1972)) are examples of subjective methods, where the circulation type is manually assigned according to pre-defined sets of circulation types. At the earliest stage, these classifications were based on the application of weather maps with subjectively evaluated pressure fields regarding the positions of pressure systems, airflow characteristics, and weather types in the area of interest. With the capacity to handle large amounts of data by computers advanced, automated, and objective methods have been developed, such as cluster analysis, which are general tool for finding groups in data, and eigenvector methods, such as principal component analysis (PCA) and empirical orthogonal functions (EOF). In EOF analysis, one projects the original large-scale climate data on an orthogonal basis which is derived by computing the eigenvectors of a spatially weighted anomaly covariance matrix, so the corresponding eigenvalues provide a measure of the percent variance explained by each pattern. Often, the first EOF or PCA1 will be the North Atlantic Oscillation (NAO).

2.2.1 Circulation Patterns

The North Atlantic Oscillation is under current climate conditions the leading mode of atmospheric circulation variability over the North Atlantic region (Hurrell et al. (2003)). There is no unique definition of NAO, but it is generally measured as the variations in the pressure difference between the Azores high and the Icelandic low and presented as an index, which is often also interpreted as an indicator for the strength of the westerlies over the Eastern North Atlantic. While the pattern is present during the entire year, it is most important during winter, explaining a large part of the variability of the large-scale pressure field, being largely determinant for the weather conditions over the North Atlantic basin and over Western Europe (Pinto and Raible (2012)). The time scales of the NAO range from days to centuries, but the dominant scales are interannual to decadal. Changes in the NAO phase are associated with characteristic changes in surface temperature, precipitation, and storm tracks, not only over the North Atlantic basin and Europe but also over parts of Northern America, the Mediterranean basin, and Eurasia.

A positive NAO phase is characterized by an intensified Azores High and deeper Iceland Low leading to a stronger meridional pressure gradient over the North Atlantic, a more zonal flow regime, and stronger westerlies characterized by a succession of low-pressure centers embedded in the westerly flow. This NAO phase is associated with warmer and wetter conditions over Northern Europe and dryer conditions over Southern Europe. In the reversed case, during a negative phase of the NAO, the Azores high is weaker and the Icelandic Low is shallower, resulting in a reduced pressure gradient over the North Atlantic and weaker westerlies. This brings unstable and wetter than normal conditions over Southern Europe, while there typically are dryer and colder than normal conditions over Northern Europe.

In addition to the positive and negative phases of the NAO, meteorologists con-

ventionally recognize further two Euro-Atlantic regimes: the Scandinavian Blocking (SB) pattern, and a North Atlantic Ridge pattern (AR). The four patterns are shown in Figure 2.2. The Scandinavian Blocking pattern is associated with a primary circulation center over Scandinavia and weaker centers over western Europe and eastern Russia (Barnston and Livezey (1987)). During the positive phase of this pattern, the geopotential height anomaly over Scandinavia is positive, which can result in a high-pressure blocking system and below-average precipitation across Scandinavia. The Atlantic Ridge pattern is characterized by high pressure over the central North Atlantic at a latitude of about 55 ° N and extends towards Scandinavia. During summer, this high-pressure system can block incoming low-pressure systems from the west, which reduces the amount of precipitation that reaches Scandinavia, resulting in dry and warm weather conditions, particularly in the southern and eastern parts of the region. In contrast, during winter, the Atlantic Ridge pattern can lead to an increased risk of storms and heavy precipitation events in Scandinavia, due to the high-pressure system forcing low-pressure systems to track further north than usual. This results in an increased risk of storms and heavy precipitation events affecting the region.

Depending on which type of classification tool is used for the circulation pattern analysis, additional patterns are commonly recognized, as from a study by Grams et al. (2017), shown in Figure 2.3. Here, a larger number of regimes are used to ensure sufficient details to fully understand the variability in surface weather on timescales of several days to weeks. Weather regimes provide a meteorological explanation for multi-day fluctuations in climatic conditions. As such, the understanding of weather regimes and circulation patterns can be important for the energy and agricultural sector, resource management, and disaster preparedness and is also much used in extended-range and sub-seasonal to seasonal (S2S) weather forecasts. Certain circulation patterns can indicate the likelihood of severe weather events and are thus important for both forecasting these events, as well as understanding the mechanisms behind them (Irannezhad et al. (2017)).

2.2.2 Defining atmospheric circulation patterns by EOF analysis

Due to the large internal variability, the North Atlantic-European climate is difficult to predict. There are however many studies describing the North Atlantic variability by persistent and recurrent dynamical configurations, known as weather regimes, which are described in Chapter 2.2.1.

In Paper II of this thesis, circulation patterns are found and analyzed by the use of EOF analysis. By performing such analysis on a pressure anomaly field over the North Atlantic region, the output is a list of orthogonal patterns sorted by their relative importance for the overall spatial variability. The EOF analysis applied here was performed using the September-October-November 500 hPa geopotential height anomalies from the ERA5 reanalysis (see section 3.3) and the seasonal forecast from SEAS5 (see section 3.4) over the North Atlantic sector (30 - 88.5°N,

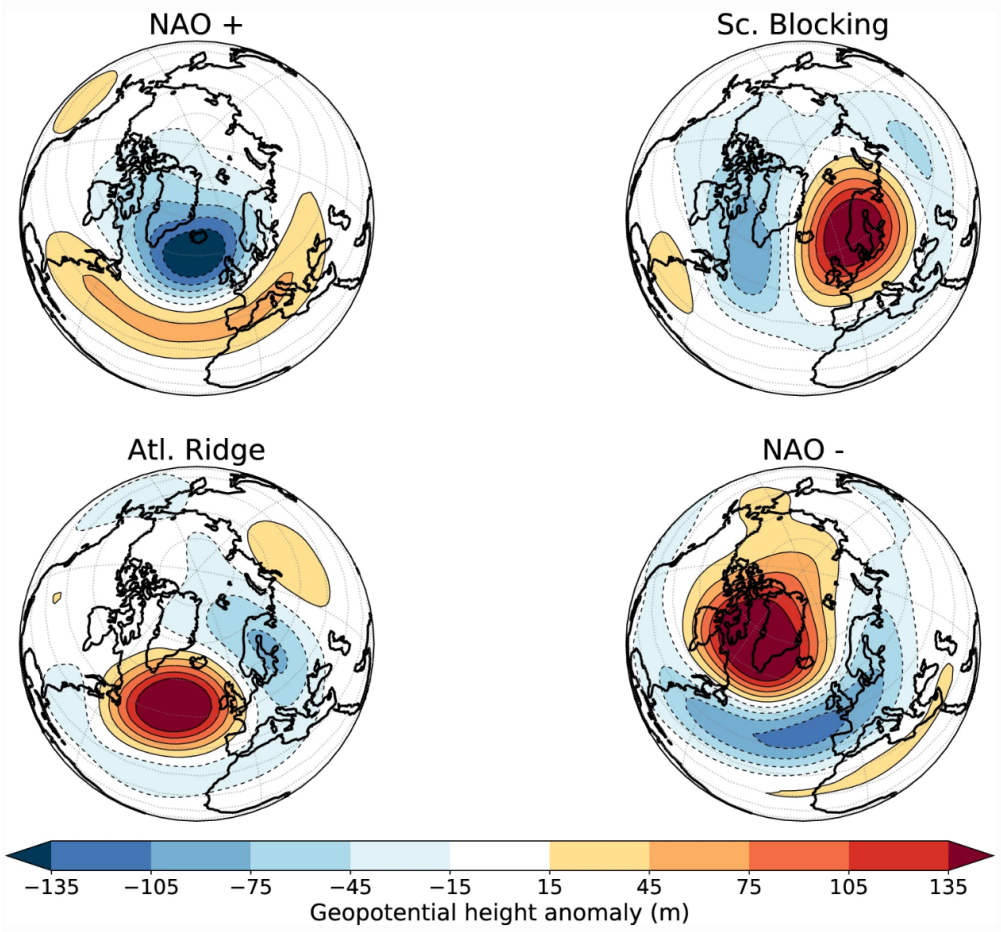

Figure 2.2: *Mean pattern of the weather regimes obtained from a combination of ERA40 and ERAInterim (1957–2014). (The Euro-Atlantic weather regimes, based on daily geopotential height data at the 500-mb isobaric level from the ERA40 and ERA-Interim reanalyses. The four regimes are the positive and negative phases of the North Atlantic Oscillation (NAO+ and NAO–, respectively), Scandinavian blocking (SB), and a North Atlantic ridge pattern (AR). Regimes patterns visualized following removal of the climatological mean seasonal cycle.) Figure from Fabiano et al. (2020).*

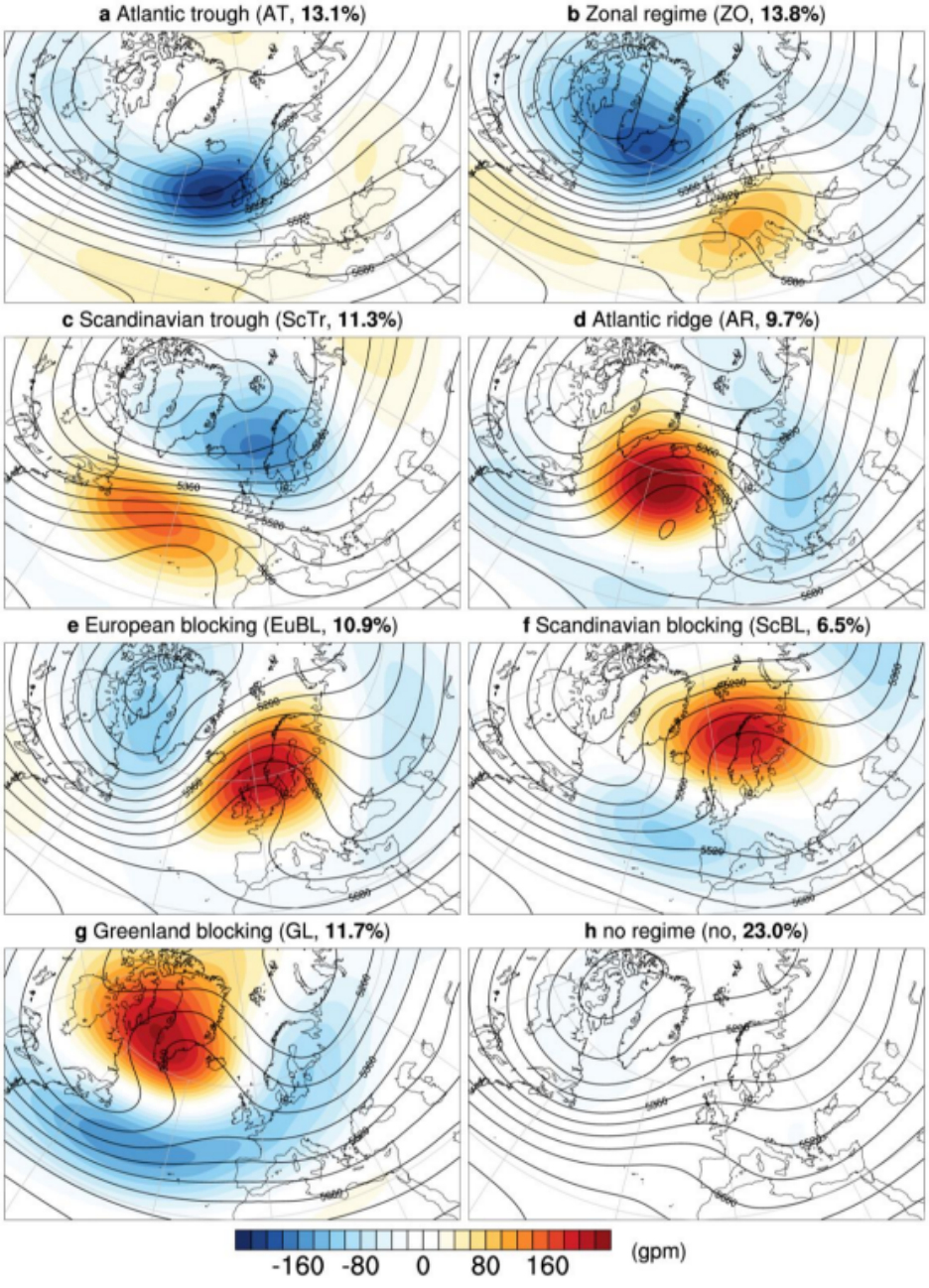

Figure 2.3: *Mean pattern of the winter weather regimes obtained from ERAInterim (1979-2015). Figure from Grams et al. (2017).*

80°W - 40°E). The first five EOFs from ERA5 SON 500 hPa geopotential height anomalies were computed using the period from 1979 to 2017. The indexes were calculated by projecting the 500 hPa geopotential height anomalies from each SEAS5 ensemble member onto the EOFs from the ERA5 500 hPa geopotential height anomalies.

2.3 Atmospheric Rivers and their connection to extreme precipitation

Atmospheric rivers (ARs) are long, narrow corridors of high water vapor content in the atmosphere. The most common ways of defining atmospheric rivers are areas where Integrated water vapor transport, $IVT \geq 250 kgm^{-1}s^{-1}$ or integrated water vapor, $IWV \geq 20$ mm are found over a contiguous region ≥ 2000 km in length (Rutz, Steenburgh and F. Ralph (2014)). Seen from a satellite image, atmospheric rivers are found as long narrow corridors of high moisture content that resemble a river, thus the phenomenon has been given its descriptive name. Benedict et al. (2019) looked at extreme precipitation events in three different regions (North, West, and East) in Norway, and found that more than 85 % of the events were connected to ARs. This is collaborated by the study of Michel et al. (2021) who found that between 70-90 % of extreme precipitation events along the coast of Norway are associated with ARs. This phenomenon is therefore an important factor for the extreme precipitation climatology of Norway. ARs are found to occur more frequently during certain weather regimes. The positive phase of NAO is found to be conducive to high precipitation values over Norway by guiding low-pressure systems to the west coast of the country and is associated with higher than normal frequency of ARs (Benedict et al. (2019) and Pasquier, Pfahl and Grams (2019)). Further, Pasquier, Pfahl and Grams (2019) found that during weather regimes such as the European Blocking, more effective moisture transport around the ridge of the high pressure and into Northern Europe was allowed, with the consequence that AR frequencies are enhanced in a region extending from Iceland to Northern Scandinavia.

The engine of atmospheric rivers is the low- and high-pressure centers that steer warm, moist air from the tropics/subtropics northward. More than 90 % of the meridional water vapor transport in midlatitudes is located in the narrow, elongated regions related to warm conveyor belts within the warm sector of extratropical cyclones (Zhu and Newell (1998)). While being responsible for the majority of water vapor transport polewards, these filaments cover less than 10 % of the area of the globe. Note that within an atmospheric river, it is not a continuous flow of moisture, but rather a consecutive incorporation of moisture from local convergence and evaporation along the track, and only in rare cases moisture from distant source regions in the tropics or subtropics. Atmospheric rivers are generally found in the vicinity of extratropical cyclones and are one part of a larger, synoptic-scale dynamical system driving the poleward transport of sensible and latent heat (Payne et al. (2020)). Over the North Pacific, for example, 85%

of ARs are paired with extratropical cyclones, consistent with their observed relationship with baroclinic instabilities and the mid-latitude storm track. However, this relationship is nuanced; only 45% of extratropical cyclones over the same region are associated with an AR. Similar non-linear relationships are observed in the North Atlantic, where the evolution and life cycle of a single AR can span that of several cyclones.

The "Atmospheric River" term was first denoted in the USA, where the water balance on the West coast strongly relies on the rainfall produced by landfalling atmospheric rivers. Thus, features of ARs are well studied in e.g. California, a region often affected by drought. Atmospheric rivers here are regarded as both beneficial and destructive, since they are known to have ended drought conditions but also to have caused substantial socio-economic damage from landslides and flooding linked to extreme precipitation. Landfalling atmospheric rivers produce heavy rainfall which can lead to flooding, and landslides and cause substantial damage, especially where the topography is steep and the flow of moist air is lifted orographically. In areas where the alignment of the coastline and a high mountain range along the coast in combination with the high moisture flux of ARs set the stage for heavy precipitation (F. M. Ralph et al. (2006) and Rutz, Steenburgh and F. Ralph (2014)). The connection between heavy precipitation events and subsequent flooding is highlighted in F. M. Ralph et al. (2006) where it was shown that all major floods in the California Russian River were associated with atmospheric rivers.

In the UK, ARs were demonstrated to be a critical mechanism in extreme winter floods by Lavers et al. (2011), where they showed that ARs deliver moisture for the 10 largest winter flood events since 1970 in a range of British basins. In recent years, the awareness of landfalling ARs and their association with extreme precipitation in Norway has increased substantially. A. Stohl, Forster and H. Sodemann (2008) and Sodemann and Stohl (2013) demonstrate the important connection between moisture transport and high-impact Norwegian weather. A. Stohl, Forster and H. Sodemann (2008) show that the extreme weather event "Kristin" in September 2005 was indeed an atmospheric river rooted in the tropical western North Atlantic. When impinging upon the mountainous area in southwest Norway the AR created an extreme precipitation event followed by flooding and landslides that led to the loss of human life and caused considerable infrastructure damage. The work of Michel et al. (2021) described regional and seasonal aspects, and found that for the coastal areas in Norway, autumn is the season where both most extreme cases occur, and when most cases are connected to ARs.

2.4 Estimation of Extreme Precipitation and Design Values

Extreme precipitation events can have significant impacts on infrastructure, by causing flooding, landslides, and erosion. To design infrastructure that can withstand such events, engineers use design values for extreme precipitation. The design values are estimates of the likelihood of exceeding a certain amount of precipitation, in a given area over specific time intervals. The design values are based on historical precipitation data and statistical analysis.

The Intensity-Duration-Frequency (IDF) relationship is a tool that helps to determine the design values for extreme precipitation. It describes the likelihood of a precipitation amount exceeding a certain level over a specific duration and frequency of occurrence. For example, an IDF curve can show that a certain level of precipitation (intensity) is expected to occur once every 10 years (frequency) for a duration of 1 hour (duration). IDF curves are used in the planning of infrastructure to ensure that the design values are consistent with the expected precipitation events in a given area. They are also used to determine the size and capacity of stormwater management systems, such as detention ponds and culverts, to ensure that they can handle the expected precipitation events. Design values for extreme precipitation and the IDF relationship are important tools in infrastructure planning to ensure the safety and reliability of infrastructure against the impacts of extreme precipitation events. Critical infrastructure such as dams and nuclear power facilities, which pose a significant threat to society if destroyed, require a risk assessment with sufficiently long return periods for the design values, and in such cases, PMP is often used.

2.4.1 Generalized Extreme Value Distribution

Return values in the form of IDF are most commonly calculated by fitting the Generalized Extreme Value (GEV) Distribution to a block maxima, as the seasonal or annual maximum precipitation, or "peak over threshold" (POT), then in the form of a fit to the Generalized Pareto Distribution.

According to the extreme value theorem, appropriately renormalized block maxima values–such as the annual or seasonal maxima–of a set of independent and identically distributed random variables will follow a generalized extreme value (GEV) distribution if a limit distribution exists (e.g. Coles (2001)). As the record length approaches infinity, the cumulative distribution function converges to $G(x)$ of the form

$$G(x) = \begin{cases} \exp\left\{ -\left[1 + \xi\left(\frac{x-\mu}{\sigma}\right)\right]^{-1/\xi} \right\} & \text{for } \xi \neq 0 \text{ and } 1 + \xi\left(\frac{x-\mu}{\sigma}\right) > 0, \\ \exp\left\{ -\exp\left[-\left(\frac{x-\mu}{\sigma}\right)\right] \right\} & \text{for } \xi = 0. \end{cases} \tag{2.1}$$

Here, the location parameter μ determines the position, the scale parameter σ ($\sigma > 0$) determines the width, and the shape parameter ξ determines the slope of the distributions for large values of x. Dependent on ξ, the distribution can take three different forms:

- Type I/Gumbel ($\xi = 0$)
- Type II/Fréchet ($\xi > 0$)
- Type III/Weibull ($\xi < 0$)

For $\xi < 0$, the Weibull distribution, the tail has a finite upper value; for $\xi > 0$, the Fréchet distribution, the tail is heavy with a power law form; for $\xi = 0$ one obtains a Gumbel distribution with an exponential form (light tails). The three different forms are shown in an example of a return level plot in Figure 2.4.

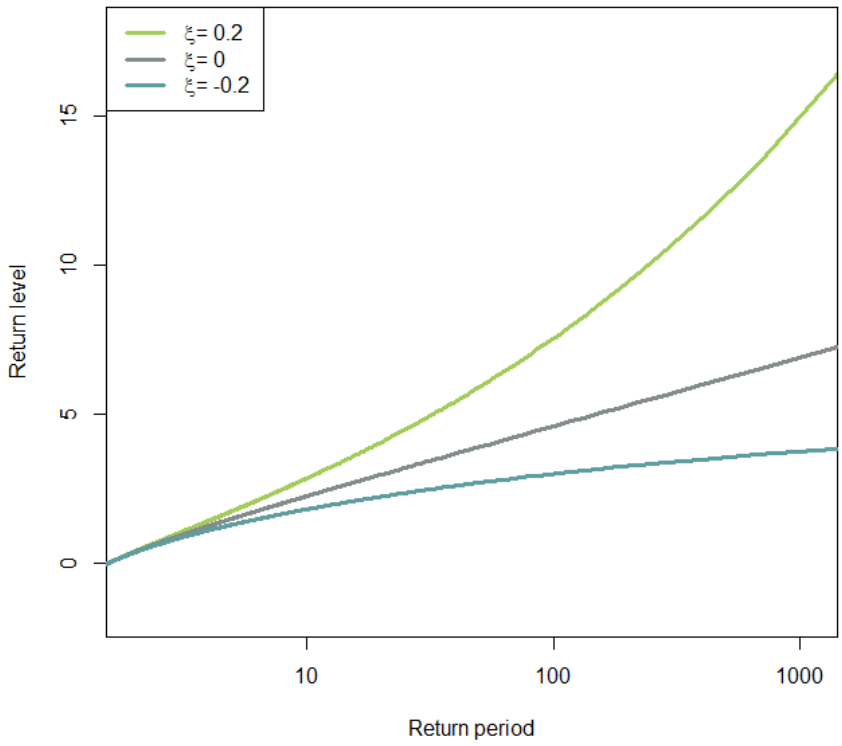

Figure 2.4: *Return level plot showing the GEV distribution with shape parameters* $\xi = -0.2$, $\xi = 0$ *and* $\xi = 0.2$

From the GEV distribution, return levels can be derived, where a return level represents the level of an extreme event that is expected to be exceeded on average once in a specified time period, often referred to as the return period. The probability p that a maximum larger than a certain value x_p occurs within a year (if the

block length is a year) is given by $P(x > x_p) = G(x_p) = 1 - p$. The value x_p is the return value and the corresponding return period is $T_p = 1/p$ years. Within a year, the return value x_p is exceeded with a probability of p, and thus on average x_p is exceeded only once every T_p years. The cumulative distribution function $G(x)$ in (2.1) is invertible and the quantile function for the GEV distribution thus has an explicit expression. The return value x_p is given by the value of the quantile function in $1-p$, that is, the quantile that has probability p of being exceeded in a particular year. As mentioned above, the shape parameter (ξ) is important for the tail of the distribution, and therefore for the return values with long return periods.

Dyrrdal et al. (2016) investigated which of the three categories of annual maximum daily precipitation in Norway belongs to and found that ξ is mainly negative in the western part of Norway, while it is largely positive in the eastern part, and suggested a dependence on dominating precipitation systems and orographic enhancement. This is also found in Ragulina and Reitan (2017) who showed how ξ decreased with elevation and that ξ differed between Norway and other parts of the world.

2.4.2 Probable Maximum Precipitation

When designing hydraulic structures such as dams, reservoirs, and levees, as well as in the design of infrastructure such as roads and bridges, the design value "Probable Maximum Precipitation" is a crucial estimate. PMP is also used as an input for the estimation of probable maximum flood, PMF. There are various methods for calculating PMP, and the most appropriate method depends on the climatic and orographic conditions of a specific location. The methods vary with the amount and quality of data available, basin size and location, basin and regional topography, storm types producing extreme precipitation, and climate. The conventional ways of estimating PMP can broadly be categorized into two groups, physical methods and statistical methods. The WMO manual provides this list of currently used PMP methods (WMO (2009)):

(a) The local method (local storm maximization or local model:)
The observed maximum storm is used to estimate PMP;

(b) The transposition method (storm transposition or transposition model):
An extraordinarily large storm close by is transposed to the watershed area;

(c) The combination method (temporal and spatial maximization of storm or storm combination or combination model):
The creation of artificial storms with prolonged duration is achieved by combining two or more storms in a specific area. This technique can be used in extensive watersheds and necessitates meteorological expertise.;

(d) The inferential method (theoretical model or ratiocination model):
A simplified physical equation describing the 3-D spatial structure of a storm is created. This method can be applied in medium to large watersheds and requires upper meteorological measurements in the area;

(e) The generalized method (generalized estimation):
This method entails separating observed rainfall into convergence and orographic rainfall within a large, meteorologically homogeneous region. This process is both time-intensive and costly, and necessitates a comprehensive dataset of long-term rainfall measurements in the area. Nevertheless, the outcomes are likely to be highly accurate. Referred to as a storm area approach.;

(f) The statistical method (statistical estimation):
This method is proposed by Hershfield (Hershfield (1961)). The regional generalized method is combined with data from multiple rain gauges to apply the hydrological frequency analysis method. The area should be smaller than $1000km^2$ and meteorologically homogeneous. Referred to as a storm area approach.

In very large watersheds there are in addition two other methods that can be used:

(a) The major temporal and spatial combination method:
Hydro-meteorological methods are applied on the part of PMP that has the larger temporal and spatial influence on PMF, while the common correlation method and flood distribution method are applied on the part of PMP with a smaller influence. The method combines temporal and spatial conditions.;

(b) The storm simulation method based on historical floods:
Hydrological watershed models are applied in producing a storm with the potential to create an observed historical flood, and PMP is estimated by maximizing moisture.

The complex topography and sparse station network in Norway make it difficult to perform a detailed analysis of extreme precipitation and to transpose a precipitation event from one location to another. Consequently, it was decided to apply statistical methods for Norway. In WMO's latest manual on PMP estimation (WMO (2009)), it is suggested to consider whether physical-based approaches can be utilized in areas with steep topography. As mentioned in the introduction (Section 1), a number of studies have investigated the use of numerical weather prediction models (NWPs) for PMP estimation (Ohara et al. (2011), Ishida et al. (2015b) and Ishida et al. (2015a)). Ishida et al. (2015a) alter boundary and initial conditions to maximize precipitation over targeted catchments, by aiming to shift the location of an atmospheric river to hit their area of interest, as illustrated in Figure 2.5. This is done in combination with increasing humidity at the boundaries of the model domain. In Norway, and in western Norway in particular, extreme precipitation is often strongly connected to atmospheric rivers (Azad and Sorteberg (2017), Benedict et al. (2019) and Michel et al. (2021)). Thus, the method used by Ishida et al. (2015b) would be natural to employ for Norwegian conditions. However, as discussed in Toride et al. (2019), there can be introduced disturbances to the fields beyond what is realistic by systematically saturating all boundaries.

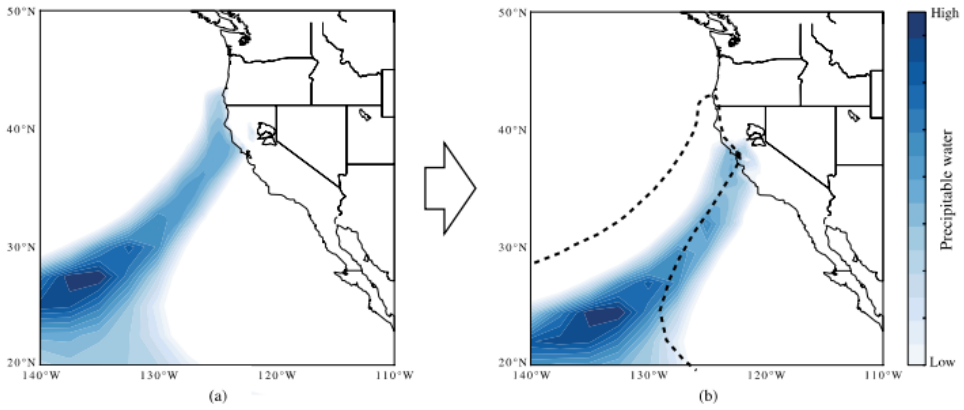

Figure 2.5: *How boundary conditions in a numerical weather prediction model can be changed to make an AR hit a selected watershed more directly. From Ishida et al. (2015a).*

Recently, there has also been a debate on the concept of PMP itself, and there are arguments that the upper limit of precipitation cannot be specified in a deterministic way (Papalexiou and Koutsoyiannis (2006), Micovic, Schaefer and Taylor (2015) and Rouhani and Leconte (2016)). Koutsoyiannis (1999) examined the work of Hershfield and concluded that, based on the GEV distribution, the return value of the estimated PMP by Hershfield's method corresponds to a return period of 60 000 years. Papalexiou and Koutsoyiannis (2006) suggested estimating design values of maximum precipitation using observed data fitted to the GEV, rather than by the much used moisture maximization method, and thus related the PMP value to a probability, in contrast to a deterministic PMP estimate. Alaya, Zwiers and Zhang (2020) advise to distinguish between the "theoretical PMP" which is an unknown upper limit for precipitation and the "operational PMP" which involves a number of assumptions, steps, and data that are uncertain and can be obtained by engineers to provide guidance for design decisions. The PMP is a rational engineering solution to the problem of establishing a plausible upper limit to extreme precipitation values that can be used by engineers where scientific knowledge does not provide the desired guidance.

2.4.3 Estimation of PMP in Norway

Due to challenges connected to sparse observation net in complex topography, not allowing for a sufficiently detailed analysis of extreme precipitation, the PMP estimation option of transposing precipitation events to new locations was regarded as inadequate for Norway. Alternatively, the estimation was done purely by statistical methods, and a standardized statistical approach based on the method developed at The National Environment Research Council (NERC) in Great Britain in 1975 is still used to estimate PMP (NERC (1975) and Førland (1992b)). The method is based on point measurements at meteorological stations and uses empirical growth factors to derive estimates for longer return periods (Dyrrdal et

al. (2016)). This approach is also vulnerable to subjective choices, such as which observation sites to use in the estimate, that can affect the resulting PMP values. This is in particular the case for areas where access to observations is limited, and the representativeness of the existing in-situ observation is inadequate due to complex terrain.

In this method a precipitation value MT can be described as a function of the precipitation value with a 5-year return period M5, which is estimated by the Gumbel method (Gumbel (2004)). MT is then calculated by

$$MT = M5e^{C[ln(T-0.5)-1.5]} \tag{2.2}$$

where T refers to the return period so that MT is precipitation with a T year return period (e.g. M5 is the precipitation with a 5 year return period). C is a geographically varying factor empirically derived as a function of M5, and defined differently for England/Wales and Scotland/North Ireland. When the method was adopted for use in Norway, it was adjusted to Norwegian conditions (Førland (1992b)). The NERC method is also referred to as the "growth factor method" or the M5 method, as the MT/M5 ratio is known as the "growth factor". The M5 is adjusted by a factor of 1.13 (recommended by WMO) to represent an arbitrary 24-h period, as the observation times are between 06 and 06 UTC. The resulting estimates are point estimates, and to apply them to an area, as a catchment, Areal Reduction Factors (ARF) must be used.

2.4.4 PMP in a changing climate

According to WMO, PMP estimates should be calculated without considering the effects of changing conditions. However, as the climate continues to change, it is becoming increasingly important to review PMP estimates to account for the rise in global temperature, altered storm tracks and precipitation patterns, and the intensification of extreme precipitation events (Papalexiou and Montanari (2019)). The atmosphere's water-holding capacity is expected to increase at the Clausius-Clapeyron (C-C) rate by about 7% per 1 °C warming (Collins et al. (2013)), which may lead to more intense extreme precipitation events and thus directly affect the PMP (Alaya, Zwiers and Zhang (2020)). X. Chen, Hossain and Leung (2017) reported an increase in PMP in the Pacific Northwest US of around 50% +/- 30% by 2099, under the high Representative Concentration Pathway scenario, RCP8.5, highlighting the importance of revisiting PMP estimates to ensure the safety and reliability of critical infrastructure in the face of a changing climate. In a changing climate, extreme precipitation events are projected to be more frequent and intense, resulting in unprecedented precipitation events (Trenberth et al. (2003)), which means that dams and other similar structures are vulnerable to future climate change (Kunkel et al. (2013)). A change in PMP estimates will have consequences for the estimation of Probable Maximum Flood (PMF), for which PMP is an input parameter. The changing climate also has direct implications for PMF, as the dominant flood-generating process is changing from snowmelt to precipitation in some areas in the Nordic countries (Vormoor et al.

(2015)). Along with structural safety, the hydrologic safety of water infrastructures is therefore gaining more attention, since overtopping or embankment failure would bring catastrophic human and societal loss (Casagli et al. (2006), X. Chen, Hossain and Leung (2017), Choi et al. (2020) and Williams (2021)). This means that PMP estimates may need to be reexamined and updated to reflect the changing climate and its effects on extreme weather. The recent advancements for modernizing PMP estimates by employing numerical atmospheric models to enable a more physics-based estimation of PMP give the possibility to utilize climate models with future projections as input for PMP studies, and has the potential to quantify the sensitivity of PMP to climate change (Rastogi et al. (2017), Thuy, Kawagoe and Sarukkalige (2019) and Sarkar and Maity (2020)).

Chapter 3

Data Sets and Models

We have applied a range of data products to investigate extreme precipitation in Norway and to evaluate PMP methodology. This chapter describes different data sets and models; the global climate model EC-Earth, the high resolution regional numerical weather prediction model AROME-MetCoOp, the reanalysis data-set ERA5, the seasonal forecasting system SEAS5, and the gridded observational dataset seNorge used in the thesis.

3.1 Climate model: EC-Earth

The global climate model EC-Earth has been used to produce a data set with 30 years of model data for the present climate. The simulation was done with EC-Earth v2.3 (Hazeleger et al. (2010)) with a horizontal resolution of ∼25 km and 91 vertical hybrid levels (T799 L91). The 30 years of simulation was constructed by 6 independent members spanning 5 years (2002-2006). The approach for generating a data set with ensemble members that can be considered to be independent is described in Haarsma et al. (2013). Observed greenhouse gas and aerosol concentrations were used, together with a daily satellite product for sea surface temperature. The simulations produced by EC-Earth were used as input for the regional numerical weather prediction model AROME-MetCoOp for extreme precipitation events for the analysis in Paper I.

The event identified by the highest daily precipitation values over a constraint area in Western Norway (57.1 °N to 63.2 °N and 2.6 °N to 9.3 °N) from the 30 years of EC-Earth simulations was selected for further study. For this event, an ensemble of 10 members was established. Each perturbation will represent a plausible realization of a possible extreme precipitation event over the Norwegian West Coast. The 10 ensembles were then downscaled using the NWP model AROME-MetCoOp.

3.2 Numerical weather prediction model: AROME-MetCoOp

AROME-MetCoOp is the operational weather prediction model used at the Norwegian Meteorological Institute, and as such has been tuned and adapted to the specifications of the Nordic model domain (Müller et al. (2017) and Bengtsson et al. (2017)). It is based on AROME (Applications of Research to Operations at Mesoscale) (Seity et al. (2011)), a non-hydrostatic atmospheric model system. It is run with the standard operational domain for Scandinavia, AROME-MetCoOp, covering the entire of Norway, as well as Sweden, Denmark, and Finland. The horizontal resolution is 2.5 km, on a 750 by 960 grid, with 65 vertical layers. AROME-MetCoOp later became the control run of MetCoOp Ensemble Prediction System (MEPS). The operational AROME-MetCoOp's ability to predict precipitation is documented in Müller et al. (2017) and Frogner et al. (2019), where forecast skills compared with the global European Centre for Medium-Range Weather Forecast's Integrated Forecasting System (ECMWF-IFS) showed that AROME-MetCoOp clearly adds value to the forecast product for both precipitation and temperature. It permits convection, though the focus of this study is related to large-scale advective precipitation. The high horizontal resolution gives a good representation of the terrain and how it influences the spatial precipitation distribution.

The simulations by AROME-MetCoOp are here initialized and forced by EC-Earth fields at the lateral and upper boundaries, for the use of the analysis in Paper I. 10 ensemble members for one extreme precipitation event were analyzed in terms of precipitation amounts in two selected catchments in addition to the importance of position and orientation of the moisture flow between the individual ensemble members.

3.3 Reanalysis dataset: ERA5

ERA5 is the most recent global reanalysis product from ECMWF, and provides atmospheric, land, and ocean climate variables from 1950 to present, at hourly resolution (Hersbach et al. (2020)). It is based on the IFS cycle Cy41r2, and is the fifth generation reanalysis product from ECMWF. Successive atmospheric reanalysis has offered a higher horizontal resolution, more sophisticated model physics core dynamics, and data assimilation. ERA5 has a horizontal resolution of 31 km, whereas its predecessor, ERA-Interim, has 80 km. It also provides an enhanced number of output parameters, including 3-hourly uncertainty information derived from an ensemble. Data from ERA5 is used in Paper II of this thesis. Together with data from the seasonal prediction system SEAS5, the ERA5 data is used in the study of large-scale circulation patterns connected to extreme precipitation events in Norway.

3.4 Seasonal Prediction System: SEAS5

The 25 member ensemble hindcast data set of the ECMWF's seasonal prediction system SEAS5 (Johnson et al. (2019)) is utilized in this thesis. SEAS5 is a coupled atmosphere-ice-ocean model with a horizontal resolution of around 35 km. SEAS5's atmospheric component is based on cycle 43r1 of the ECMWF-IFS (R. G. Owens (2018)). The spectral horizontal resolution is T319 and there are 91 vertical layers. The NEMO ocean model (Nucleus for European Modelling of the Ocean (Madec et al. (2017))) and LIM2 sea-ice model (Louvian-la-Neuve Sea Ice Model (Fichefet and Maqueda (1997))) are coupled to the atmospheric system, and have a horizontal resolution of 0.25-degrees. The atmospheric and ocean-ice model systems are initialized by the ERA-Interim (Dee et al. (2011)) and OCEAN5 reanalysis (Zuo et al. (2018)), respectively.

The ensemble members are generated from perturbations to the ocean and atmosphere initial conditions and from stochastic model perturbations. The SEAS5 seasonal re-forecast consists of 25 members initiated monthly, and each member spans over 7 months for the years 1981 to present. In this study, we use the hindcast data from 1981 to 2018. The individual ensemble member forecasts need to be independent for the statistical analysis of extreme precipitation. Because of the chaotic nature of the atmospheric system, we assume that precipitation events are not predictable more than a few weeks in advance and, thus, a specific first month of the model run is discarded to avoid dependent events.

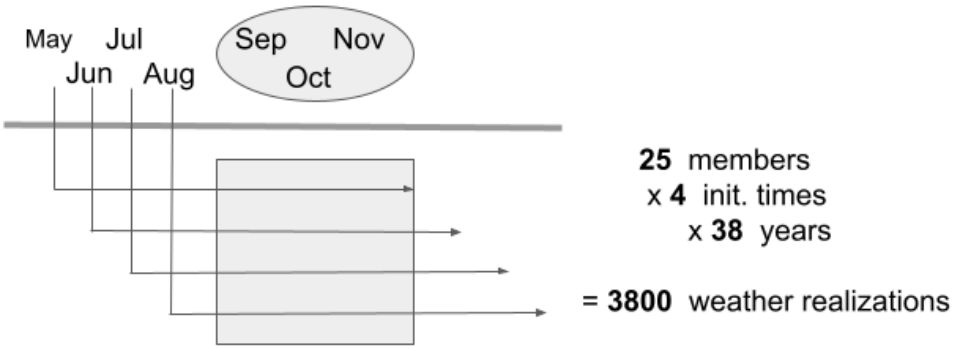

Figure 3.6: *Illustration of how members and initialization times are selected and retrieved from SEAS5.*

For the analysis of both Paper II and Paper III we analyze the autumn season (September, October, and November; SON), and, thus 4 initialization months (May, June, July, and August) which span over the SON months are used, as are

illustrated in Figure 3.6. The events for the seasonal 3-day maximum precipitation values are used. This yields 100 seasonal weather realizations for each year between 1981 and 2018, in total 3800 weather realizations representing the current climate.

3.5 Observational dataset: seNorge

seNorge is a long-term gridded observational dataset containing daily total precipitation, daily mean temperature, and daily minimum and maximum temperatures covering the time period 1957 to present (Lussana et al. (2018)). The data are provided on a high-resolution grid with 1 km grid spacing. The grids are based on in situ observation records from the Norwegian Meteorological Institute's (MET Norway) station network, which consists of around 600 precipitation stations. The majority of the stations are owned by MET Norway, but a growing part is owned by other organizations, such as The Norwegian Public Roads Administration and other public institutions. The observations are collected and stored at MET Norway where the data undergo a quality control routine.

Measuring precipitation, especially solid precipitation, in combination with wind is a challenge due to the wind blowing precipitation over and around the precipitation gauge preventing the true amount from being measured. The observed precipitation values are therefore corrected for under-catch, according to the method proposed by Wolff et al. (2015).

The spatial domain covers the Norwegian mainland, plus an adjacent strip of land extending into Sweden, Finland, and Russia in order to cover catchments that drain to Norway, and to reduce boundary effects along the Norwegian border. Two distinct statistical interpolation methods have been developed, one for temperature and the other for precipitation. They are both based on a spatial scale-separation approach where, at first, the analysis (i.e., predictions) at larger spatial scales is estimated. Subsequently, they are used to infer the small-scale details down to a spatial scale comparable to the local observation density. For precipitation, in addition to observational data, spatial interpolation makes use of information provided by a climate model. The analysis evaluation is based on cross-validation statistics and comparison with a previous seNorge version. The analysis quality is presented as a function of the local station density.

Even if seNorge is presented on a 1x1 km grid resolution, the resolution representativeness is perhaps at 10-40 km scale, due to the distance between in-situ observation stations on which the grid is based on. The representative resolution will depend on the observation station density, which is more sparse in high altitudes and in the northern part of Norway. According to Bandhauer et al. (2022) an effective resolution of 10 km can at best be expected in southern Norway, while the resolution is around 40 km or larger in the interior of the Norwegian mountain ridge and in the northern part of the domain (C. Lussana et al. (2019) and Band-

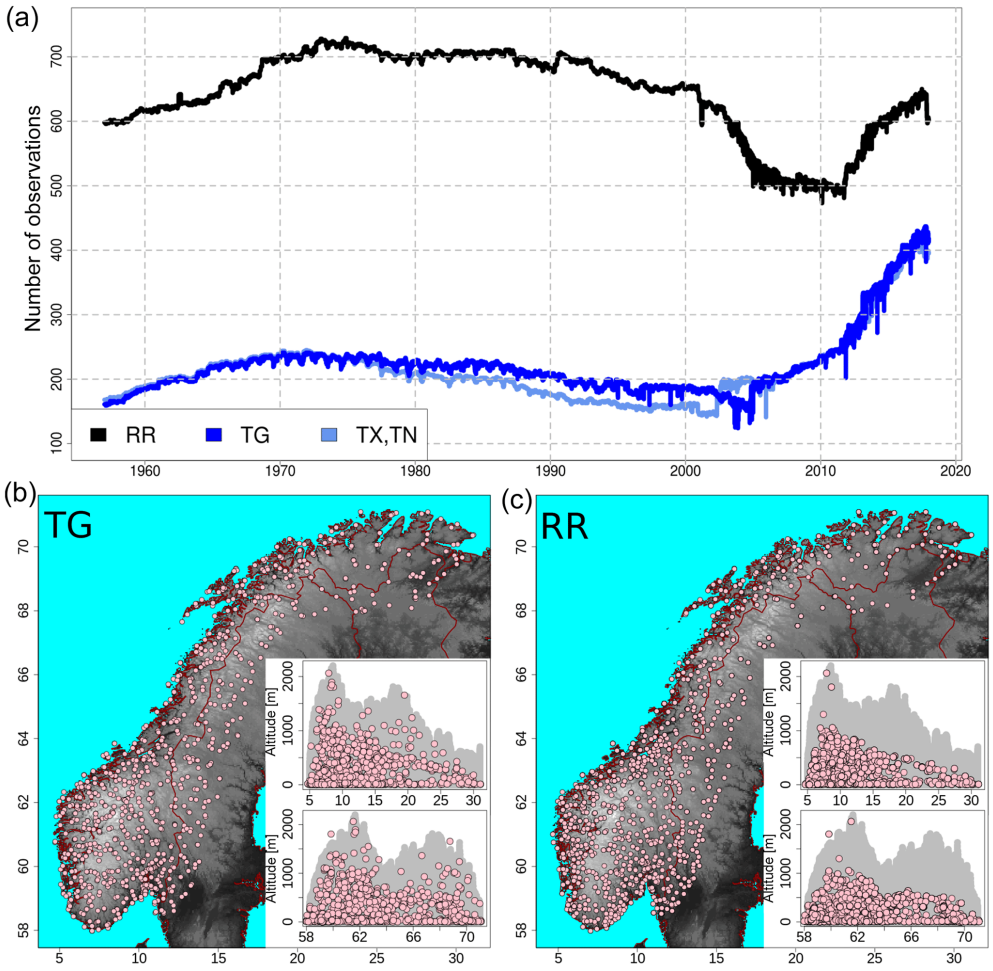

Figure 3.7: *The observational network over the Norwegian mainland for the four variables daily total precipitation (RR), daily mean temperature (TG), daily maximum temperature (TX), and daily minimum (TN).* ***(a)*** *shows the number of observations available over time. Panels* ***(b,c)*** *show the observational networks for TG* ***(b)*** *and RR* ***(c)****. The pink dots mark station locations with more than 1 year of data. The inset graphs in* ***(b,c)*** *show altitude above mean sea level as a function of latitude (top graph) and longitude (bottom graph), where the gray area shows the altitude of the terrain at grid points and the pink dots are the altitudes of stations. Figure from C. Lussana et al. (2019).*

hauer et al. (2022)).

Precipitation data from seNorge is used for the analysis in Paper III of this thesis, where seasonal maximum precipitation is fitted to the GEV distribution and further used in combination with data from the seasonal forecasting system SEAS5.

Chapter 4

Summary of papers

4.1 Paper I: Changing Lateral Boundary Conditions for Probable Maximum Precipitation Studies: A Physically Consistent Approach

Objective

To investigate a new approach for changing lateral boundary conditions in PMP estimates when a physical numerical model is used. A special focus is on numerical and dynamical consistency in the PMP experiments.

Summary

We used the ensembles from simulations with the global climate model EC-Earth as input data for a regional model in order to analyze extreme precipitation on catchment scale in two selected catchments in Norway. 10 ensembles of one extreme event were analyzed, where each member will represent a plausible realization of a possible extreme precipitation event over the Norwegian West Coast.

Author's contributions

I planned the analysis together with my supervisors and did the analysis and plotting. The model runs, both EC-Earth and AROME-MetCoOp simulations were enabled by the project group in the project TWEX (NFR-255037). The text was written in cooperation with my supervisors.

Main findings

- By using global climate ensemble runs we are able to change boundary- and initial conditions in a numerical weather prediction model in a physically and dynamically consistent way.
- The precipitation amount in selected catchments is increased 75 % by the member that has an AR hitting more directly over the catchment.
- Local orographic effects play an important role in the resulting precipitation amounts, implying that there is not a linear relationship between AR intensity and precipitation amounts.
- The precipitation amounts in the selected catchments were altered, but compared to PMP values estimated by the traditional method, the values were underestimated.
- While this shows promising results, the approach is computationally costly and also requires subjective choices, as to which model to use, model set-up, and how to perturb the ensemble members.

Main conclusion

This approach enables a physically consistent way to alter lateral boundary- and initial conditions for extreme precipitation event analysis over targeted catchments, but at the same time it is costly and perhaps not feasible for deriving PMP estimates over entire Norway.

4.2 Paper II: Recent changes in circulation patterns and their opposing impact on extreme precipitation at the west coast of Norway

Objective

To investigate whether event sampling by restructuring the SEAS5 seasonal prediction system ensembles could be utilized for extreme precipitation analysis over Norway in order to understand recent changes in observed precipitation amounts. In addition, we seek to find whether the large sample size yields more robust estimates for return values in terms of smaller confidence intervals compared to equivalent estimates from ERA5.

Summary

By the use of a novel approach where all the ensembles of different initialization times are collected from the seasonal forecasting model SEAS5, we analyze extreme precipitation events on the west coast of Norway. 3-day maximum precipitation events are investigated and linked to dominant large-scale precipitation patterns. The events are also fitted to the GEV distribution and compared to the corresponding fit for 3-day seasonal maximum events retrieved from ERA5.

Author's contributions

I planned the analysis in close cooperation with my supervisors. I retrieved the data and did the majority of the analysis and plotting with guidance from one of my supervisors. A part of the analysis was done by one of the co-authors. In the end, I wrote the paper in cooperation with the co-authors.

Main findings

- We find that the confidence interval of GEV analysis is strongly reduced when using the resampled dataset from SEAS5 compared to data from ERA5.
- When analyzing circulation patterns connected to extreme precipitation events on the West coast of Norway, we find that two patterns have trends over the period 1981-2018, with opposing impacts on the precipitation events.
- The two opposing impacts on precipitation events are concurrent with the stationary precipitation amounts found for the west coast of Norway for the autumn season.

Main conclusion

We find two circulation patterns connected to the extreme value statistics for the West coast of Norway. The patterns exhibit trends over the recent decades with opposing impacts on the precipitation values.

4.3 Paper III: Towards a new framework for PMP estimates in Norway by combining an ensemble data set and gridded observations

Objective

The aim of paper III is to analyze the statistical properties of the parameters involved in the fit to the GEV distribution for the large ensemble data set used in Paper II, along with the gridded observational data set seNorge. Further, the objective is to re-parameterize the GEV distribution in order to derive return values, with a special focus on return values with long return periods approaching the level of PMP.

Summary

Data from the seasonal forecast model SEAS5 are fitted to a GEV distribution and compared to an equivalent GEV distribution for the gridded observational data set seNorge. We propose a method to estimate return values by combining the spatially detailed information in seNorge to estimate the bulk of the distribution and the longer SEAS5 data series to estimate the tail behavior. Using a re-parameterized GEV distribution, the information from the two data sets may be combined in two ways. First, we considered an independent estimation of the median parameter η based on the seNorge data and the growth curve based on the SEAS5 data. Alternatively, we considered estimating the shape parameter (ξ) based on the SEAS5 data, while the location (μ) and scale (σ) are estimated based on the seNorge data. In this way, we were able to make use of the long data series provided by SEAS5 to estimate the tail behavior of the quantile curve.

Author's contributions

I planned the analysis together with the co-authors and did the data acquisition and analysis. The paper draft was written in close cooperation with the co-authors.

Main findings

- We demonstrated how the size of the underlying data set used to fit the GEV distribution influences the estimated parameters.
- We are able to utilize a re-parameterized version of the GEV to combine the large sample size data from SEAS5 with the gridded observational data set from seNorge.
- We arrive at return values with a much smaller confidence interval than by using the gridded observation data set alone, especially for return values with long return periods.

Main conclusion

We find that by using the re-parameterized version of the GEV distribution we can obtain reliable estimates for return values with long return periods for parts of Norway, where the product is trusted. This re-parameterization is based on a combination of two datasets, which ensures physical properties are taken into account for the return value estimation. The approach is thought to be most reliable in coastal areas, where large-scale precipitation dominates, and the station density is adequate.

4.3.1 Summary of answers to the research questions

This section summarizes the answers to the research questions related to this thesis:

1. **Can the initial and boundary conditions for numerical PMP studies be altered in a physically and dynamically consistent way (Paper I)?**
   We found that by using an ensemble of simulations from the global climate model EC-Earth as input for the NWP model AROME-MetCoOp we are able to change the lateral boundary conditions that result in altered precipitation amounts in two selected catchments. However, the proposed method is computation-consuming, and the results will depend on model configuration choices.

2. **Can the large ensemble data set acquired from SEAS5 give insight on extreme precipitation in Norway (Paper II)?**
   The study demonstrates the possibility of utilizing SEAS5 as a tool for investigating extreme precipitation, both in terms of physical properties for extreme precipitation events and extreme value statistics. We found that two atmospheric circulation patterns are related to extreme value statistics for a region on the west coast of Norway. The two patterns exhibit opposing trends in recent decades, with opposing impacts on the precipitation values.

3. **How can a physical model-based ensemble data set be utilized for estimates with long return periods (Paper III)?**
   The increased sample size attained from the large ensemble data set SEAS5 strongly reduces the confidence interval for return values. In order to accommodate the coarse spatial resolution of SEAS5, the data set is combined with the finer resolution gridded observational data set through a re-parameterization of the GEV distribution.

4. **Are we able to propose a method for estimates of PMP (Paper III)?**
   We are able to propose a method for retrieving robust return values for long return periods. By exploiting a modeling system that is able to produce a large sample size of representative events of the current climate, we are able to obtain a clearer picture of the spatial distribution of the shape parameter, which is decisive for a robust estimate of return levels with long return periods. We are able to make use of the long data series provided by SEAS5 to estimate the tail behavior of the quantile curve with the result that the return values have a much smaller confidence interval than by using the gridded observation data set alone, especially for return values with long return periods. This is an exploratory method and a demonstration of how modeling systems can be exploited in this area of research.

Chapter 5

Discussion and future perspectives

WMO has recommended, if possible, to use physical-based approaches for estimating PMP in areas where orographic enhancement of precipitation is considerable, and the methodology for PMP estimation is currently under scrutiny. Today's methodology for estimating PMP in Norway is the approach developed at NERC and standardized to fit Norwegian conditions. It is highly sensitive to available observation data and in addition influenced by which data points are included, which is a choice made subjectively. While the fit to the GEV distribution also is sensitive to available data, the increased sample size in the methods of Paper II and Paper III ensures a more robust estimate with a smaller confidence interval compared to using e.g. ERA5 or seNorge alone. Estimates of return values with long return periods have previously been extensively extrapolated.

The concept of PMP has been criticized by hydrologists as it assumes a physical upper bound of precipitation amounts possible. At the same time, extreme value theory indicates that this bound does not necessarily exist. This thesis explores alternative methods for PMP estimation and suggests combining a physical model-based prediction system with existing gridded observation data to obtain return values with robust estimates for long return periods. In this way, we utilize the increased sample size derived from a physical model-based product, while at the same time, we account for the finer-scaled spatial variability by combining the data with the gridded observational dataset. This involves a shift from the traditionally deterministic way of regarding the PMP estimate, towards the probabilistic extreme value distribution.

Paper I demonstrated how ensembles from the global climate model EC-Earth can be used as input data for the regional fine scale AROME-MetCoOp for PMP estimation in two selected catchments in Norway. The analysis was inspired by other studies using atmospheric model-based approaches, where PMP is obtained by modifying the initial and boundary conditions of extreme precipitation events (Ohara et al. (2011) and Ishida et al. (2015b)). Often in such studies, moisture availability is increased, usually by setting relative humidity to 100%, air temperature increased, convergent wind fields artificially generated, and initial or boundary conditions are spatially shifted. However, the physical consistency of these approaches has been questioned. The method proposed in Paper I is able to

shift the boundary and initial conditions but with a special focus on a physically consistent methodology. The use of several ensemble members gives an indication of how sensitive an extreme precipitation event caused by an atmospheric river is to shifts in moisture and wind fields. According to X. Chen, Hossain and Leung (2017) model-based methods in the context of PMP estimates have not been widely validated, and their physical basis has not been thoroughly established. The approaches assume that extreme precipitation is more sensitive to the variables that are modified in the simulations. For example, the relative humidity maximization approach assumes that storm magnitude is more responsive to relative humidity levels, while the wind perturbation approach assumes that moisture convergence is more critical to the intensity of a storm. Spatially shifting initial and boundary conditions can be challenging to interpret, as this induces a shift in land surface conditions, resulting in drastic changes in storm characteristics and PMP estimation, especially in regions where surface heterogeneity drives precipitation variability. By using a model-chain, and utilizing both a global climate and a regional scale model, relevant variables are jointly altered in a physically consistent way. Although the study of Paper I showed promising results, it also revealed a high need for computational resources. Perhaps this approach will be more plausible when operational forecast centers build longer archives of ensemble forecasts that can be utilized.

While Paper II had a focus on the large-scale dynamical features connected to extreme precipitation in Norway, it also demonstrated how a modeling system like SEAS5 can be used to generate plausible current climate weather events from the different ensembles and lead times, which allows for robust analysis on physical properties of extreme events, as well as statistical. The study gave insight into trends in atmospheric circulation patterns, over the period 1981-2018, that are connected to precipitation amounts on the west coast of Norway.

In Paper III the same data set is further applied, and together with the gridded observational dataset seNorge, the SEAS5 hindcast is the foundation for estimates of return values with long return periods. The two data sets are combined through a re-parameterization of the GEV distribution with a normalized "growth curve", where the location parameter from seNorge determines the correct level of the curve for short return periods, while the scale and shape parameter is determined by the fit to the SEAS5 data. As an alternative, to ensure appropriate levels of the curve for return values at longer return periods, also the scale parameter is taken from seNorge, while the shape is from SEAS5. We are thus able to make use of the long data series provided by SEAS5 to estimate the tail behavior of the quantile curve with the result that the return values have a much smaller confidence interval than by using the gridded observation data set alone, especially for return values with long return periods. By utilizing the large sample size of representative events in the current climate, a clearer understanding of the shape parameter in the GEV distribution is obtained. This parameter is crucial for a robust estimation of return levels with long return periods, as it strongly affects the tail of the frequency curve. The study in Paper III found a negative shape

parameter in certain regions of Norway, which indicates an upper limit value in the resulting curve. This is particularly noticeable in areas heavily affected by large-scale precipitation processes, as opposed to inland regions where convective precipitation is more significant. The asymptotic form of the curve means that the return levels reach a maximum value. If this is a suitable level for design values such as PMP, depends on the ability of SEAS5 to capture extreme precipitation caused by small-scale processes. In addition, while the coarse spatial resolution of the ensemble data from SEAS5 is taken into account by combining it with seNorge through a re-parameterized version of the GEV distribution, the underlying spatial density of observation stations in the gridded product can affect the results. seNorge is presented on a 1x1 km grid resolution, but the resolution representativeness is perhaps at 10-40 km scale, due to the distance between the in-situ observations used as input data to the spatial interpolation algorithm applied to establish the gridded values (C. Lussana et al. (2019)). The estimates presented in this thesis are therefore thought to be most reliable in areas with high station density, and where the dominating precipitation process is large-scale precipitation, such as the western coastal areas and mainly in the southern parts of Norway. Although there is a large station density in the southeast parts of Norway, the mixture of precipitation processes complicates the parameter estimation in the fit to the GEV. The shape derived from SEAS5 is robust, but due to the fact that the precipitation process is also influenced by convective precipitation, which is parameterized in the atmospheric model, the estimates are more uncertain in these areas. The seNorge dataset fitted to the GEV distribution is in Paper III shown to be influenced by outliers in the underlying data, which makes the uncertainty high in the same places.

Both data sets are fitted to the GEV distribution, for 3-day seasonal maximum precipitation events. A disadvantage of using block maxima is that events that are the highest value for the season (or year), but not in fact an extreme value, are part of the data sample fitted to the GEV. At the same time, if there is more than one extreme during the block length, only the largest is included. By choosing Peak-Over-Threshold (POT) rather than block maxima, this issue can be avoided. When using POT, the data are fitted to the Generalized Pareto distribution and not the GEV (Coles (2001)). For POT the threshold level should be carefully selected, so that it is high enough to apply the Generalised Pareto distribution, but low enough to include as many data points as possible (Maraun and Widmann (2018)). Another disadvantage of POT is the potential clustering of data, which might lead to the inclusion of events that are not independent, which is the reason for choosing block maxima in the present analysis.

A preliminary comparison of the return levels, with a return period of 50 000 years, to the traditionally calculated PMP values indicates that estimates found here are lower, see Figure 5.8 (left panel). The figure shows the fraction between the original PMP and the 50 000 year return value for points in Norway. The 50 000 year return period values are in some places $\frac{1}{3}$ (or less) of the original PMP values. A part of the underestimation can be attributed to the coarse model res-

olution of SEAS5. The topography is heavily smoothed, which gives a reduced orographic effect and as a consequence lower precipitation estimates. Another noticeable feature of the figure is the large spatial variability in the fraction values. The original estimates are point estimates, and as they are sensitive to subjective choices as well as data availability, spatial consistency is not guaranteed, in contrast to the spatially consistent approach presented here. The right panel in Figure 5.8 shows the fraction between the estimates (in the left panel) normalized to the normal precipitation sum for SON, and a more spatial consistent pattern is detectable, indicating that the differences between the estimates are connected to the climatology. Further, it should be noted that the comparison needs to be considered with caution, as the original PMP values are point estimates, and the areal reduction factor is not applied. Exploiting the point-rainfall product for SEAS5 (Hewson and Pillosu (2021)), would make the comparison of existing PMP estimates more straightforward, as they are point estimates, and will be a task for future studies.

The technique proposed here holds great potential, and in future work, it would be natural to combine the large ensemble with other data sets, such as high-resolution reanalysis or hindcasts over Scandinavia (e.g. NORA3 (Haakenstad and Breivik (2022)), CARRA (Schyberg et al. (2020)) and CERRA (Verrelle et al. (2022))), where convection is treated explicitly, for e.g. statistical downscaling of SEAS5, or developing a correction scheme based on the reanalysis. This could provide a source for comparison of the findings presented in this thesis and could also be extended to areas beyond the Norwegian mainland. If operational services build up archives of precipitation analysis (archive of operational EPS reforecasts), this could be utilized as initial conditions for regional NWP models (as the method in Paper I). A more thorough evaluation of the existing PMP estimates, with a comparison of the estimates proposed here, is also warranted. In addition, a discussion on the level of today's estimates is due, as well as whether the concept of PMP serves the needs of end users.

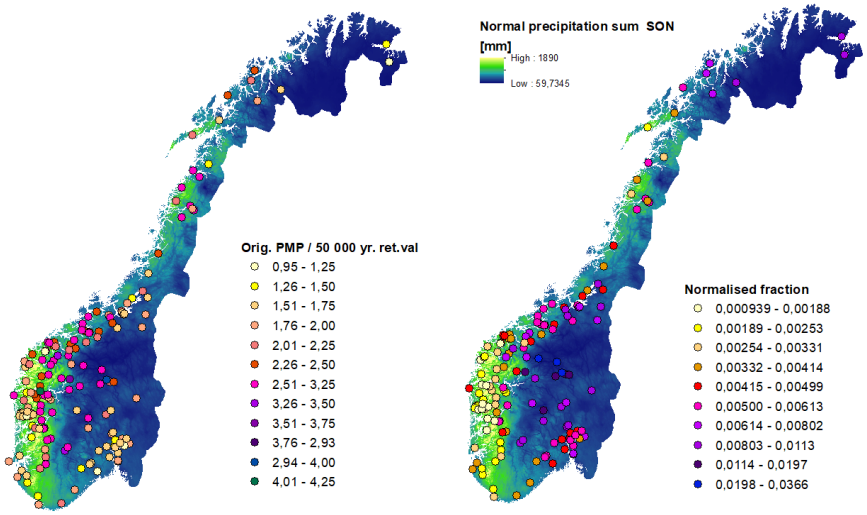

Figure 5.8: *Left panel: A comparison of original PMP estimates and the new estimated return values shown as a fraction between the original PMP and the 50 000 year return value for points in Norway. Both the original PMP values and the return values are for 72 hours duration, in September-October-November. Right panel: The fraction shown in the left panel normalized to the normal seasonal (SON) precipitation sum. The normal period 1991-2020 is used.*

Abbreviations

AR	North Atlantic Ridge
AR	Atmospheric River
ARF	Areal Reduction Factor
AROME	Applications of Research to Operations at Mesoscale
ECMWF	European Centre for Medium-Range Weather Forecast
EOF	Empirical Orthogonal Function
EPS	Ensemble Prediction System
GEV	Generalized Extreme Value Distribution
IDF	Intensity - Duration - Frequency
IFS	Integrated Forecasting System
IVT	Integrated Water Vapour Transport
IWV	Integrated Water Vapour
MEPS	MetCoOp Ensemble Prediction System
NAO	North Atlantic Oscillation
NEMO	Nucleus for European Modelling of the Ocean
NERC	The National Environment Research Council
NWP	Numerical Weather Prediction
PCA	Principal Component Analysis
PMF	Probable Maximum Flood
PMP	Probable Maximum Precipitation
POT	Peak Over Threshold
RCP	Representative Concentration Pathway
SON	September-October-November
SB	Scandinavian Blocking
WMO	World Meteorological Organisation

Bibliography

Alaya, M. A. Ben, F. W. Zwiers and X. Zhang (2020). 'Probable maximum precipitation in a warming climate over North America in CanRCM4 and CRCM5'. In: *Climatic Change* 158 (3-4). ISSN: 15731480. DOI: 10.1007/s10584-019-02591-7.

Azad, Roohollah and Asgeir Sorteberg (2017). 'Extreme daily precipitation in coastal western Norway and the link to atmospheric rivers'. In: *Journal of Geophysical Research: Atmospheres* 122.4, pp. 2080–2095. DOI: 10.1002/2016JD025615. URL: https://agupubs.onlinelibrary.wiley.com/doi/abs/10.1002/2016JD025615.

Bandhauer, Moritz et al. (2022). 'Evaluation of daily precipitation analyses in E-OBS (v19.0e) and ERA5 by comparison to regional high-resolution datasets in European regions'. In: *International Journal of Climatology* 42 (2). ISSN: 10970088. DOI: 10.1002/joc.7269.

Barnston, A. G. and R. E. Livezey (1987). 'Classification, seasonality and persistence of low-frequency atmospheric circulation patterns'. In: *Monthly Weather Review* 115 (6). ISSN: 00270644. DOI: 10.1175/1520-0493(1987)115<1083:CSAPOL>2.0.CO;2.

Benedict, Imme et al. (2019). 'Large-Scale Flow Patterns Associated with Extreme Precipitation and Atmospheric Rivers over Norway'. In: *Monthly Weather Review* 147.4, pp. 1415–1428. DOI: 10.1175/MWR-D-18-0362.1. URL: https://doi.org/10.1175/MWR-D-18-0362.1.

Bengtsson, Lisa et al. (2017). 'The HARMONIE-AROME model configuration in the ALADIN-HIRLAM NWP system'. In: *Monthly Weather Review* 145 (5). ISSN: 15200493. DOI: 10.1175/MWR-D-16-0417.1.

Casagli, N. et al. (2006). 'Analysis of the landslide triggering mechanism during the storm of 20th-21st November 2000, in Northern Tuscany'. In: *Landslides* 3 (1). ISSN: 1612510X. DOI: 10.1007/s10346-005-0007-y.

Chen, D. and Y. Chen (2003). 'Association between winter temperature in China and upper air circulation over East Asia revealed by canonical correlation analysis'. In: *Global and Planetary Change* 37 (3-4). ISSN: 09218181. DOI: 10.1016/s0921-8181(02)00206-0.

Chen, X. and F. Hossain (2018). 'Understanding Model-Based Probable Maximum Precipitation Estimation as a Function of Location and Season from Atmospheric Reanalysis'. In: *Journal of Hydrometeorology* 19.2, pp. 459–475. DOI: 10.1175/JHM-D-17-0170.1. URL: https://doi.org/10.1175/JHM-D-17-0170.1.

Chen, X., F. Hossain and L.R. Leung (2017). 'Probable Maximum Precipitation in the U.S. Pacific Northwest in a Changing Climate'. In: *Water Resources Research* 53 (11). ISSN: 19447973. DOI: 10.1002/2017WR021094.

Choi, Ji-Hyeok et al. (2020). 'Resolving Emerging Issues with Aging Dams under Climate Change Projections'. In: *Journal of Water Resources Planning and Management* 146 (5). ISSN: 0733-9496. DOI: 10.1061/(asce)wr.1943-5452.0001204.

Coles, Stuart (2001). *An introduction to statistical modeling of extreme values*. Springer Series in Statistics. London: Springer-Verlag. ISBN: 1-85233-459-2.

Collins, Matthew et al. (2013). 'Long-term Climate Change: Projections, Commitments and Irreversibility. In: Climate Change 2013: The Physical Science'. In: *Climate Change 2013 the Physical Science Basis: Working Group I Contribution to the Fifth Assessment Report of the Intergovernmental Panel on Climate Change* (January 2014).

Dee, D P et al. (2011). 'The ERA-Interim reanalysis: configuration and performance of the data assimilation system'. In: *Quarterly Journal of the Royal Meteorological Society* 137.656, pp. 553–597. DOI: 10.1002/qj.828. URL: https://rmets.onlinelibrary.wiley.com/doi/abs/10.1002/qj.828.

Dyrrdal, Anita Verpe et al. (2016). 'Estimating extreme areal precipitation in Norway from a gridded dataset'. In: *Hydrological Sciences Journal* 61 (3). ISSN: 21503435. DOI: 10.1080/02626667.2014.947289.

Fabiano, F. et al. (2020). 'Euro-Atlantic weather Regimes in the PRIMAVERA coupled climate simulations: impact of resolution and mean state biases on model performance'. In: *Climate Dynamics* 54 (11-12). ISSN: 14320894. DOI: 10.1007/s00382-020-05271-w.

Fichefet, T. and M. A. Morales Maqueda (1997). 'Sensitivity of a global sea ice model to the treatment of ice thermodynamics and dynamics'. In: *Journal of Geophysical Research: Oceans* 102.C6, pp. 12609–12646. DOI: https://doi.org/10.1029/97JC00480. eprint: https://agupubs.onlinelibrary.wiley.com/doi/pdf/10.1029/97JC00480. URL: https://agupubs.onlinelibrary.wiley.com/doi/abs/10.1029/97JC00480.

Førland, E J (1992a). 'Manual for beregning av påregnelige ekstreme nedbørverdier (in Norwegian)'. In: *DNMI rapport* 92/21.

— (1992b). 'Manual for beregning av påregnelige ekstreme nedbørverdier (in Norwegian)'. In: *DNMI rapport* 92/21.

Frogner, Inger Lise et al. (2019). 'Convection-permitting ensembles: Challenges related to their design and use'. In: *Quarterly Journal of the Royal Meteorological Society* 145 (S1). ISSN: 1477870X. DOI: 10.1002/qj.3525.

Grams, C. M. et al. (Aug. 2017). 'Balancing Europe's wind-power output through spatial deployment informed by weather regimes'. In: *Nature Climate Change* 7.8, pp. 557–562. ISSN: 17586798. DOI: 10.1038/NCLIMATE3338.

Gumbel, E.J. (2004). *Statistics of Extremes*. Dover publications, New York. Unabridged republication of the edition published by Columbia University Press, New York, 1958.

Haakenstad, Hilde and Øyvind Breivik (2022). 'NORA3. Part II: Precipitation and Temperature Statistics in Complex Terrain Modeled with a Nonhydrostatic

Model'. In: *Journal of Applied Meteorology and Climatology* 61 (10). ISSN: 15588432. DOI: 10.1175/jamc-d-22-0005.1.

Haarsma, Reindert J et al. (2013). 'More hurricanes to hit western Europe due to global warming'. In: *Geophysical Research Letters* 40.9, pp. 1783–1788. DOI: 10.1002/grl.50360. URL: https://agupubs.onlinelibrary.wiley.com/doi/abs/10.1002/grl.50360.

Hazeleger, Wilco et al. (2010). 'EC-Earth: A Seamless Earth-System Prediction Approach in Action'. In: *Bulletin of the American Meteorological Society* 91.10, pp. 1357–1364. DOI: 10.1175/2010BAMS2877.1. URL: https://doi.org/10.1175/2010BAMS2877.1.

Hersbach, Hans et al. (2020). 'The ERA5 global reanalysis'. In: *Quarterly Journal of the Royal Meteorological Society* 146 (730). ISSN: 1477870X. DOI: 10.1002/qj.3803.

Hershfield, David M. (1961). 'Estimating the Probable Maximum Precipitation'. In: *Journal of the Hydraulics Division* 87 (5). ISSN: 0044-796X. DOI: 10.1061/jyceaj.0000651.

Hess, P. and H. Brezowsky (1952). *Katalog der Grosswetterlagen Europas. Ber. dt. Wetterdienst in der US-Zone 33*.

Hewson, Timothy David and Fatima Maria Pillosu (2021). 'A low-cost post-processing technique improves weather forecasts around the world'. In: *Communications Earth and Environment* 2 (1). ISSN: 26624435. DOI: 10.1038/s43247-021-00185-9.

Hurrell, James W. et al. (2003). 'An overview of the north atlantic oscillation'. In: *Geophysical Monograph Series*. Wiley-Blackwell Publishing Ltd. ISBN: 9781118669037. DOI: 10.1029/134GM01.

Irannezhad, Masoud et al. (2017). 'Analysing the variability and trends of precipitation extremes in Finland and their connection to atmospheric circulation patterns'. In: *International Journal of Climatology* 37. ISSN: 10970088. DOI: 10.1002/joc.5059.

Ishida, K et al. (2015a). 'Physically Based Estimation of Maximum Precipitation over Three Watersheds in Northern California: Atmospheric Boundary Condition Shifting'. In: *Journal of Hydrologic Engineering* 20.4, p. 4014052. DOI: 10.1061/(ASCE)HE.1943-5584.0001026.

— (2015b). 'Physically Based Estimation of Maximum Precipitation over Three Watersheds in Northern California: Relative Humidity Maximization Method'. In: *Journal of Hydrologic Engineering* 20.10, p. 4015014. DOI: 10.1061/(ASCE)HE.1943-5584.0001175.

Johnson, Stephanie J. et al. (2019). 'SEAS5: The new ECMWF seasonal forecast system'. In: *Geoscientific Model Development* 12.3. ISSN: 19919603. DOI: 10.5194/gmd-12-1087-2019.

Kelder, T. et al. (Dec. 2020). 'Using UNSEEN trends to detect decadal changes in 100-year precipitation extremes'. In: *npj Climate and Atmospheric Science* 3.1. ISSN: 23973722. DOI: 10.1038/s41612-020-00149-4.

Koutsoyiannis, Demetris (1999). 'A probabilistic view of Hershfield's method for estimating probable maximum precipitation'. In: *Water Resources Research* 35 (4). ISSN: 00431397. DOI: 10.1029/1999WR900002.

Kunkel, Kenneth E. et al. (2013). 'Probable maximum precipitation and climate change'. In: *Geophysical Research Letters* 40 (7). ISSN: 00948276. DOI: 10.1002/grl.50334.

Lamb, Hubert Horace (1972). 'British Isles weather types and a register of the daily sequence of circulation patterns 1861-1971'. In.

Lavers, David A. et al. (2011). 'Winter floods in Britain are connected to atmospheric rivers'. In: *Geophysical Research Letters* 38.23. L23803, n/a–n/a. ISSN: 1944-8007. DOI: 10.1029/2011GL049783. URL: http://dx.doi.org/10.1029/2011GL049783.

Lussana, C et al. (2018). 'seNorge2 daily precipitation, an observational gridded dataset over Norway from 1957 to the present day'. In: *Earth System Science Data* 10.1, pp. 235–249. DOI: 10.5194/essd-10-235-2018. URL: https://www.earth-syst-sci-data.net/10/235/2018/.

Lussana, C. et al. (2019). 'SeNorge_2018, daily precipitation, and temperature datasets over Norway'. In: *Earth System Science Data* 11 (4). ISSN: 18663516. DOI: 10.5194/essd-11-1531-2019.

Madec, Gurvan et al. (2017). *NEMO ocean engine*. URL: http://hdl.handle.net/2122/13309.

Maraun, Douglas and Martin Widmann (2018). *Statistical Downscaling and Bias Correction for Climate Research*. DOI: 10.1017/9781107588783.

Michel, Clio et al. (2021). 'Characterization of the atmospheric environment during extreme precipitation events associated with atmospheric rivers in Norway - Seasonal and regional aspects'. In: *Weather and Climate Extremes* 34. ISSN: 22120947. DOI: 10.1016/j.wace.2021.100370.

Micovic, Z, M G Schaefer and G H Taylor (2015). 'Uncertainty analysis for Probalbe Maximum Precipitation estimates'. In: *Journal of Hydrology* 521, pp. 360–373. URL: http://dx.doi.org/10.1016/j.jhydrol.2014.12.033.

Müller, Malte et al. (2017). 'AROME-MetCoOp: A Nordic Convective-Scale Operational Weather Prediction Model'. In: *Weather and Forecasting* 32.2, pp. 609–627. DOI: 10.1175/WAF-D-16-0099.1. URL: https://doi.org/10.1175/WAF-D-16-0099.1.

NERC (1975). *Flood Studies Report, Vol. II*.

Ohara, N et al. (2011). 'Physically Based Estimation of Maximum Precipitation over Three Watersheds in Northern California'. In: *Journal of Hydrologic Engineering* 16.4, pp. 351–361. DOI: 10.1061/(ASCE)HE.1943-5584.0000324.

Papalexiou, Simon Michael and Demetris Koutsoyiannis (2006). 'A probabilistic approach to the concept of Probable Maximum Precipitation'. In: *Advances in Geosciences* 7, pp. 5–54.

Papalexiou, Simon Michael and Alberto Montanari (2019). 'Global and Regional Increase of Precipitation Extremes Under Global Warming'. In: *Water Resources Research* 55.6. ISSN: 19447973. DOI: 10.1029/2018WR024067.

Pasquier, J. T., S. Pfahl and C. M. Grams (2019). 'Modulation of Atmospheric River Occurrence and Associated Precipitation Extremes in the North Atlantic Region by European Weather Regimes'. In: *Geophysical Research Letters* 46 (2). ISSN: 19448007. DOI: 10.1029/2018GL081194.

Payne, Ashley E. et al. (2020). 'Responses and impacts of atmospheric rivers to climate change'. In: *Nature Reviews Earth and Environment* 1 (3). ISSN: 2662138X. DOI: 10.1038/s43017-020-0030-5.

Philipp, Andreas et al. (2010). 'Cost733cat - A database of weather and circulation type classifications'. In: *Physics and Chemistry of the Earth* 35 (9-12). ISSN: 14747065. DOI: 10.1016/j.pce.2009.12.010.

Pinto, Joaquim G. and Christoph C. Raible (2012). 'Past and recent changes in the North Atlantic oscillation'. In: *Wiley Interdisciplinary Reviews: Climate Change* 3 (1). ISSN: 17577799. DOI: 10.1002/wcc.150.

R. G. Owens, T D Hewson (2018). 'ECMWF Forecast User Guide'. In: *ECMWF*. DOI: 10.21957/m1cs7h.

Ragulina, Galina and Trond Reitan (2017). 'Generalized extreme value shape parameter and its nature for extreme precipitation using long time series and the Bayesian approach'. In: *Hydrological Sciences Journal* 62.6, pp. 863–879. DOI: 10.1080/02626667.2016.1260134. eprint: https://doi.org/10.1080/02626667.2016.1260134. URL: https://doi.org/10.1080/02626667.2016.1260134.

Ralph, F. Martin et al. (2006). 'Flooding on California's Russian River: Role of atmospheric rivers'. In: *Geophysical Research Letters* 33.13. L13801, n/a–n/a. ISSN: 1944-8007. DOI: 10.1029/2006GL026689. URL: http://dx.doi.org/10.1029/2006GL026689.

Rastogi, Deeksha et al. (2017). 'Effects of climate change on probable maximum precipitation: A sensitivity study over the Alabama-Coosa-Tallapoosa River Basin'. In: *Journal of Geophysical Research* 122 (9). ISSN: 21562202. DOI: 10.1002/2016JD026001.

Rouhani, H and R Leconte (2016). 'A novel method to estimate the maximization ratio of the Probalbe Maximum Precipitation (PMP using regional climate model output)'. In: *Water Resources Research* 52, pp. 7347–7365. DOI: doi:10.1002/2016WR018603.

Rutz, J.J., W.J. Steenburgh and F.M. Ralph (2014). 'Climatological Characteristics of Atmospheric Rivers and Their Inland Penetration over the Western United States'. In: *Monthly Weather Review* 142 (2), pp. 905–921. DOI: 10.1175/MWR-D-13-00168.1. URL: https://doi.org/10.1175/MWR-D-13-00168.1.

Salas, Jose D. et al. (2014). *Uncertainty of the PMP and PMF*. DOI: 10.1201/b16683.

Sarkar, Subharthi and Rajib Maity (2020). 'Estimation of Probable Maximum Precipitation in the context of climate change'. In: *MethodsX* 7. ISSN: 22150161. DOI: 10.1016/j.mex.2020.100904.

Schaller, Natalie et al. (2020). 'The role of spatial and temporal model resolution in a flood event storyline approach in western Norway'. In: *Weather and Climate Extremes* 29. DOI: https://doi.org/10.1016/j.wace.2020.100259.

Schyberg, H. et al. (2020). 'Arctic regional reanalysis on single levels from 1991 to present.' In: *Copernicus Climate Change Service (C3S) Climate Data Store (CDS)*. DOI: DOI:10.24381/cds.713858f6.

Seity, Y et al. (2011). 'The AROME-France Convective-Scale Operational Model'. In: *Monthly Weather Review* 139.3, pp. 976–991. DOI: 10.1175/2010MWR3425.1. URL: https://doi.org/10.1175/2010MWR3425.1.

Sodemann, H and A Stohl (2013). 'Moisture Origin and Meridional Transport in Atmospheric Rivers and Their Association with Multiple Cyclones'. In: *Monthly Weather Review* 141.8, pp. 2850–2868. DOI: 10.1175/MWR-D-12-00256.1. eprint: http://dx.doi.org/10.1175/MWR-D-12-00256.1. URL: http://dx.doi.org/10.1175/MWR-D-12-00256.1.

Stohl, A., C. Forster and H. Sodemann (2008). 'Remote sources of water vapor forming precipitation on the Norwegian west coast at 60°N–a tale of hurricanes and an atmospheric river'. In: *Journal of Geophysical Research: Atmospheres* 113.D5. D05102, n/a–n/a. ISSN: 2156-2202. DOI: 10.1029/2007JD009006. URL: http://dx.doi.org/10.1029/2007JD009006.

Thuy, Le Thi Thanh, Seiki Kawagoe and Ranjan Sarukkalige (2019). 'Estimation of probable maximum precipitation at three provinces in Northeast Vietnam using historical data and future climate change scenarios'. In: *Journal of Hydrology: Regional Studies* 23. ISSN: 22145818. DOI: 10.1016/j.ejrh.2019.100599.

Toride, Kinya et al. (2019). 'Model-based Probable Maximum Precipitation estimation: How to estimate the worst-case scenario induced by atmospheric rivers?' In: *Journal of Hydrometeorology* 20.12, pp. 2383–2400. DOI: 10.1175/JHM-D-19-0039.1. URL: https://doi.org/10.1175/JHM-D-19-0039.1.

Trenberth, K. E. et al. (2003). 'The changing character of precipitation'. In: *Bull. Amer. Meteor. Soc.* 84, pp. 1205–1217.

Tveito, O. E. (2021). 'Norwegian standard climate normals 1991-2020 - the methodological approach'. In: *Report no. 05/2021* (05).

Verrelle, A. et al. (2022). 'CERRA-Land sub-daily regional reanalysis data for Europe from 1984 to present.' In: *Copernicus Climate Change Service (C3S) Climate Data Store (CDS).* DOI: DOI:10.24381/cds.a7f3cd0b.

Vormoor, K. et al. (2015). 'Climate change impacts on the seasonality and generation processes of floods - Projections and uncertainties for catchments with mixed snowmelt/rainfall regimes'. In: *Hydrology and Earth System Sciences* 19 (2). ISSN: 16077938. DOI: 10.5194/hess-19-913-2015.

Williams, David John (2021). *Lessons from tailings dam failures—where to go from here?* DOI: 10.3390/min11080853.

WMO (2009). 'Manual for Estimation of Probable Maximum Precipitation, 3rd edition, WMO - No. 1045, Geneva, ISBN 978-92-63-11045-9'. In: *World Meteorological Organization.*

Wolff, M. A. et al. (2015). 'Derivation of a new continuous adjustment function for correcting wind-induced loss of solid precipitation: Results of a Norwegian field study'. In: *Hydrology and Earth System Sciences* 19 (2). ISSN: 16077938. DOI: 10.5194/hess-19-951-2015.

Zhu, Yong and Reginald E. Newell (1998). 'A Proposed Algorithm for Moisture Fluxes from Atmospheric Rivers'. In: *Monthly Weather Review* 126.3, pp. 725–735.

Zuo, Hao et al. (Aug. 2018). *OCEAN5: The ECMWF Ocean Reanalysis System and its Real-Time analysis component*. DOI: 10.21957/la2v0442. URL: https://www.ecmwf.int/node/18519.

Part II

Papers

Paper I

Changing Lateral Boundary Conditions for Probable Maximum Precipitation Studies: A Physically Consistent Approach

Changing Lateral Boundary Conditions for Probable Maximum Precipitation Studies: A Physically Consistent Approach

KARIANNE ØDEMARK,[a,b] MALTE MÜLLER,[a,b] AND OLE EINAR TVEITO[a]

[a] *Norwegian Meteorological Institute, Oslo, Norway*
[b] *Department of Geosciences, University of Oslo, Norway*

(Manuscript received 12 March 2020, in final form 17 September 2020)

ABSTRACT: This article presents a conceptual study toward establishing a new method for altering lateral boundary conditions in numerical model based estimates for probable maximum precipitation (PMP). We altered an extreme event in a physically and dynamically consistent way in a regional convective-scale weather prediction model (AROME-MetCoOp) by applying fields from a global ensemble climate model approach based on EC-EARTH. Ten ensemble members are downscaled with the regional model, which results in 10 different realizations of an extreme precipitation event for the west coast of Norway. We show how the position and orientation of the moisture flow is different between the individual ensemble members, which leads to relatively large changes in precipitation values for a selected catchment. For example, the modification of the moisture transport on scales of several hundred kilometers impacts the extreme precipitation amount by about 75% among the model members. Compared with historical rainfall records, precipitation changes of 62% and 71% are found for two selected catchments. Although the present study is restricted to one particular extreme event that is modified 10 times with the ensemble approach, there is a considerable spread of the moisture transport compared to the spread of the moisture transport of extreme precipitation events of the past 40 years. We conclude that the described approach is a step toward a new method to derive PMP values for a given catchment; however, a larger amount of events and larger ensembles would have to be considered to estimate PMP values.

KEYWORDS: Extreme events; Precipitation; Numerical analysis/modeling; Numerical weather prediction/forecasting; Reanalysis data

1. Introduction

When designing water management infrastructure, such as dams, an assessment of the theoretically maximum probable precipitation (PMP) is necessary. PMP is defined as "the greatest depth of precipitation for a given duration meteorologically possible for a given size storm area at a particular location at a particular time of year, with no allowance made for long-time climatic trends." (WMO 2009). So far, the "moisture maximization of extreme rainstorm observations" approach has been widely applied to estimate PMP. However, recent studies highlight some underlying deficiencies with the method, the results are influenced by subjective judgments of method for moisture maximization and the availability of atmospheric moisture measurements (Micovic et al. 2015). At the Norwegian Meteorological Institute (MET Norway), a standardized statistical approach based on the NERC method is used to estimate PMP (NERC 1975; Førland 1992). This approach is also vulnerable to subjective choices that strongly can affect the PMP estimates. This is in particular the case for areas where access to observations is limited.

The concept of PMP itself has recently been debated, and there are arguments that the upper limit of precipitation cannot be specified in a deterministic way (Papalexiou and Koutsoyiannis 2006; Micovic et al. 2015; Rouhani and Leconte 2016). Ben Alaya et al. (2018) points out the difference between theoretical and operational PMP. The theoretical PMP is an unknown upper limit for precipitation, whereas operational PMP is a rational engineering solution, meaning not purely based on scientific knowledge, to provide a possible magnitude of extreme precipitation values. Hence, whether the theoretical upper limit exists or not, an operational PMP can be obtained by engineers to provide guidance for design decisions. It is important that the theoretically physical upper limit is not confused with the rational concept, as it reduces its credibility and usefulness (Klemeš 1993). When deciding on operational PMP values, the best possible knowledge should be used. The most recent World Meteorological Organization manual for estimation of PMP (WMO 2009) recommends to apply physically based atmospheric models, especially for areas where orographic precipitation is significant. A number of studies have investigated the use of numerical weather prediction models (NWPs) for PMP estimation (Ohara et al. 2011; Ishida et al. 2015a,b). Ohara et al. (2011) studied PMP for a catchment in California and applied a regional-scale high-resolution physical atmospheric model. Other studies have also applied NWP-based methods to estimate PMP, where the approach is based on physical maximization of a historical extreme rainstorm. Ishida et al. (2015a) alters boundary and initial conditions to maximize precipitation over targeted catchments. Chen and Hossain (2018) pointed out that there seems to have emerged a consensus that using a physical numerical model is the way ahead for a new PMP methodology, but that there is lacking a consensus on how to physically "maximize" the historical storms within numerical models for PMP estimation. Maximizing relative humidity is often

Denotes content that is immediately available upon publication as open access.

Corresponding author: Karianne Ødemark, karianneo@met.no

DOI: 10.1175/JHM-D-20-0070.1

applied, though the question is how large effect this will give when the humidity in a historical extreme precipitation event is quite high already. Toride et al. (2019) points out that systematically saturation of all boundaries potentially introduces disturbances to the fields beyond what is realistic. In addition, a sudden change at the boundaries of the model domain can induce physical and dynamical inconsistencies.

Chen and Hossain (2018) found that there are different dominant parameters that control the storms at different locations across the continental United States. This study found that in some regions moisture availability together with vertical wind are the factors controlling the precipitation outcome, while in other regions instability controls the magnitude of the storm. The most successful approach for maximizing precipitation is by altering the parameters that will lead to the largest effect on precipitation values. A necessity is thus to know what type of atmospheric conditions lead to extreme precipitation in the area of interest.

In Norway, and in western Norway in particular, extreme precipitation is often strongly connected to atmospheric rivers (ARs) (Azad and Sorteberg 2017; Benedict et al. 2019). ARs are long, narrow patches of high vapor transport. The direction and location of the AR constrains which part of an area receives the highest amount of precipitation (Rutz et al. 2014). Ishida et al. (2015a) changed the boundary conditions in a numerical prediction model in order to place an AR to hit the selected watershed, and, in turn, increasing the amount of precipitation over the watershed.

While Ishida et al. (2015a) focused on a watershed in California, and several of the aforementioned studies are focused on numerical based methods for estimating PMP for regions in the United States, there are not yet any studies on the subject for Norway. The argument for using NWP models to estimate PMP is especially valid in areas with complex orography (WMO 2009), and the west coast of Norway has a steep topography with mountainous areas and long fjords along the coast. The largest extreme precipitation events, which are connected to the large-scale moisture flow across the Atlantic Ocean are found in western Norway (Azad and Sorteberg 2017), which is the focus area in the present study.

In the present study, we discuss an alternative method to change the boundary conditions, with emphasis on making the numerical based approach physically consistent. The aim is to make a framework with a coherent physical set up for manipulating the initial and boundary conditions. The approach utilizes synthetic events, with the advantage that we are not bound by historical events. We use a model chain, where data from a global climate model (EC-EARTH; Hazeleger et al. 2010) is applied as input to a regional weather prediction model (AROME-MetCoOp; Müller et al. 2017) in order to resolve the spatial characteristics of catchments at the Norwegian west coast. For a specific extreme precipitation event in a present-day climate simulation with EC-Earth a set of 10 perturbed ensemble members are produced and further downscaled with AROME-MetCoOp. Hence, the boundary conditions for the regional model are changed and the location of the maximum moisture flow is altered. The perturbation of the input data produces 10 ensemble members that can be considered as 10 possible realizations of a weather situation that can result in an extreme precipitation event. The realizations are starting from nearly the same atmospheric state and are equally likely. The resulting precipitation at two selected catchments are evaluated and put in context with the larger-scale differences between the ensemble members and their spread with respect to extreme events which occurred between 1981 and 2018, in order to describe what setups are conducive for the highest precipitation values.

2. Data and methods

The global climate model EC-Earth has been used to produce a dataset with 30 years of model data for present climate. The simulation was done with EC-Earth v2.3 (Hazeleger et al. 2010) with a horizontal resolution of ~25 km and 91 vertical hybrid levels (T799 L91). The 30 years of simulation were constructed by six independent members spanning 5 years (2002–06). The approach for generating a dataset with ensemble members that can be considered to be independent is described in Haarsma et al. (2013). Observed greenhouse gas and aerosol concentrations were used, together with a daily satellite product for sea surface temperature.

From the 30 years of simulations, the event identified by highest daily precipitation values over a constraint area in western Norway (57.1°–63.2°N and 2.6°–9.3°N) was selected for further study. For this event an ensemble of 10 members was established. The ensemble was constructed by stochastically perturbing the model physics tendencies (SPTT) 5 days ahead of the event, which is similar to the method used for the operational ensemble weather forecast at European Centre for Medium-Range Weather Forecasts (ECMWF; Owens and Hewson 2018). Only the lateral initial and boundary conditions are changed and the surface forcing is kept constant. Surface forcing, as SST changes, are important for extreme precipitation; however, this study is focused on changes in lateral initial and boundary conditions. Each perturbation will represent a plausible realization of a possible extreme precipitation event over the Norwegian west coast. See Schaller et al. (2020) for more details on the model setup.

Although the spatial resolution of the global climate model is considered high in comparison with state-of-the-art climate model, it is still too coarse to properly resolve the kilometer-scale orographic effects important for catchment-scale precipitation estimates. To study precipitation on catchment scale a regional weather forecast model (AROME-MetCoOp; Müller et al. 2017) was used to downscale the 10 ensemble members. It is based on AROME (Applications of Research to Operations at Mesoscale; Seity et al. 2011), a non-hydrostatic atmospheric model system used operationally at the Norwegian Meteorological Institute. It is run with the standard operational domain for Scandinavia, AROME-MetCoOp, covering the entirety of Norway, as well as Sweden, Denmark, and Finland. The horizontal resolution is 2.5 km, on a 750 × 960 grid, with 65 vertical layers. The simulations are initialized by the EC-Earth fields 36 h before the extreme event and are forced by EC-Earth fields at the lateral and upper boundaries.

AROME-MetCoOp's ability to predict precipitation is documented in Müller et al. (2017), where forecast skills compared with the global ECMWFs Integrated Forecasting System (IFS) showed that AROME-MetCoOp clearly adds value to the forecast product for both precipitation and temperature. Since March 2014 when AROME-MetCoOp became the operational model at MET Norway it has been tuned and adapted to the specifications of our Nordic model domain, and as such it is the preferred choice of model to simulate precipitation in Norway. It permits convection, though the focus of this study is related to large-scale advective precipitation. The high horizontal resolution gives a good representation of the terrain and how it influences the spatial precipitation distribution. For the 10 members downscaled with AROME-MetCoOp, we have analyzed precipitation in two selected catchments, as well as the moisture flow at larger scales.

To compare the modeled precipitation values and in situ observations, we have retrieved observations and model data for an event with heavy precipitation (see Fig. A1 in the appendix). Daily accumulation values from three stations in the vicinity of each of the catchments are used. The event from 2013 is from the very beginning of the operational setup of AROME-MetCoOp. In this event the model underestimates precipitation compared with the observed values. For the event in 2016, the model values are comparable to the observed precipitation values. This is an example of the models ability to estimate high precipitation values, but it should be interpreted carefully. To say something conclusive about the model prediction ability, there is a need to validate the model over more than two single cases by the use of skill scores and other suitable parameters. This was done in Müller et al. (2017), and they showed that for an extreme precipitation event in 2014 and in the same area as the catchments studied here (west coast of Norway) the model performed well.

So far, the main approaches discussed in the literature to maximize precipitation with numerical models, are either to increase relative humidity, shift the boundary conditions in space, or a combination of the two (Ohara et al. 2011; Ishida et al. 2015a,b). When shifting boundary conditions the main goal is to make a historical rainstorm hit over a targeted area. To estimate the highest possible precipitation values over a catchment, the location of vapor flux is decisive.

Figure 1 shows the vertically integrated water vapor transport (IVT) corresponding to an AR simulated by EC-Earth. A detailed description of the representation of ARs in EC-Earth is given in Whan et al. (2020), where they show that the simulation of AR frequency and intensity in EC-Earth is comparable to ERA-Interim. A further evaluation of EC-Earth's ability to represent extreme IVT in the North Atlantic area has been performed in Hegdahl et al. (2020). They found that the 98th percentile of the IVT in EC-Earth is similar to ERA-Interim, which confirms that results from EC-Earth can be used to identify atmospheric rivers.

Traditional PMP values are calculated for the two catchments by the current standard method at MET Norway (Førland 1992), a statistical approach based on the NERC method (NERC 1975). The precipitation values from the

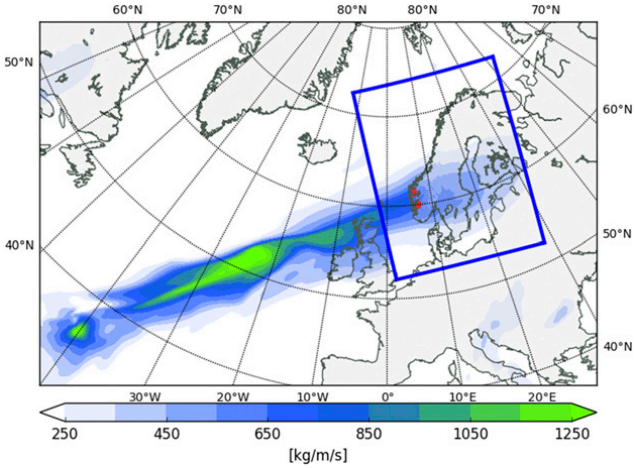

FIG. 1. Daily mean IVT simulated in EC-Earth for one of the ensemble members. Inside of the blue box, which represents the domain of AROME-MetCoOp, the displayed IVT values are from the regional model. The two red dots indicate where the two catchments used in the present study are located.

model ensemble are compared with the statistical PMP, as well as observations and return values from relevant stations in MET Norway's station network. The return values are obtained from a fit to a generalized extreme value (GEV) distribution. The GEV is fitted to peak over threshold (POT) values from the observation series, where the 99.5th percentile threshold is used. The estimates have been calculated using the extRemes package in R (Gilleland and Katz 2016).

The IVT values in the ensemble are put in context with extreme events which occurred between 1980 and 2018. Observations of precipitation from six stations in and around the two catchments were used to select events where the daily precipitation amount exceeds the 99.5 percentile value. Data from 1980 through 2018 are used for each station. For the stations in Jølstra the 99.5th percentile values are 66.5, 49.1, and 58.2 mm, while for the stations located near Opo the values are 50.0, 76.9, and 47.0 mm. Only the dates that have precipitation values above the threshold and at the same time cooccur for all three stations in the group are used further. At the observation sites precipitation is measured from 0600 UTC one day to 0600 UTC the next day, so it is likely that most of the precipitation fell on the first of these two dates, but is registered on the last. Therefore, IVT from the day before the precipitation date is retrieved from ERA5 (Hersbach et al. 2018). ERA5 is the recently released reanalysis product from ECMWF, which comes with a finer spatial and temporal (hourly) resolution, uses a more advanced assimilation system, and includes more sources of observational data than the previous reanalysis product, ERA-Interim (Dee et al. 2011). For each extreme precipitation event selected for the two catchments the IVT pattern from ERA5 is analyzed and compared to the AROME-MetCoOp ensemble.

In the next section, the results in terms of precipitation amounts, of catchment averages and gridpoint values, of the position and direction of the IVT, and of the realism of the IVT

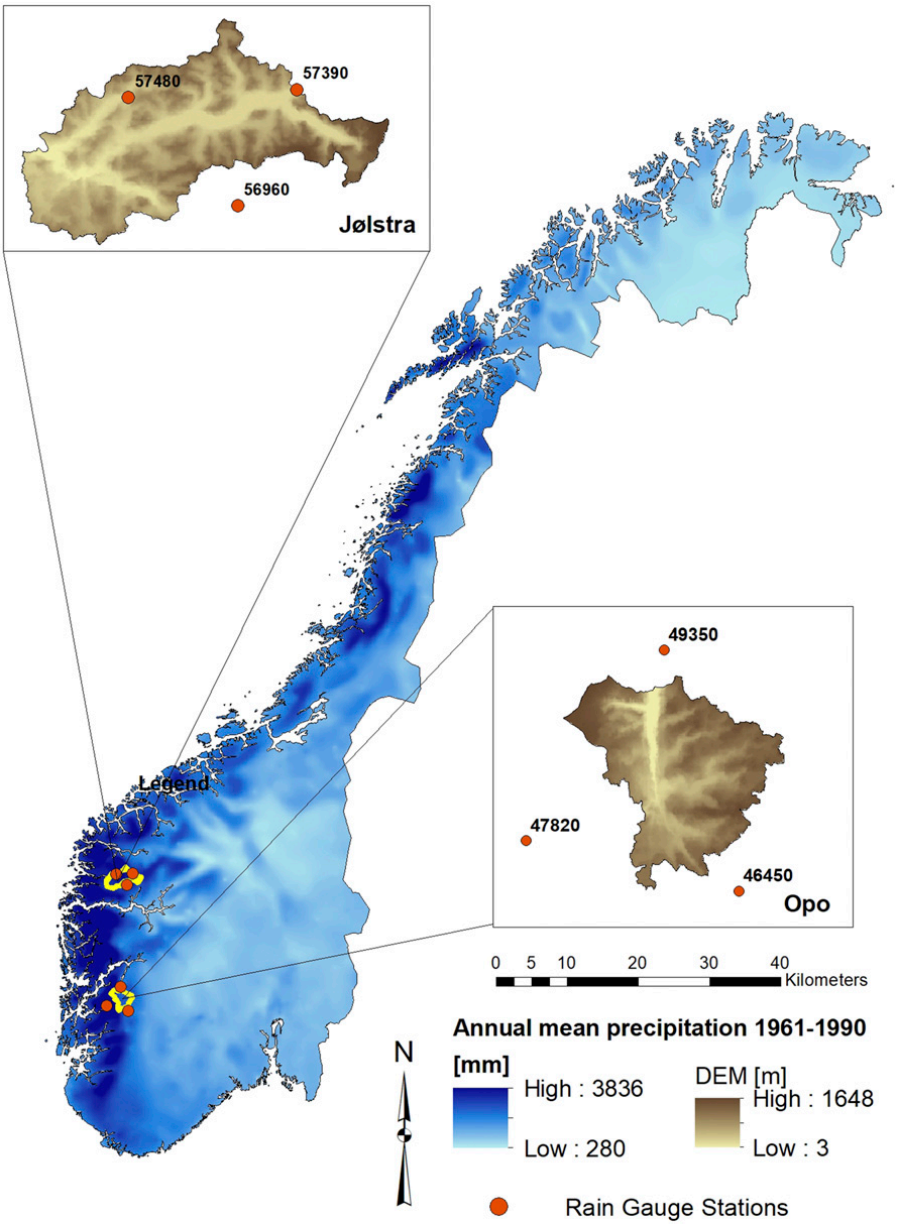

FIG. 2. Map over Norway showing annual mean precipitation and the location of the two selected catchments, Jølstra and Opo. Rain gauge stations used are indicated with orange dots. The boxes show the topography within the catchments. The annual mean precipitation is for the reference period 1961–90 (Lussana et al. 2018).

in the model ensemble are compared to historical extremes and presented in detail.

3. Results

Although all of the 10 ensemble members have the same synoptic structure, the perturbations result in variations of the IVT which in turn change the local-scale precipitation values. In the following, we will focus on the connection between the large-scale IVT changes close to the boundary of the regional model and the precipitation amounts in the two catchments Jølstra and Opo. These catchments are located in the western part of Norway (Fig. 2) and have catchment areas of 717 and 362 km^2, respectively. The distance between the catchments are about 180 km and they are both located in regions with complex mountainous topography. They are therefore representative for areas that are strongly impacted by AR induced precipitation extremes.

Precipitation stations in and near the Jøstra catchment have annual mean precipitation amounts ranging from 1630 to 2666 mm (annual total, the 1961–90 reference period is used). The catchments elevation ranges from 0 m MSL at the outlet to 1648 m MSL as the highest elevation, and 43% of the catchment is categorized as bare mountain while 31% is categorized

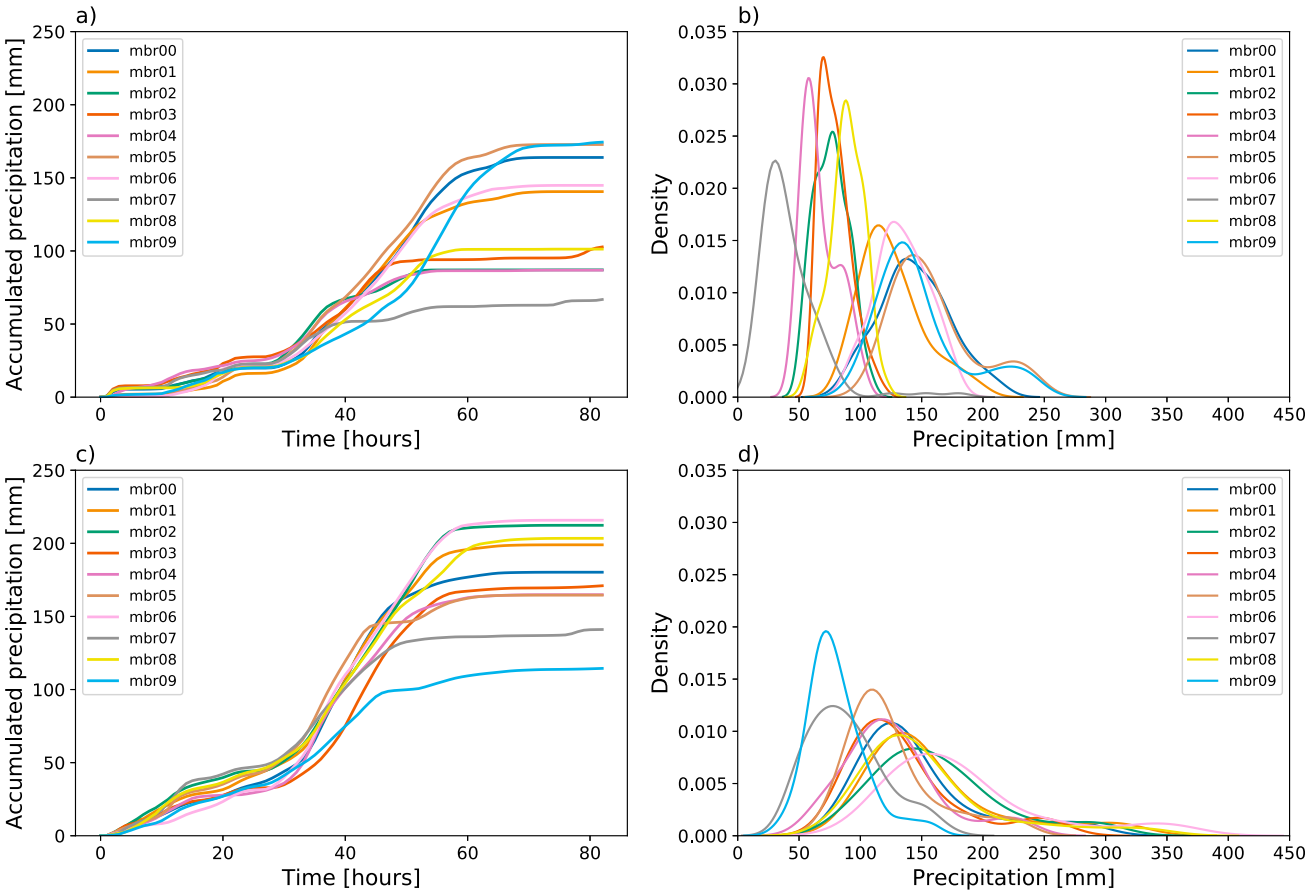

FIG. 3. Accumulated precipitation (area average) in the two catchments, (a) Jølstra and (c) Opo, and probability density distribution of the accumulation for all grid boxes within the catchments [(b) Jølstra and (d) Opo] for all ensemble members in the AROME-MetCoOp simulation. The gridbox values are accumulated over 48 h (during the 48 h with largest accumulation).

as forest. Observation stations in the vicinity of the Opo catchment have mean annual totals ranging from 1628 to 2685 mm. Opo is also a mountain catchment with 66% categorized as bare mountain and 20% forest. Its lowest point is 88 m MSL, and the highest is 1635 m MSL. See the inset figures in Fig. 2 for an elevation model of the two catchments and the mean annual precipitation in the map of Norway in the same figure.

Analyzing the evolution of accumulated precipitation (catchment average) for Jølstra and Opo in the AROME-MetCoOp simulations reveals that some of the ensemble members have significant different accumulated precipitation values (Figs. 3a,c). In Jølstra (Fig. 3a), most of the members have highest precipitation accumulation during the second and third day of the model run (between hours 30 and 60), after which the accumulation stops, except member 9 which has a different timing than the others. The members with highest precipitation accumulation (members 5 and 9) have about 75 mm higher precipitation than in the two lowest (members 2 and 4), while in Opo (Fig. 3c) the members with highest and lowest precipitation values have a difference of about 100 mm.

Area averages can conceal the large variations of precipitation values over an area and one single gridpoint value is not likely to represent the catchment wide rainfall. In Figs. 3b and 3d, 48-h accumulated precipitation values in all the grid boxes within the catchments are shown. Accumulated values of 247 and 241 mm can be found in Jølstra for two of the members and values above 300 mm for several of the members in Opo, with 364 mm as the highest value. For 24-h accumulation, the maximum amounts are 183 mm for Jølstra and 203 mm for Opo (not shown).

Daily accumulation in historical rainfall events for stations in the vicinity of the catchments show that the 24-h accumulation in the ensemble members are producing precipitation well above what is recorded (Fig. 4). The maximum model value for Jølstra is 62% higher than the highest recorded rainfall, for Opo the model maximum is 71% higher than the highest recorded rainfall.

Compared to PMP values calculated with MET Norway's standardized statistical method, accumulated values from the model are somewhat lower. In Table 1 PMP estimates are given for 24, 48, and 72 h for Jølstra and Opo. For accumulation over 48 h (Figs. 3b,d), the highest values are around 250 mm in the model (for Jølstra), while the original PMP value is 470 mm. For 24 h the model has an accumulation of 183 mm, while the PMP is 360 mm. For both durations the model results are about 50% of the statistically derived PMP. For Opo the model values are closer to the statistical PMP, here the 24-h

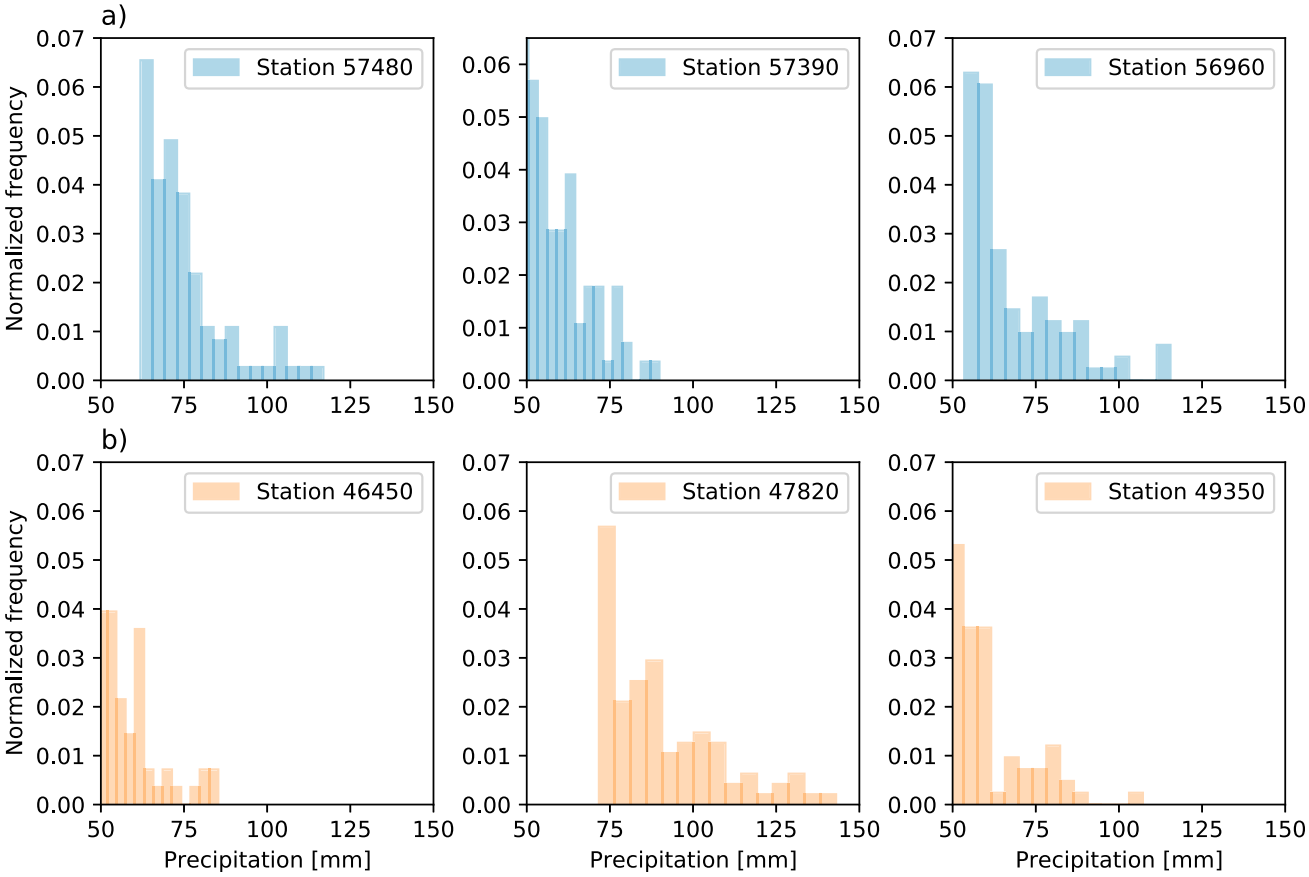

FIG. 4. Historical rainfall records for the 100 highest 24-h events selected from the station's entire time series, for observation stations near the (a) Jølstra and (b) Opo catchments.

model value is about 60% of the original PMP, and the 48-h value is 78%. The return values obtained from a fit to a generalized extreme value (GEV) distribution for the same six stations as in Fig. 4 are shown in Fig. 5. For 24-h precipitation the model results have return periods laying between a couple of thousand years and on the order of 10^4 years. For the longest return periods in the figure the values must be read with caution, as the confidence intervals are very large, but still interesting as a way to put the model results and original PMP in context.

To understand what is causing the differences in precipitation amounts between the AROME-MetCoOp members, the IVT location and magnitude is shown in Figs. 6 and 7, where the left panels in Fig. 6 show the IVT during the time with largest precipitation accumulation. The map shows the orientation of the IVT and displays where the strongest vapor transport is positioned and, thus, which coastal area is targeted. The right panels of the figure give more detail of the AR's position and its evolution in time. In Fig. 7 cross sections upstream and close to each of the two catchments are used to show the IVT magnitude and its progression in time near the catchments. Looking at the three ensemble members in Fig. 6, the AR is located farther north in member 9 and it hits the Jølstra catchment more directly. The ARs in members 4 and 6 are located south of this catchment, which corresponds to member 9 producing the most precipitation here. For catchments average values, member 9 produces the most in Jølstra with 175 mm, while members 4 and 6 have around 90 and 145 mm (Fig. 3). For Opo, member 9 produces the least (around 115 mm) and member 6 produces the highest values (220 mm).

In the right panels in Fig. 6 the temporal evolution with latitude is given, which shows that the IVT in member 9 indeed is stronger just north of 60°N, while members 4 and 6 are located just south of 60°N. This is confirmed by looking at the IVT magnitude just upstream of the Jølstra catchment (Fig. 7), where member 9 has a higher magnitude than the other members, and the duration with such high values extends longer than in the others members. For Opo, the difference in the location of the AR is not as pronounced. IVT magnitude just upstream of the catchment shows that the member producing the highest accumulated precipitation is similar to the IVT values in the member producing least precipitation. This suggest that there are additional factors that cause differences in precipitation amounts. The catchment is smaller, and it

TABLE 1. PMP values for Jølstra and Opo calculated by MET Norway's standard statistical method.

Catchment	24 h	48 h	72 h
Jølstra PMP (mm)	360	470	560
Opo PMP (mm)	355	465	550

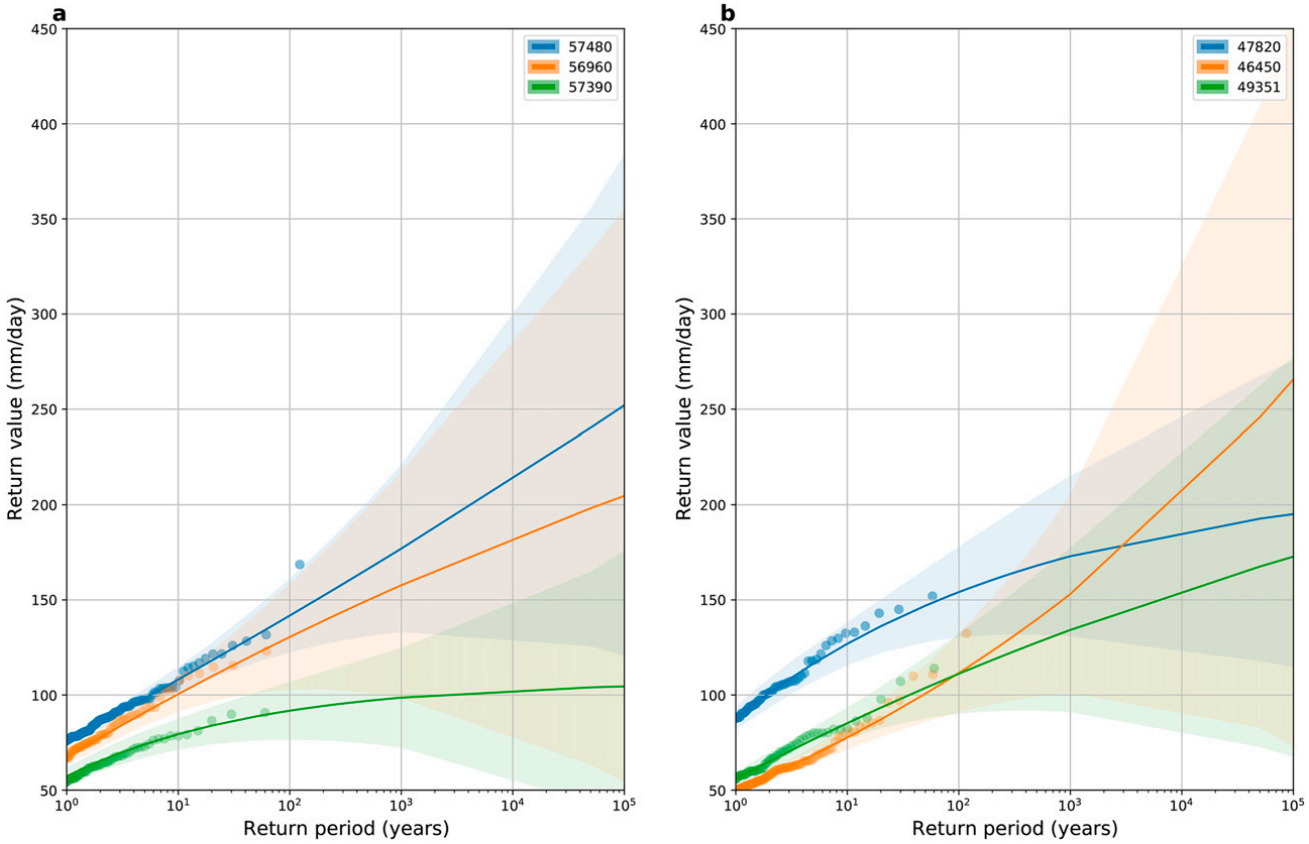

FIG. 5. Generalized extreme value distribution for three observation stations in (a) the area near the Jølstra catchment and (b) near the Opo catchment.

might be more sensitive to local orographic effects. When looking closer at the surface wind patterns during the time where the accumulation is greatest, the wind in member 6 turns to a more (steep) southwesterly direction than member 9 does (not shown). This can explain the precipitation amount in the member, which has a more preferable wind direction for producing precipitation. The catchment is situated downstream of a southwest–northeast-oriented fjord (Åkrafjorden).

Among all the members in the ensemble the distance between the ARs are not more than 270 km. The AR located farthest south is at the southern tip of Norway, and the AR located farthest north is near the point farthest west in Norway. For Jølstra this results in a change in accumulated precipitation of about 75% for the member that has the AR more directly toward the catchment's location compared to the member with the AR not as favorable located. Thus, with this approach it is possible to shift the boundary conditions and, in turn, impact the areas which receive most precipitation. In general, the IVT of the ensemble members shows shifts of the AR location, as well as (in some members) the direction of the moisture flow, which has an impact of the resulting precipitation.

To better understand the limitations of our approach, due to the choice of one particular extreme event, we compare the IVT of the AROME-MetCoOp ensemble members with historical (1981–2018) extreme events (above the 99.5% threshold) which occurred in the two catchments (Figs. 8 and 9). The composite map in Fig. 8 reveals that the moisture transport is located farther north in the events occurring in the catchment here (Fig. 8a), while there are higher IVT values in the events occurring in the catchment farthest south (Fig. 8b). Although the spatial spread of the IVT in the AROME-MetCoOp ensemble is as large as several hundred kilometers, it is still somewhat smaller than the one of the historical extreme events. The magnitude of extreme IVT, however, is consistent with the historical one (Fig. 9).

4. Discussion and outlook

One of the advantages of using numerical models for estimating PMP is the capability of producing data in areas where the observation network is limited. This ensures a complete spatial coverage, and the level of detail is determined by the spatial resolution of the model. The model simulations have to be sufficiently long, in order to get time series for a robust detection of events with return periods on the order of hundreds of years, which makes the computational cost high. To estimate PMP, which at least should exceed a return period on the order of 10 000–40 000 years (O. E. Tveito, MET Norway, 2020, personal communication), the magnitude of computational cost will make the task unrealistic in practice. A way to work around this is to select only the most extreme precipitation events and simulate these, as done in literature as well as in this study. The main approaches to maximize precipitation with numerical models are either to increase relative humidity, shift the boundary conditions in space, or a combination of the two. When

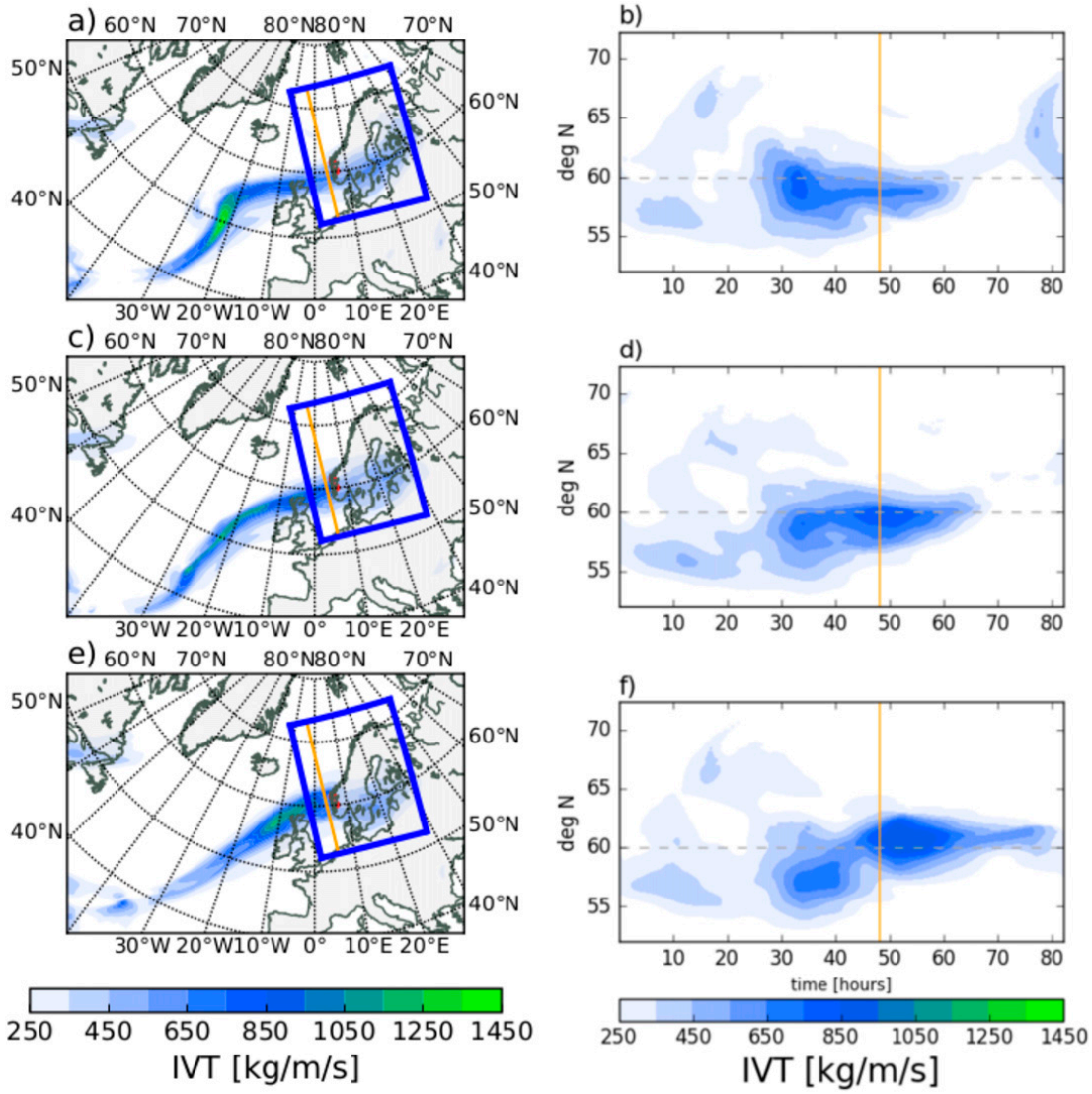

FIG. 6. Snapshot of IVT in EC-Earth ensemble (a) member 4, (c) member 6, and (e) member 9. The AROME-MetCoOp domain is shown by the blue box in the figures on the left, and the orange line shows the cross section for the Hovmöller diagrams on the right. The Hovmöller diagrams show IVT in EC-Earth ensemble (b) member 4, (d) member 6, and (f) member 9. The orange line in the Hovmöller diagrams indicate the time of the snapshot of IVT in the left panels, and the dashed gray line indicates the 60°N latitude.

shifting boundary conditions the goal is to make a historical rainstorm hit over a targeted area. To estimate the highest possible precipitation values over a catchment, the location of vapor flux is decisive. The approach presented here is to utilize a global climate model, which produces a 30-yr present-day climate simulation and to select the most extreme precipitation event. This event is perturbed and 10 different ensemble members of the extreme event are downscaled with a regional weather prediction model. Thus, we have 10 different alterations of the lateral initial and boundary conditions for the regional model runs, which in turn provides 10 different realizations of an extreme precipitation event. Alteration of the initial and boundary conditions are done in a physically and dynamically consistent way.

In the present study we performed a detailed analysis on the effect of the large-scale modification of the IVT on the precipitation on catchment scale. Two catchments are selected, which are frequently impacted by AR induced extreme precipitation events and are embedded in the complex topography of western Norway. For one of the catchments we find that the AR is shifted by about 270 km, which has a downstream impact on the amount of precipitation by about 75%. For the other catchment, the main reason for a change of precipitation is not the translation of the AR, but the change in direction of the main vapor transport.

The two catchments are situated in complex terrain and, while this region in Norway is the wettest part of the country, local differences exist. This is illustrated by Fig. 5 where the generalized extreme value distributions for two of the stations in each catchment area are shown. In particular, one of the stations in Opo (Fig. 5b) shows a strikingly different distribution than the other

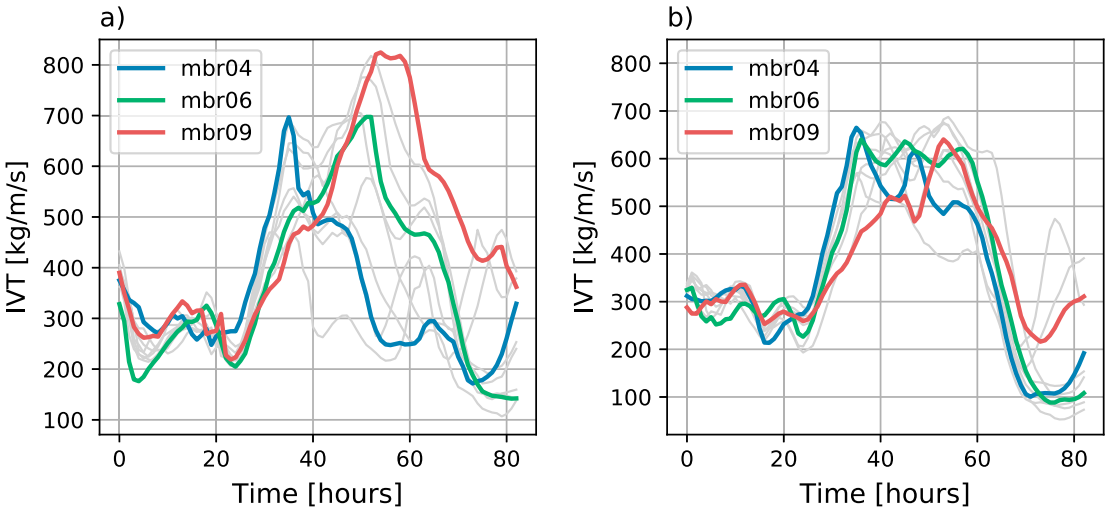

FIG. 7. IVT in AROME-MetCoOp upstream of the two catchments, (a) Jølstra and (b) Opo. The evolution of IVT in time is shown along a 7.5-km-long cross section located west of the corresponding catchment.

two, even though they are located only 25 km apart. Compared with statistically derived PMP estimates the model results are lower, but return periods on the order of 10^4 years are reached.

The comparison with ERA5 reanalysis data shows that the models are capturing the IVT extremes and that the different ensemble members cover partly the range of IVT extremes observed in the past 40 years. This is especially true for the northernmost catchment, where the AROME-MetCoOp well matches IVT values from the past events farther away from the west coast of Norway. For the other catchment, the ARs in the ensemble are not targeting the catchment as successful. The event detection in the very first step of the model chain selected events from daily precipitation covering all of the west coast. In further studies this step should be refined and the event detection could be done on a more local scale.

Here, we have demonstrated the use of a method that is not bounded to the relatively short history of observed events, but utilizes a model chain to create physically consistent synthetic events and is giving reasonable results. However, estimating PMP values takes more than the highest value out of 10 ensemble members, and the approach presented here is to be regarded as a step toward a comprehensive method. The suggested approach will modify the boundary and initial conditions in a physical and dynamical way ensuring the physics to remain realistic.

We conclude that the described approach can be used as a method to alter the initial and boundary conditions in order to derive PMP values for a given catchment. To ensure that the model setup for estimating PMP is done in the most physically realistic manner, there is a need to investigate how alterations of one rainfall event changes the precipitation pattern over selected catchments. We can show that small changes in position and orientation of the moisture flow, induced by the ensemble approach, lead to relative large changes in precipitation values.

Our study has a specific focus on the large-scale precipitation events caused by ARs and orographic precipitation,

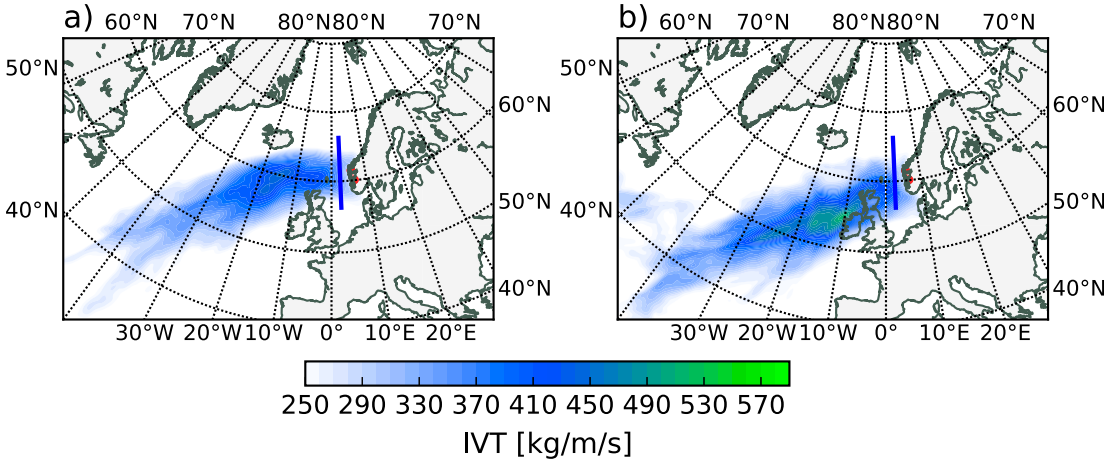

FIG. 8. Map of IVT composite from the events with precipitation above the 99.5% threshold from the stations in the (a) Jølstra area and (b) Opo area. Data are taken from the ERA5 reanalysis dataset. The blue line indicates the cross section used in Fig. 9.

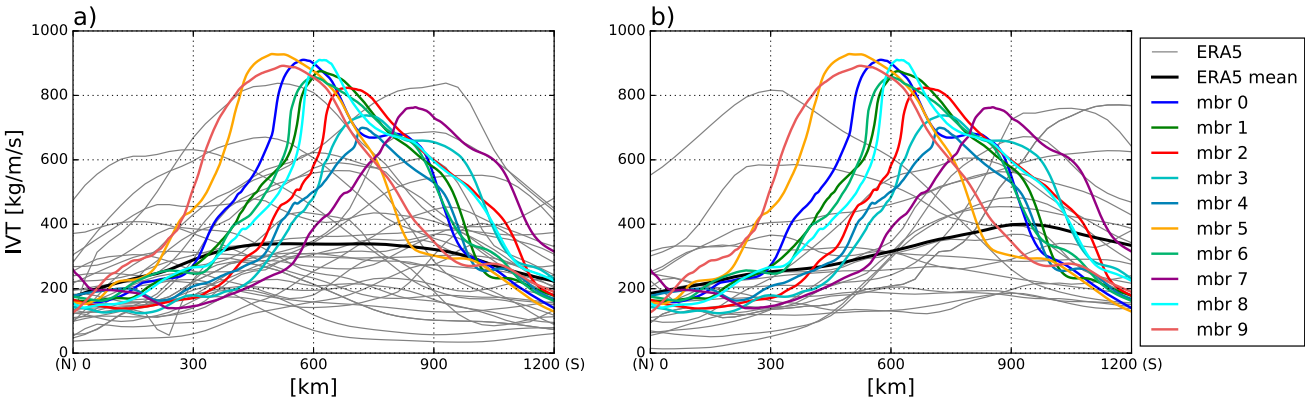

FIG. 9. IVT in ERA5 along the cross section given by the blue line in Fig. 8, for the same events (gray thin lines). The thick gray line shows the mean IVT in the events. The colored lines show the IVT values in the AROME-MetCoOp ensemble.

which is the major mechanism for extreme precipitation at the Norwegian west coast. Convective events producing heavy precipitation are neglected although, farther inland convective events can cause extreme precipitation amounts that result in damages to infrastructure with severe consequences for society. This has not been the focus in this study, nevertheless, the model in use is a convection permitting model, and has the ability to be applied in a convective historical storm.

PMP estimates are, together with snowmelt, input parameters for watershed models when estimating probable maximum flood (PMF). In this framework, the determination of precipitation phase is important. The aim of the study presented in this paper is to investigate if the ensemble approach can be an alternative to the physically more inconsistent artificial manipulations of initial and boundary conditions in the NWP model, and not in the detail of precipitation phase, though that would be needed in the determination of PMF.

In general, in order to utilize an ensemble approach for the estimation of PMP more of the most extreme precipitation events would have to be resimulated. To meet these challenges with realistic computational costs, a possible approach could be to utilize already established ensembles from numerical seasonal or weather forecasting systems. Multiyear hindcast datasets of seasonal prediction systems are available; their different ensemble members can provide for a valuable extreme event dataset. From this dataset there is a possibility to find the most extreme precipitation events and to downscale to catchments of interest. This is a proposed outlook that should be explored, and if it is found feasible, it has the potential to cover catchments for larger areas than in this case study.

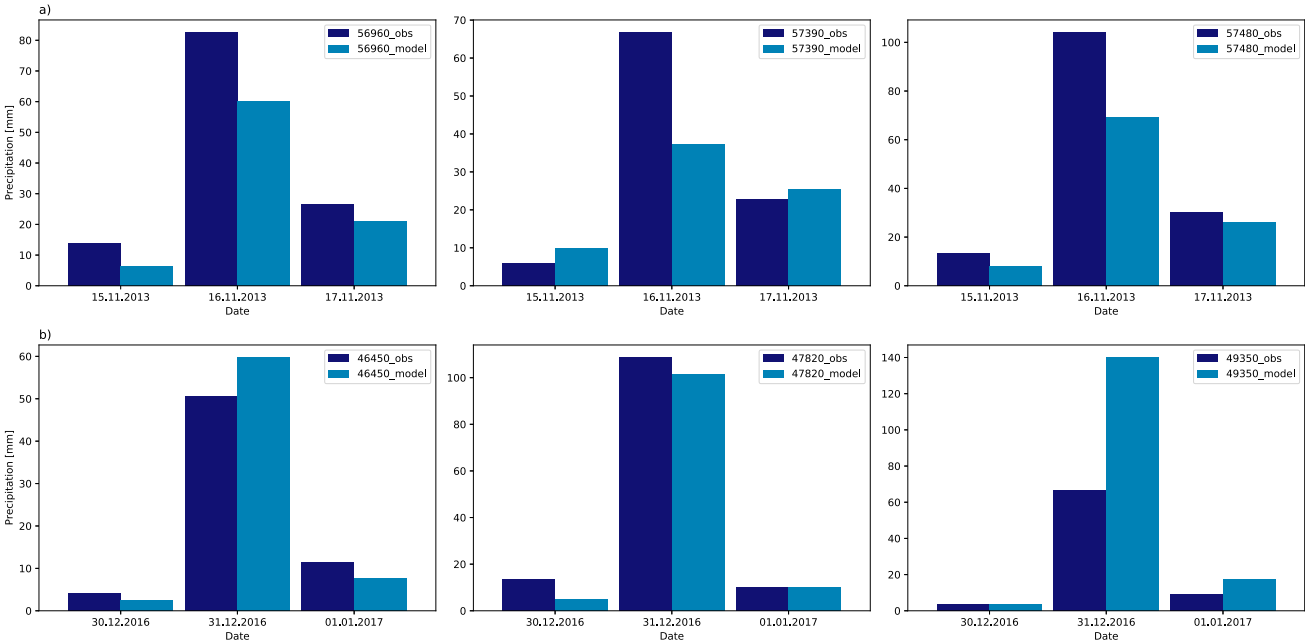

FIG. A1. Comparison of precipitation values from AROME-MetCoOp and observations from three stations near (a) the Jølstra catchment and (b) the Opo catchment from two extreme precipitation events. Daily accumulated values are shown over three days. The observations are done from 0600 to 0600 UTC, and the model values are calculated over the same time period.

Acknowledgments. The study is supported by the Norwegian Research Council and Energi Norge through the project FlomQ (NFR-235710/E20). MM has received support from the project TWEX (NFR-255037) funded through the Norwegian Research Council. We acknowledge the TWEX project team for providing the model simulations, and we are thankful for discussions with this group, especially Jana Sillmann and Nathalie Schaller. We are also thankful for helpful discussions with Thordis L. Thorarinsdottir and Morten A. Ø. Køltzow.

APPENDIX

Comparison of AROME-MetCoOp and Observations

A comparison of precipitation values from AROME-MetCoOp and observations from three stations near the Jølstra and Opo catchment from two extreme precipitation events is shown in Fig. A1.

REFERENCES

Azad, R., and A. Sorteberg, 2017: Extreme daily precipitation in coastal western Norway and the link to atmospheric rivers. *J. Geophys. Res. Atmos.*, **122**, 2080–2095, https://doi.org/10.1002/2016JD025615.

Ben Alaya, M. A., F. Zwiers, and X. Zhang, 2018: Probable maximum precipitation: Its estimation and uncertainty quantification using bivariate extreme value analysis. *J. Hydrometeor.*, **19**, 679–694, https://doi.org/10.1175/JHM-D-17-0110.1.

Benedict, I., K. Ødemark, T. Nipen, and R. Moore, 2019: Large-scale flow patterns associated with extreme precipitation and atmospheric rivers over Norway. *Mon. Wea. Rev.*, **147**, 1415–1428, https://doi.org/10.1175/MWR-D-18-0362.1.

Chen, X., and F. Hossain, 2018: Understanding model-based probable maximum precipitation estimation as a function of location and season from atmospheric reanalysis. *J. Hydrometeor.*, **19**, 459–475, https://doi.org/10.1175/JHM-D-17-0170.1.

Dee, D. P., and Coauthors, 2011: The ERA-Interim reanalysis: Configuration and performance of the data assimilation system. *Quart. J. Roy. Meteor. Soc.*, **137**, 553–597, https://doi.org/10.1002/qj.828.

Førland, E. J., 1992: Manual for beregning av påregnelige ekstreme nedbørverdier (in Norwegian). DNMI Rep. 21/92, 44pp.

Gilleland, E., and R. Katz, 2016: Extremes 2.0: An extreme value analysis package in R. *J. Stat. Software*, **72**, 1–39, https://doi.org/10.18637/jss.v072.i08.

Haarsma, R. J., W. Hazeleger, C. Severijns, H. de Vries, A. Sterl, R. Bintanja, G. J. van Oldenborgh, and H. W. van den Brink, 2013: More hurricanes to hit western Europe due to global warming. *Geophys. Res. Lett.*, **40**, 1783–1788, https://doi.org/10.1002/grl.50360.

Hazeleger, W., and Coauthors, 2010: EC-Earth: A seamless Earth-system prediction approach in action. *Bull. Amer. Meteor. Soc.*, **91**, 1357–1364, https://doi.org/10.1175/2010BAMS2877.1.

Hegdahl, T. J., K. Engeland, M. Müller, and J. Sillmann, 2020: An event-based approach to explore selected present and future atmospheric river–induced floods in western Norway. *J. Hydrometeor.*, **21**, 2003–2021, https://doi.org/10.1175/JHM-D-19-0071.1.

Hersbach, H., and Coauthors, 2018: Operational global reanalysis: Progress, future directions and synergies with NWP. ERA Rep. Series 27, 63 pp., https://www.ecmwf.int/sites/default/files/elibrary/2018/18765-operational-global-reanalysis-progress-future-directions-and-synergies-nwp.pdf.

Ishida, K., M. L. Kavvas, S. Jang, Z. Q. Chen, N. Ohara, and M. L. Anderson, 2015a: Physically based estimation of maximum precipitation over three watersheds in Northern California: Atmospheric boundary condition shifting. *J. Hydrol. Eng.*, **20**, 04014052, https://doi.org/10.1061/(ASCE)HE.1943-5584.0001026.

——, ——, ——, ——, ——, and ——, 2015b: Physically based estimation of maximum precipitation over three watersheds in Northern California: Relative humidity maximization method. *J. Hydrol. Eng.*, **20**, 04015014, https://doi.org/10.1061/(ASCE)HE.1943-5584.0001175.

Klemeš, V., 1993: Probability of extreme hydrometeorological events - a different approach. *IAHS Publ.*, **213**, 167–176.

Lussana, C., T. Saloranta, T. Skaugen, J. Magnusson, O. E. Tveito, and J. Andersen, 2018: seNorge2 daily precipitation, an observational gridded dataset over Norway from 1957 to the present day. *Earth Syst. Sci. Data*, **10**, 235–249, https://doi.org/10.5194/essd-10-235-2018.

Micovic, Z., M. G. Schaefer, and G. H. Taylor, 2015: Uncertainty analysis for probable maximum precipitation estimates. *J. Hydrol.*, **521**, 360–373, http://doi.org/10.1016/j.jhydrol.2014.12.033.

Müller, M., and Coauthors, 2017: AROME-MetCoOp: A Nordic convective-scale operational weather prediction model. *Wea. Forecasting*, **32**, 609–627, https://doi.org/10.1175/WAF-D-16-0099.1.

NERC, 1975: *Meteorological Studies*. Vol. II, *Flood Studies Report*, National Environmental Research Council, 91 pp.

Ohara, N., M. L. Kavvas, S. Kure, Z. Q. Chen, S. Jang, and E. Tan, 2011: Physically based estimation of maximum precipitation over American River Watershed, California. *J. Hydrol. Eng.*, **16**, 351–361, https://doi.org/10.1061/(ASCE)HE.1943-5584.0000324.

Owens, R. G., and T. Hewson, 2018: ECMWF forecast user guide. ECMWF, https://doi.org/10.21957/m1cs7h.

Papalexiou, S. M., and D. Koutsoyiannis, 2006: A probabilistic to the concept of Probable Maximum Precipitation. *Adv. Geosci.*, **7**, 51–54, https://doi.org/10.5194/adgeo-7-51-2006.

Rouhani, H., and R. Leconte, 2016: A novel method to estimate the maximization ratio of the Probable Maximum Precipitation (PMP) using regional climate model output. *Water Resour. Res.*, **52**, 7347–7365, https://doi.org/10.1002/2016WR018603.

Rutz, J. J., W. J. Steenburgh, and F. M. Ralph, 2014: Climatological characteristics of atmospheric rivers and their inland penetration over the western United States. *Mon. Wea. Rev.*, **142**, 905–921, https://doi.org/10.1175/MWR-D-13-00168.1.

Schaller, N., and Coauthors, 2020: The role of spatial and temporal model resolution in a flood event storyline approach in western Norway. *Wea. Climate Extremes.*, **29**, 100259, https://doi.org/10.1016/j.wace.2020.100259.

Seity, Y., 2011: The AROME-France convective-scale operational model. *Mon. Wea. Rev.*, **139**, 976–991, https://doi.org/10.1175/2010MWR3425.1.

Toride, K., 2019: Model-based probable maximum precipitation estimation: How to estimate the worst-case scenario induced by atmospheric rivers? *J. Hydrometeor.*, **20**, 2383–2400, https://doi.org/10.1175/JHM-D-19-0039.1.

Whan, K., J. Sillmann, N. Schaller, and R. Haarsma, 2020: Future changes in atmospheric rivers and extreme precipitation in Norway. *Climate Dyn.*, **54**, 2071–2084, https://doi.org/10.1007/s00382-019-05099-z.

WMO, 2009: Manual on estimation of probable maximum precipitation (PMP). Tech. Rep. WMO-1045, 257 pp., http://www.wmo.int/pages/prog/hwrp/publications/PMP/WMO%201045%20en.pdf.

Paper II

Recent changes in circulation patterns and their opposing impact on extreme precipitation at the west coast of Norway

Weather and Climate Extremes 39 (2023) 100530

Contents lists available at ScienceDirect

Weather and Climate Extremes

journal homepage: www.elsevier.com/locate/wace

Recent changes in circulation patterns and their opposing impact on extreme precipitation at the west coast of Norway

Karianne Ødemark [a,b,*], Malte Müller [a,b], Cyril Palerme [a], Ole Einar Tveito [a]

[a] Norwegian Meteorological Institute, Oslo, Norway
[b] Department of Geosciences, University of Oslo, Norway

ARTICLE INFO

Keywords:
Extreme precipitation
Circulation patterns
Ensemble data set
Trends

ABSTRACT

Understanding recent and future changes of extreme precipitation is essential for climate change adaptation. Here, we use 3800 extreme precipitation events produced by an ensemble seasonal prediction system. The ensemble represents the climate from 1981 to 2018 and we analyse 3-day maximum precipitation events in September–October–November for the west coast of Norway. Two dominant atmospheric patterns, described by an empirical orthogonal function (EOF) analysis, are related to the results of the extreme value statistics. The principal components of the second and third mode of EOFs have significant trends over the last 40 years, but with an opposing impact on the return values of extreme precipitation. This explains the observed stationarity of extreme precipitation over recent decades at the west coast of Norway, which was also found in previous studies. The second mode of EOFs also shows a relation to the sea-ice coverage in the Barents and Kara Seas, which suggests a connection between the decline of sea-ice to the changes in the atmospheric pattern.

1. Introduction

Extreme precipitation events can lead to excess surface water and floods and are becoming an amplifying societal cost as a result of urbanization and our warming climate. A warmer climate will lead to an increase in the intensity (Boucher et al., 2013; Kharin et al., 2013; Fischer and Knutti, 2016) as well as the frequency (Fischer and Knutti, 2016; Papalexiou and Montanari, 2019) of the heaviest precipitation events. For example, for each additional degree Celcius of the global temperature, the most intense precipitation events which are observed today will likely occur twice as often (Myhre et al., 2019). Detailed knowledge about extreme precipitation events is important for advanced predictions on weather-to-climate time scales. When determining the climatic estimates which critical infrastructures are designed after, it is crucial to understand potential risks caused by extreme weather, so the constructions will endure the strain caused by current and future climate.

For statistical analysis of extreme precipitation events long time series are required, which is a major challenge when using observational or reanalysis data. Kelder et al. (2020) have demonstrated how an ensemble hindcast data set from a seasonal prediction system can be utilized to retrieve a large number of plausible weather event realizations. In their case, a 3800 year long data set was constructed to study extreme precipitation in the period from 1981 to 2018. They showed that by using this large ensemble the confidence intervals for the extreme value distribution are considerably smaller than by using data from a reanalysis only. Hence, the increased number of events by a factor of 100, provides the opportunity to significantly reduce uncertainties in the statistical analysis, and in turn, to improve design values, especially for values with high return periods.

In addition, these large ensemble data sets give us the opportunity to investigate different physical drivers for high impact weather events and can potentially improve our understanding of the relation between extreme precipitation with other dynamical components in the coupled Earth's system, such as atmospheric weather patterns, sea-ice variability, or land- and ocean-surface conditions.

Precipitation in Norway is to a large extent dominated by the large-scale atmospheric circulation (Azad and Sorteberg, 2017) which in turn is driven by the Earth's energy balance through complex processes. There has been tremendous effort on understanding connections between atmospheric circulation and various drivers of the coupled Earth's system (Vihma, 2014; Bintanja et al., 2020). The poleward shift in the North Atlantic storm track can through deviations in strength and location of cyclones lead to changes in regional climate (Wickström et al., 2020). There is still no consensus of the dominant mechanism causing the shift, and several mechanisms may act in parallel (Tamarin-Brodsky and Kaspi, 2017). Reductions of sea-ice and snow cover is a part of a complex climate system feedback, that together with

* Corresponding author at: Norwegian Meteorological Institute, Oslo, Norway.
E-mail address: karianneo@met.no (K. Ødemark).

https://doi.org/10.1016/j.wace.2022.100530
Received 16 November 2021; Received in revised form 9 November 2022; Accepted 18 November 2022
Available online 23 November 2022

changes in atmospheric and ocean circulation can change the energy balance (Serreze and Barry, 2011). Several studies connect changes in mid-latitude weather to changes in atmospheric circulation caused by the decreasing sea-ice coverage in the Arctic (Screen, 2017; Kolstad and Screen, 2019). The changes in atmospheric circulation seen is found to be dependent on the geographical region of sea-ice loss. Specifically, Sun et al. (2015) found that sea ice loss in the Atlantic sector caused a weakening of the upper-level westerly winds, whereas sea ice loss in the Pacific sector caused a strengthening. Other studies highlight ocean variability as an important mechanism (Sato et al., 2014; Tokinaga et al., 2017). Some skepticism about the importance of sea-ice in driving mid-latitude weather extremes has been expressed (Blackport et al., 2019), however, the comprehensive study performed in the Polar Amplification Model Intercomparison Project's (PAMIP) (Smith et al., 2019) contribution to the sixth Coupled Model Intercomparison Project (CMIP6) (Eyring et al., 2016) find that simulations from 16 models show a weakening of mid-latitude tropospheric westerly winds in response to projected Arctic sea ice loss (Smith et al., 2022). The modelled response is robust among the models, but the response is weak relative to inter-annual variability.

Weather regimes favourable for precipitation extremes in the North Atlantic Region are dominated by negative geopotential height anomalies that enhances extratropical cyclone activity as described in Pasquier et al. (2019). These regimes are associated with higher than normal frequencies of Atmospheric Rivers (ARs), which are narrow filaments of high water vapour transport. More than 90% of the meridional water vapour transport in midlatitudes is located in these narrow, elongated regions related to warm conveyor belts within the warm sector of extratropical cyclones (Zhu and Newell, 1998) . While being responsible for the majority of water vapour transport polewards, ARs cover less than 10% of the area of the globe (Gimeno et al., 2014). They transport water at volumetric flow rates similar to those of the world's largest rivers. Landfalling atmospheric rivers cause heavy rainfall and potentially flooding, especially where the flow of moist air is lifted orographically in areas with steep topography. In the past decades, the awareness of landfalling ARs and their association with extreme precipitation in Norway has increased dramatically. Stohl et al. (2008) and Sodemann and Stohl (2013) provide evidence for the important connection between moisture transport and high impact Norwegian weather. Stohl et al. (2008) show that the extreme weather event "Kristin" in September 2005 was indeed an atmospheric river with a large flux of warm moist air detectable across the North Atlantic. When impinging upon the mountainous area in southwest Norway the AR created an extreme precipitation event followed by flooding and landslides and caused a considerable infrastructure damage and loss of human life. While Stohl et al. (2008) described one particular event, Benedict et al. (2019) found that more than 85% of extreme precipitation events on the west coast of Norway during the cold season are connected to ARs. However, extreme precipitation amounts are not linearly linked to the strength and intensity of the AR, but local conditions are important factors influencing precipitation amounts (Ødemark et al., 2020; Michel et al., 2021). The southern west coast of Norway is the wettest region in the country, where the annual precipitation can exceed 3000 mm. The annual precipitation in this region shows an increasing trend (Kuya et al., 2021). However, there are inter-seasonal variations. For the fall season, which is the focus in the present study, no trend is found. Further, Kelder et al. (2020) analysed variability in precipitation in autumn at the west coast of Norway and found no trend in extreme precipitation for this period.

A critical factor determining the intensity of precipitation is the flow direction of the moisture transport, as it is most efficient when hitting the mountain range at an perpendicular angle (Michel et al., 2021). The complex terrain on the Norwegian coast is characterized by intricate fjords adjacent to steep mountains, which can give rise to very local weather and climate conditions due to the direction of the moisture flow (Ødemark et al., 2020), which in turn is controlled by the large-scale atmospheric circulation. Michel et al. (2021) give a broad overview of the characteristics of the atmospheric environment during extreme precipitation events in Norway, with both regional and seasonal aspects. This study investigates how dominant long-term and large-scale atmospheric patterns relate to extreme precipitation events in Norway. Several studies have examined the connection between the probability of extreme events to changes in atmospheric circulation (Francis and Vavrus, 2012; Coumou et al., 2014; Horton et al., 2015). An increase in the occurrence or persistence of high-amplitude wave patterns is expected to alter the likelihood of extreme events. Francis and Vavrus (2012) describes how a slower progression of upper-level waves associated with Arctic amplification would cause mid-latitude weather patterns to be more persistent, which may lead to an increased probability of extreme weather events, such as drought, flooding, cold spells, and heat waves.

A special emphasis in this study is to investigate whether there are dominant long-term atmospheric weather patterns that are conducive for extreme precipitation events, and further whether there are changes in these patterns over time. In the present study, a sample of 3800 extreme precipitation events, following the method in Kelder et al. (2020), and the related mean seasonal atmospheric states obtained from a hindcast data set of a seasonal forecasting system is analysed. This gives us the opportunity to study the interconnections and changes of the occurrence of extreme precipitation with dominant seasonal atmospheric weather patterns over the last 40 years. In the following section the SEAS5 seasonal prediction system (Johnson et al., 2019) and the method for constructing the combined data set are described in more detail together with the method for analysing dominant long term atmospheric patterns. In Section 3 we elaborate on the results and a discussion and conclusions follow in Section 4.

2. Data and method

In this study we utilize a 25 member ensemble hindcast data set of the European Centre for Medium-Range Weather Forecast's (ECMWF's) seasonal prediction system SEAS5. SEAS5 is a coupled atmosphere–ice–ocean model with a horizontal resolution of around 35 km. SEAS5's atmospheric component is based on cycle 43r1 of the ECMWF-Integrated Forecasting System (IFS) (ECMWF, 2016). The spectral horizontal resolution is T319 and there are 91 vertical layers. The NEMO ocean model (Nucleus for European Modelling of the Ocean, Madec et al. (2017)) and LIM2 sea-ice model (Louvian-la-Neuve Sea Ice Model, Fichefet and Maqueda (1997)) are coupled to the atmospheric system, and have a horizontal resolution of 0.25-degrees. The atmospheric and ocean-ice model systems are initialized by the ERA-Interim (Dee et al., 2011) and OCEAN5 reanalysis (Zuo et al., 2018), respectively.

The ensemble members are generated from perturbations to the ocean and atmosphere initial conditions and from stochastic model perturbations. The SEAS5 hindcast consists of 25 members initiated monthly, and each member spans over 7 months for the years 1981 to present. In this study we use the hindcast data from 1981 to 2018.

The members of individual ensemble forecasts need to be independent for the statistical analysis of extreme precipitation. Because of the chaotic nature of the atmospheric system, we assume that precipitation events are not predictable more than a few weeks in advance and, thus, the first month of the model run is discarded to avoid dependent events. It can be argued that due to the slowly varying components of the atmosphere–ocean system, extreme precipitation events might cluster beyond the discarded first month of the model run. However, Kelder et al. (2020) showed that when removing the first month of the ensemble members they can be considered to represent independent extreme precipitation events.

In the present study we analyse the fall season (September, October and November; SON), and, thus 4 initialization months (May, June, July, August) which span over the SON months are used. This yields 100 seasonal weather realizations for each year between 1981 and

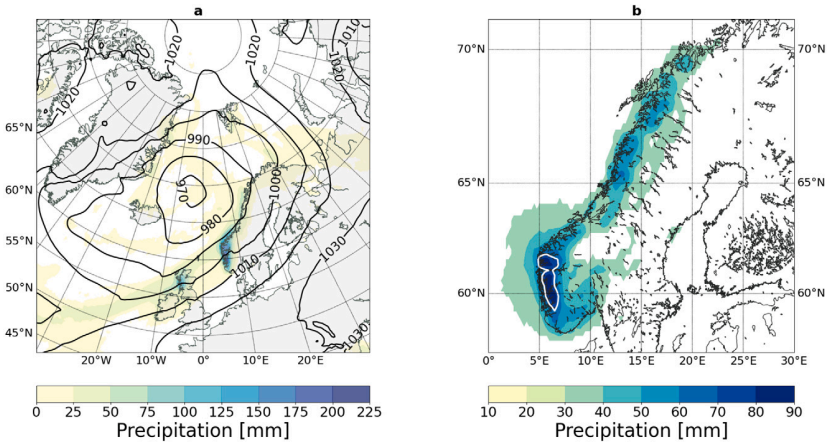

Fig. 1. **a** The synoptic situation during the extreme precipitation event 26–28 October 2014. Contours show MSLP October 26th at 12:00 UTC and precipitation values are accumulated from 26th 00:00 UTC to 29th 00:00 UTC. **b** The 98th percentile of 3-day precipitation in SON, data taken from ERA5. The white contour line indicates the chosen study region, defined by the area where the 98th percentile of the 3-day precipitation in ERA5 exceeds 70 mm.

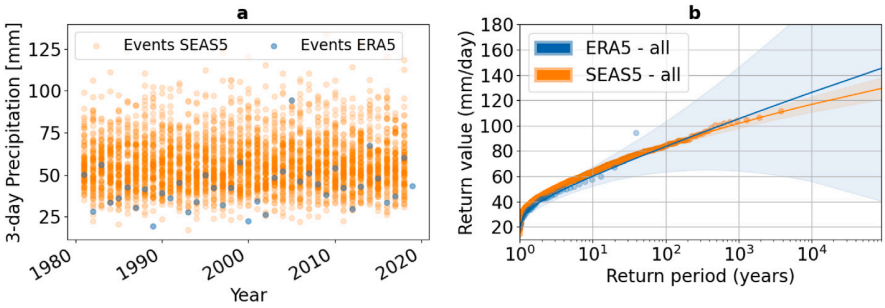

Fig. 2. **a** All seasonal max 3-day precipitation events retrieved from SEAS5 (orange dots) and equivalent from ERA5 (blue dots). **b** Generalized Extreme Value (GEV) distributions from SEAS5 (in orange) and ERA5 (in blue). Shaded areas indicate the 95% confidence interval.

2018, and in total 3800 weather realizations representing the current climate. The region of interest is located on the west coast of Norway, a region where the highest annual mean precipitation of Europe is observed and where multi-day heavy precipitation events occur frequently (Lavers and Villarini, 2015; Azad and Sorteberg, 2017). Indeed, as shown in Michel et al. (2021), this region is subject to the highest frequency of heavy precipitation events in the country, defined as the occurrences above the 99.5th percentile of the observed daily precipitation over the period 1979–2018. Further, they found the fall season being the season when most heavy precipitation events occur. As an example, one of the largest extreme precipitation events at the west coast of Norway occurred in October 2014. The synoptic atmospheric condition during this extreme precipitation event was characterized by a low pressure system located over the northern part of the Norwegian Sea, which brought warm and moist air-masses, associated with an AR, towards the west coast of Norway (Fig. 1a). Over the course of three days, the low pressure system moved slowly northeast which led to persistent precipitation in nearly the same region on the coast. This led to severe floods in several rivers with considerable damage to buildings and infrastructures.

In order to detect the extreme precipitation events in the SEAS5 hindcast data, we define our study region by using the 98th percentile of seasonal (SON) 3-day precipitation from the ERA5 reanalysis within a domain on the Norwegian south west coast for the period from 1981 to 2018 (Hersbach et al., 2018). The area where the percentile precipitation values exceed this threshold is highlighted in Fig. 1b. The area average seasonal maxima for 3-day accumulated precipitation in the selected region are combined from all relevant ensemble members and lead times in SEAS5, to construct the data-set used for the following statistical analysis. This means the data-set consists of 3800 seasonal maximum 3-day precipitation values that are fitted to a generalized extreme value (GEV) distribution to obtain return values. For comparison, we have fitted a generalized extreme value distribution to equivalent data from ERA5. The GEV-analysis is carried out applying the extRemes package in R (Gilleland and Katz, 2016).

Kelder et al. (2020) examined SEAS5 and ERA5 precipitation maxima over Norway. By comparing 3-day precipitation values with observational gridded data they concluded to apply a bias correction factor of 1.74 for precipitation in Norway. We apply the same factor here. The bias correction is a simple scaling of SEAS5 to ERA5, where we use a constant ratio between the mean of ERA5 and SEAS5 SON precipitation maxima.

The seasonal mean state of the atmosphere's circulation can be characterized by a principal component analysis of the 500 hPa geopotential anomaly for SON from the ERA5 reanalysis. The Empirical Orthogonal Function (EOF) analysis applied here was performed using the SON 500 hPa geopotential height anomalies from ERA5 and SEAS5 over the North Atlantic sector (30–88.5°N, 80°W–40°E). The 500 hPa geopotential height anomalies were weighted by the square root of the cosine of the latitude to ensure equal-area weighting before performing the analysis (Chung and Nigam, 1999). Then, the first five EOFs from ERA5 SON 500 hPa geopotential height anomalies were computed using the period from 1979 to 2017. The indices were calculated by projecting the 500 hPa geopotential heights anomalies from each SEAS5 ensemble member onto the EOFs from the ERA5 500 hPa geopotential height anomalies.

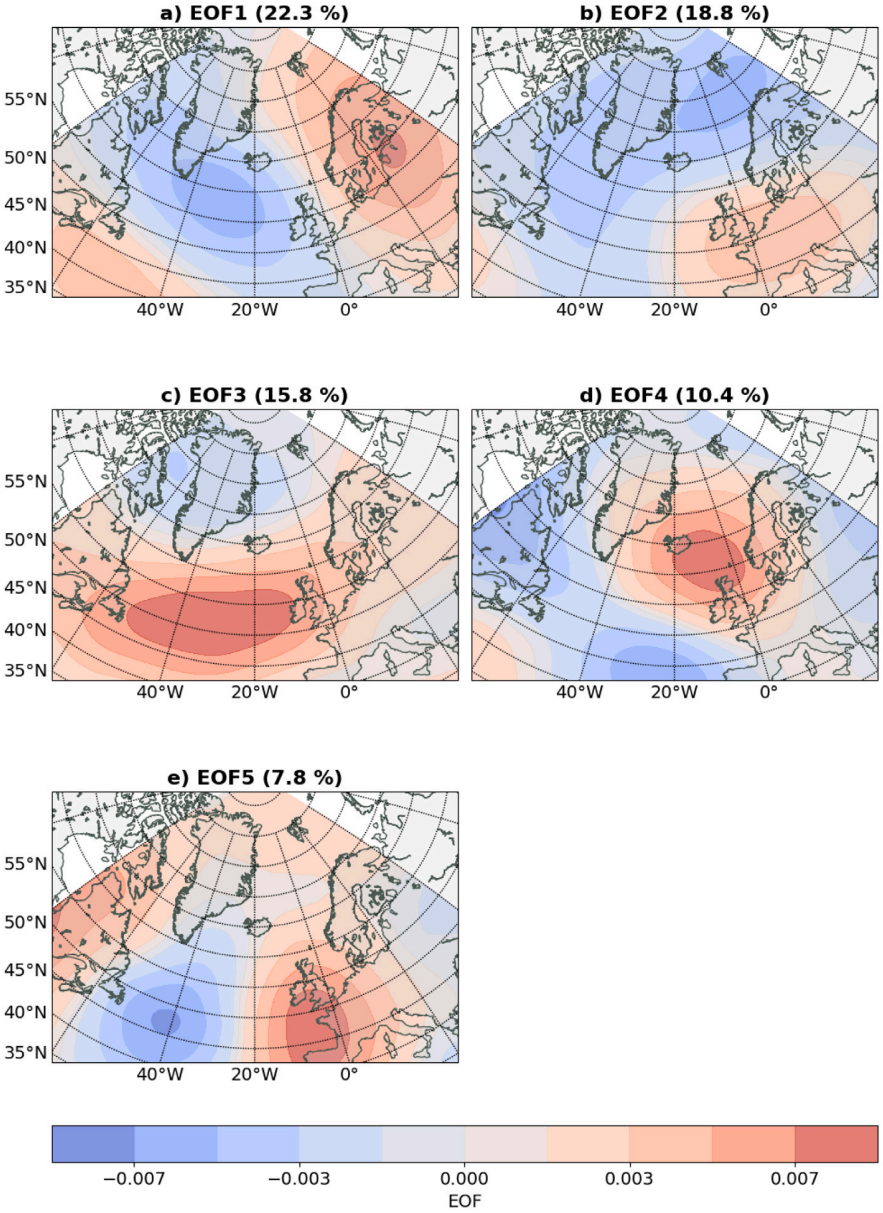

Fig. 3. The 5 first EOFs from a principal component analysis performed on the 500 hPa geopotential anomaly field for the September–October–November season. Variance explained for each EOF is given in the figure title.

The 3800 SEAS5 SON 3-day precipitation maxima now have associated seasonal indices for each of the first 5 EOFs, which can be used to analyse whether there are seasonal conditions that are connected to the extreme precipitation events. To attain this, return levels are evaluated for the different modes of EOFs for all 3800 events. Further, the main characteristics of the large-scale atmospheric setup during the extreme precipitation events in the west coast of Norway can be attained through a composite analysis of the events with the seasonal maximum 3-day precipitation in the SEAS5 data set. The SON 3-day precipitation events exceeding the 50 year return value are considered, and composite maps are made for the events according to the EOF index. The composite analysis will give the synoptic (short-term) features of different physical aspects during the extreme events. This means they will most likely not reflect the regime of the seasonal (long-term) conditions, due to atmospheric variability, but is merely used as a tool to investigate the events themselves.

3. Results

The extracted events from SEAS5 comprise a set of 3800 events, which surpass ERA5, or an observational record series from an equivalent time period, by a factor of 100. All the seasonal maximum 3-day precipitation events from SEAS5 are shown in Fig. 2a together with seasonal maximum 3-day precipitation events from ERA5. The increased sample size strongly reduces the confidence interval of the fitted distribution of extreme value statistics, as seen in Fig. 2b. For a return period of 1000 years the 95% confidence interval is ranging from 64 mm to 146 mm for data from ERA5, while for SEAS5 it is between 97 mm and 105 mm, which gives interval ranges of 82 mm and 8 mm, respectively. For a return period of 10 000 years, the confidence interval for ERA5 is −+55% of the estimated value, while for SEAS5 the interval is +−5%. In general, the confidence interval is reduced by more than a factor of 10 by using SEAS5 data compared to ERA5 data.

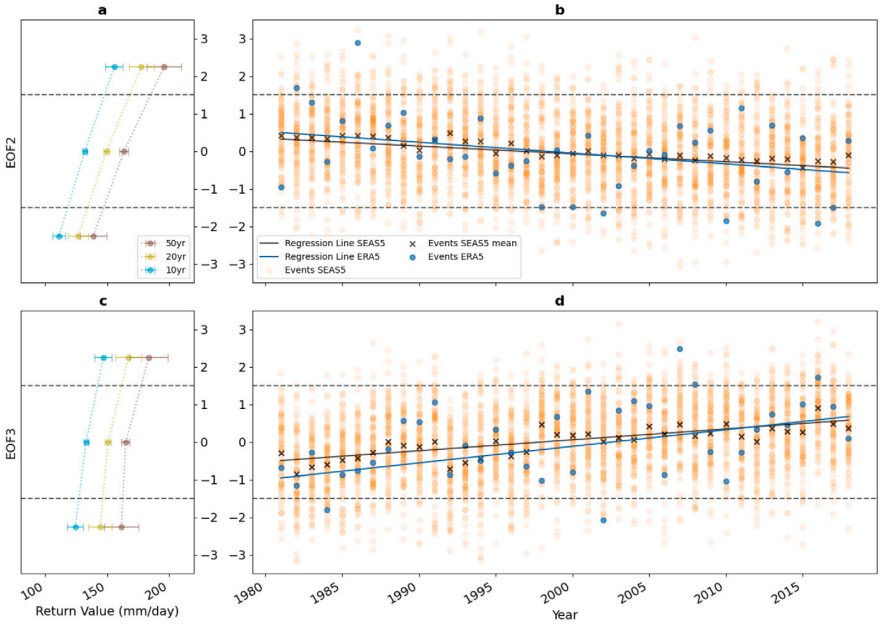

Fig. 4. The two EOFs (EOF2 top and EOF3 bottom) with the strongest connection to extreme precipitation return values. In the left panel variations in return values for return periods of 10, 20 and 50 years in the different EOF modes (positive, neutral and negative). The right panel shows the indices calculated from the EOF analysis for all events in the constructed SEAS5 data-set (orange dots) together with ERA5 data (blue dots). The black line indicates the regression line for the yearly mean of SEAS5 events (black crosses) and the blue line correspondingly for ERA5 events.

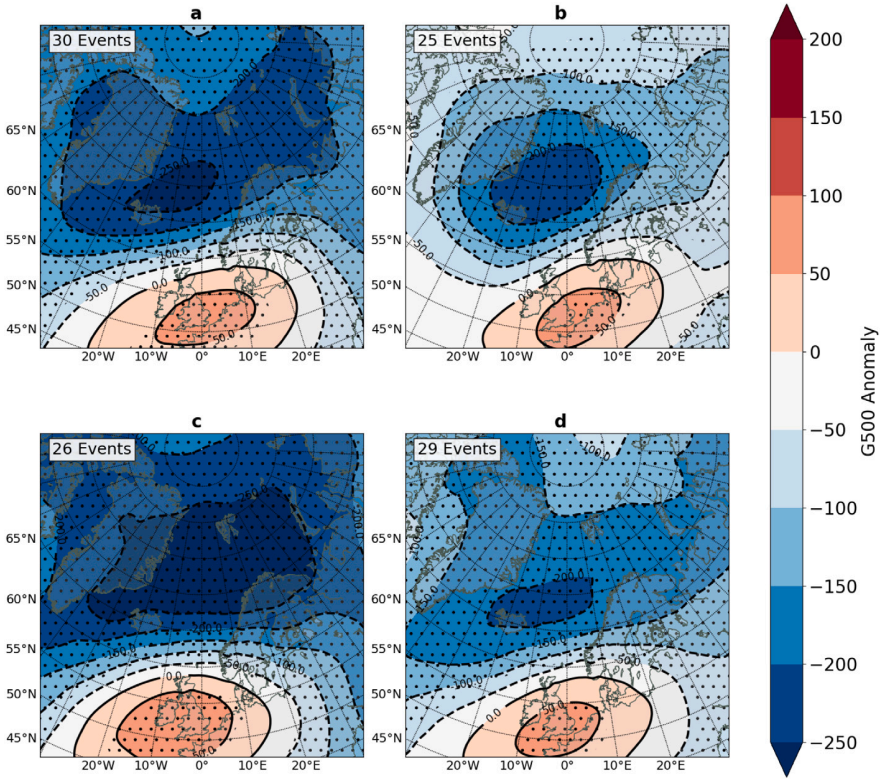

Fig. 5. Composite maps showing the geopotential height anomaly at the 500 hPa level. The anomaly is calculated relative to the season climatology, and the black dots indicate where the geopotential height anomaly is significant according to the student t-test 98% confidence, tested with False Discovery Rate approach. Composite maps in **a** and **b** show the 2nd EOF, positive and negative mode, respectively. Correspondingly in **c** and **d** for the 3rd EOF.

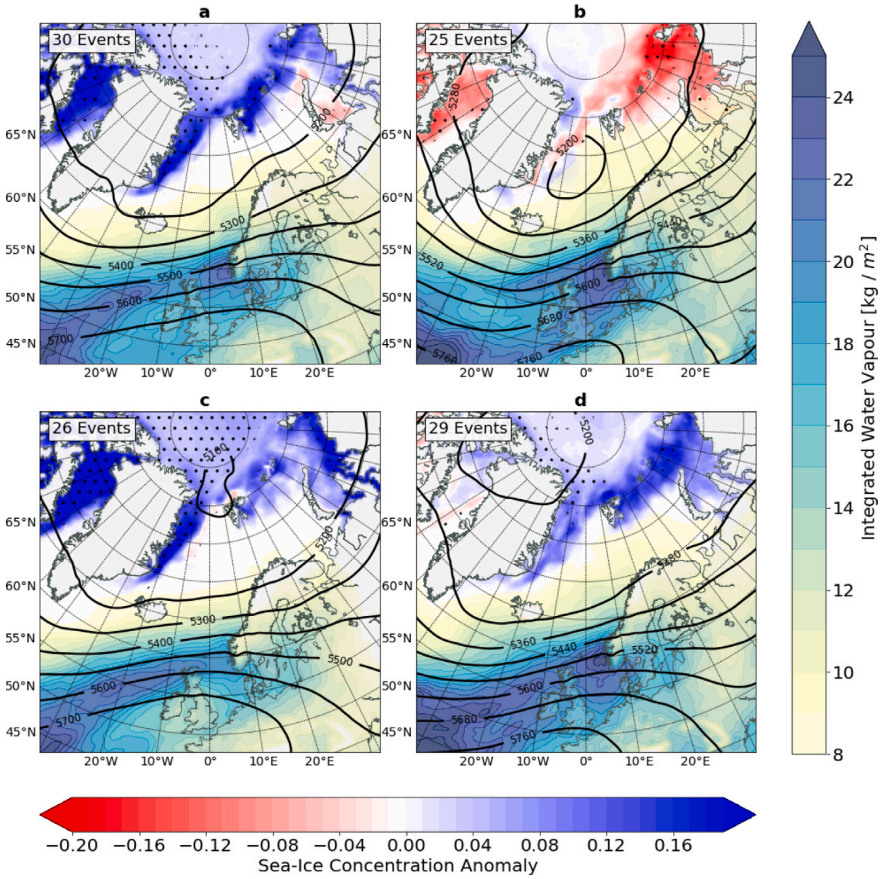

Fig. 6. Composite maps for the same events as in Fig. 5 showing sea-ice concentration anomaly calculated as the difference between the selected events and the season climatology, integrated water vapour (total column) and geopotential height at the 500 hPa level in black contours. The black dots indicate where the sea-ice concentration anomalies are significant according to the student t-test at the 95% confidence level.

The increased number of extreme events retrieved from SEAS5 opens up the possibility to analyse atmospheric properties linked to extreme events in a robust way. To identify if there are dominant circulation patterns conducive for the highest SON 3-day precipitation events in SEAS5, we are considering the first five EOFs of the 500 hPa geopotential height anomaly principal component analysis (Fig. 3). The pattern in EOF1 resembles the Scandinavian Pattern (Barnston and Livezey, 1987) which is associated with a primary circulation centre over Scandinavia and weaker centres over western Europe and eastern Russia. During the positive phase of this pattern, the geopotential height anomaly over Scandinavia is positive, which can result in a blocking system and below average precipitation across Scandinavia. The second EOF pattern has a centre of positive anomaly over western Europe and the UK and a negative anomaly field in the Arctic which stretches over Greenland and further south. It resembles the European Blocking weather regime as shown in Grams et al. (2017). There they found a positive wind speed anomaly along the coast of Norway during this regime. Further, Pasquier et al. (2019) found that this pattern allows for a more effective moisture transport around the ridge of the high pressure and into Northern Europe, with the consequence that AR frequencies are enhanced in a region extending from Iceland to Northern Scandinavia. EOF3 shows a pattern with a dipole pressure centre of positive anomaly over the Azores and negative anomaly over Iceland, which resembles the zonal regime as shown in Grams et al. (2017). The pattern has a similarity to the North Atlantic Oscillation (NAO) pattern (Barnston and Livezey, 1987; Hurrell et al., 2001), though the NAO is by definition the leading mode (1st EOF). A positive phase of this pattern is known to bring warm and wet conditions over Scandinavia (Uvo, 2003). The NAO is a leading mode of atmospheric circulation variability over the North Atlantic region. The pattern is present during the entire year, but it is more important during winter (Pinto and Raible, 2012) and relatively weak during September–October–November. The three first EOFs together explain about 57% of the variance. The positive phase of both EOF2 and EOF3 are conducive for high precipitation values over Norway by guiding low pressure systems to the west coast of the country, and are associated with higher than normal frequency of ARs (Pasquier et al., 2019).

When analysing the return values for subsets of the data corresponding to the respective values of EOF indices, we find that the second and third EOF (Fig. 3b and c) show a connection to the return values of extreme precipitation for the west coast of Norway (Fig. 4a and c). For both EOF's, using only precipitation extremes for positive EOF indices results in significantly higher return values than using events for negative EOF indices (Fig. 4a and c). Note, the sign of an EOF is ambiguous and, for the sake of simplicity, we defined the sign for EOF2 and EOF3 to positively correlate the extreme precipitation and the respective principal components.

Over the 40 year time period both EOF2 and EOF3 exhibit a trend, but with opposite signs (Fig. 4b and d). The trends were tested for significance by using the Mann–Kendall test and both trends are significant, with p-values less than 0.01, yielding a confidence level of 99%. To test the consistency with ERA5 reanalysis, the corresponding trends in EOF indices from ERA5 are included (blue dots in Fig. 4b and d). They are also significant with p-values for EOF2 and EOF3 of 0.025 and 0.0016, respectively. To test the robustness of the trends on the choice of domain for the EOF analysis, we have performed a sensitivity analysis by using five additional domains. These domains are slightly different from the original, and we perform the EOF analysis in

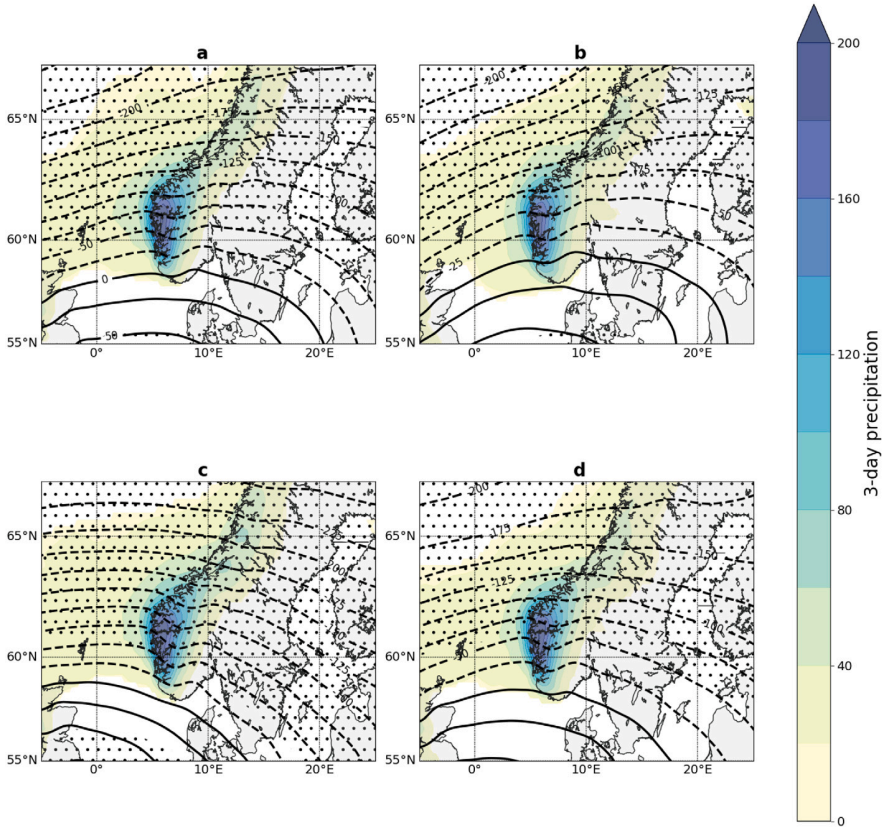

Fig. 7. Composite maps for the same events as in Fig. 6, showing the 3-day precipitation values and geopotential height anomaly at the 500 hPa level. The anomaly is calculated relative to the season climatology, and the black dots indicate where the geopotential height anomaly is significant according to the student t-test 98% confidence, tested with False Discovery Rate approach.

the same manner as the original to all five. From this we find results in agreement with the original domain, with similar trends for all the additional domains for EOF2, and for three out of five for EOF3. The results for the sensitivity analysis are summarized in Table S2 in the Supplementary Material.

Due to the difference in return values for positive and negative modes of EOF, we look closer at the precipitation events to investigate atmospheric features for events occurring during the separate modes. Composite maps can reveal characteristics of the atmospheric circulation for the selected precipitation events. Note that the pressure field during a particular event, or the composite of events, do not necessarily corresponds to the mean seasonal circulation pattern. This is due to the fact that we are considering 3-day precipitation events and the mean circulation pattern represents the whole season. We utilize only the extreme precipitation events exceeding the 50 year return value. From this subset, we further divide the events into positive and negative modes of EOF2 and EOF3 for the composites (Figs. 5 and 6). The 500 hPa geopotential anomaly composites show a dipole structure with negative anomaly situated over the Greenland and Norwegian Seas and a positive anomaly centre located over the UK and West Europe. The main difference between the patterns is seen in the extent and strength of the negative anomaly and the location of the high anomaly centre and zero-anomaly line. For the figures with positive EOF indices (Figs. 5 and 6a and c), the negative anomaly is not only deeper, but has a larger extent than for the figures showing negative EOF indices (Figs. 5 and 6b and d). The more negative geopotential height anomalies for the positive modes of the EOFs will cause stronger pressure gradients that leads to stronger flows towards the west coast, where the flow will be lifted orographically and lead to heavier precipitation.

Over the years from 1981 to 2018 EOF2 has had a negative trend, towards the indices that are associated with lower return values. The maps in Figs. 5b and 6b are the composite of events with lowest indices of EOF2, thus the composite of events which are more frequently occurring in the most recent years in the data-set. This composite map stands out from the rest, as the area with negative height anomaly is more confined than in Figs. 5 and 6a, c and d. Another notable feature in Fig. 6b is the sea-ice extent in the Barents-Kara Sea, which is smaller here compared to what is seen in Fig. 6a, c and d. Sea-ice concentration has had a decreasing trend in recent decades, and the minimum annual sea-ice extents in 2020 and 2019 are the second and third lowest on record. Sea-ice extent can influence the energy budget in the Arctic, and is connected to atmospheric circulation patterns (Vihma, 2014). Figure S1 (in the Supplementary Material) shows the SST anomaly for the same events as in Fig. 6. Although it is not significant, there is a signal of the events in Fig. 6b having higher SST values than the rest, concurrent with the events that had the lowest sea-ice extent. These are the events composed by low indices of EOF2, and given the trend found in Fig. 4b implies conditions that lead to precipitation events with lower return values on the west coast of Norway in the autumn season.

Comparing the composites of events occurring during positive and negative indices for the two EOFs, a difference in the pressure gradient can be seen in Fig. 7, where the geopotential height anomaly lines are closer in Fig. 7a and c (positive indices) compared to Fig. 7b and d (negative indices). The trend in EOF2 is thus towards events with more frequently occurring circulation with weaker pressure gradient. The weaker pressure gradient implies a weaker flow, resulting in lower precipitation amounts over the west coast of Norway. In contrast, the trend in EOF3 implies events with more frequently occurring circulation characterized by a stronger pressure gradient. This is conducive for a stronger flow, which results in precipitation events associated with higher return values.

4. Discussion and conclusions

The characteristics of extreme precipitation are expected to change drastically in our warming climate (Myhre et al., 2019). The west coast of Norway, and especially the south west coast, is subject to the largest rainfall amounts in Norway, with an annual mean precipitation exceeding 3000 mm (Lussana et al., 2018). In order to investigate the recent changes of extreme precipitation along the west coast of Norway, we are using a large ensemble generated from the SEAS5 seasonal hindcast data-set which represents the climate from 1981 to 2018 (Johnson et al., 2019). From this data-set 3800 annual 3-day precipitation maxima are extracted for the SON season and for a region on the west coast of Norway. The extreme precipitation events are analysed by means of the GEV distribution and by the preconditioning mean seasonal atmospheric patterns using EOF analysis.

The large data set offers an increased precipitation event sample size that strongly reduces the uncertainty in design value estimates. The confidence interval is reduced by more than a factor of 10 when SEAS5 events are used in a fit to the GEV distribution compared to using data from ERA5. Design values are frequently used estimates when planning and designing public buildings or communication structures, and reliable information is crucial for raising and maintaining robust infrastructures. The complex topography in Norway gives rise to large heterogeneities in precipitation extremes for different parts of the country, and limitations in observational records makes design value estimation challenging. This methodology gives the opportunity to reduce uncertainties in areas where already existing design value estimates are based on sparse observations or time limited reanalysis data-sets, and it especially strengthens the estimates for long return periods.

In addition to a more robust extreme value distribution statistics, the increased sample size allows for a more robust analysis of atmospheric properties connected to extreme events. If there are persistent and reoccurring weather patterns during a season, the seasonal mean atmospheric state will be influenced and predominated by this. For this reason, seasonal EOF indices are used to investigate whether there are conditions that are favourable for extremes during a season. We find that the return periods and return values of extreme precipitation are related to two EOF atmospheric circulation modes. The two EOFs are patterns favourable for higher precipitation amounts on the west coast of Norway and thus are also related to the probability of occurrence of extreme events: the pattern of EOF2 is associated with higher than normal air flow along the coast of Norway, which is also coupled with a more effective moisture transport into Northern Europe and enhanced AR frequencies (Pasquier et al., 2019), and the more zonal regime in EOF3 is associated with warm and wet conditions over Scandinavia (Uvo, 2003). The principal components of two EOFs exhibit significant trends over the 40 year time period, however, with an opposing impact on the extreme precipitation. In total, this leads to a virtually non-changing extreme precipitation over the west coast of Norway over the past 40 years.

Our results are consistent with Kelder et al. (2020), who analysed variability in precipitation in autumn in a similar region at the west coast of Norway and found no trend in extreme precipitation for this period. From a climate model analysis Whan et al. (2020) found that there is only little change from the past (around 1850) to the near-future periods (around 2030) in the number of Atmospheric Rivers reaching the west-coast of Norway and the extreme precipitation. However, drastic increases are found for the far-future (around 2100). Other studies on the recent changes in mean precipitation from observation records show increasing precipitation amounts for Norway, and climate predictions expect further increase in the years to come (Hanssen-Bauer et al., 2017). The annual total has had an increasing trend, with an exception for the autumn season (Kuya et al., 2021).

Circulation patterns are driven by the Earth's energy balance and are controlled by complex interactions within the coupled Earth–Atmosphere system. They are thus subject to the currently changing climate. In order to better understand the interconnected changes in the coupled ocean–ice–atmospheric system we combined the analysis of the geopotential height fields, sea-ice extent, and SST for the largest extreme events (exceeding 50 year return value) and, further, sub-divided them into the predominant EOF conditions. We have found an inherent connection of the ocean surface temperatures and sea-ice coverage in the Barents-Kara Sea for EOF2. In other words, extreme precipitation events which occur in seasons where the mean atmospheric state is dominated by a positive (negative) EOF2 atmospheric pattern are also occurring during positive (negative) anomalies of sea-ice in the Euro Atlantic sector, as well as negative (positive) ocean surface temperature anomalies.

There are a number of studies on linkages between sea-ice, ocean surface temperatures and mid-latitude weather patterns (e.g. Magnusdottir et al. (2004), Vihma (2014), Tokinaga et al. (2017)). On the one hand, SST is an important driver in planetary-scale atmospheric circulation which can again transport warm air into the Arctic and contribute to sea-ice loss (Tokinaga et al., 2017). In particular, the variability of the SST in the Gulf Stream area is potentially linked to an upper-tropospheric wave response which causes atmospheric patterns over the North Atlantic with predominant southerly winds (Sato et al., 2014), with a subsequent impact on the sea-ice coverage of the Barents-Kara Sea (Nakanowatari et al., 2014).

On the other hand, sea-ice variability for example in the Barents-Kara Sea region might have important implications on the state of the atmosphere. For example Ruggieri et al. (2016) describe a mechanism which causes an atmospheric blocking like signal over the Barents-Kara Sea region during low sea-ice conditions. Hence, the statistical correlation of SST and sea-ice variability to the extreme precipitation in relation to EOF2 suggests that this change might be connected to our warming climate. However, a more detailed study on the different Earth's system components will be necessary to disentangle the processes.

In our study, EOF3 shows a north–south dipole structure with negative pressure anomaly over Iceland and positive pressure anomaly over the Azores, thus a zonal regime that is similar to the NAO pattern. The detected change in EOF3 might be associated with a region south of Greenland with a slower warming rate than the North Atlantic Ocean in general (Rahmstorf et al., 2015), which causes a local increase of the north–south temperature gradient over the ocean surface (Harvey and Shaffrey, 2021), which again influences the pressure gradient. In isolation this trend in EOF3 leads to increasing precipitation with higher return values at the west coast of Norway. This impact is diminished by the trend in the 2nd EOF and its opposing effect on extreme precipitation.

We find two seasonal atmospheric patterns which have a connection to the extreme precipitation, but the patterns themselves have an opposing trend. Choosing different areas for the EOF analysis might remove this separation and one thus could argue that this is an artificial separation into these two patterns by the EOF method. However, for the two patterns we also find different correlations to the sea-ice extent, which supports the fact that the separation is meaningful.

The novel extreme event analysis approach presented here has proven to be useful for studying the relation of extreme precipitation with other dynamical components. The method reduces uncertainties in statistical analysis due to the increased sample size, and allows to find connections between the extreme precipitation events and atmospheric circulation patterns, sea-ice variability, or ocean-surface conditions. A natural next step would be to investigate the mechanisms causing this relationship, which can improve our understanding of the driving forces for extreme precipitation events.

CRediT authorship contribution statement

Karianne Ødemark: Conception and design of study, Acquisition of data, Analysis and/or interpretation of data, Writing – original draft. **Malte Müller:** Conception and design of study, Acquisition of data, Analysis and/or interpretation of data, Writing – review & editing. **Cyril Palerme:** Acquisition of data, Analysis and/or interpretation of data. **Ole Einar Tveito:** Analysis and/or interpretation of data, Writing – review & editing.

Declaration of competing interest

The authors declare that they have no known competing financial interests or personal relationships that could have appeared to influence the work reported in this paper.

Data availability

Data will be made available on request.

Acknowledgements

The study is supported by the Norwegian Research Council and Energi Norge, Norway through the project FlomQ (NFR-235710/E20). MM has received support from the project TWEX (NFR-255037) funded through the Norwegian Research Council. The data from SEAS5 and ERA5 data are available from the Copernicus Climate Change Service (C3S) Climate DataStore (https://cds.climate.copernicus.eu/). The authors would like to thank the editor and two reviewers for their help in improving the paper. We are also thankful for helpful input from Inger Hanssen-Bauer. All authors approved the version of the manuscript to be published.

Appendix A. Supplementary data

Supplementary material related to this article can be found online at https://doi.org/10.1016/j.wace.2022.100530.

References

Azad, R., Sorteberg, A., 2017. Extreme daily precipitation in coastal western Norway and the link to atmospheric rivers. J. Geophys. Res.: Atmos. 122 (4), 2080–2095. http://dx.doi.org/10.1002/2016JD025615, arXiv:https://agupubs.onlinelibrary.wiley.com/doi/pdf/10.1002/2016JD025615, URL https://agupubs.onlinelibrary.wiley.com/doi/abs/10.1002/2016JD025615.

Barnston, A.G., Livezey, R.E., 1987. Classification, Seasonality and Persistence of Low-Frequency Atmospheric Circulation Patterns. Mon. Weather Rev. 115 (6), 1083–1126. http://dx.doi.org/10.1175/1520-0493(1987)115<1083:CSAPOL>2.0.CO;2, URL https://journals.ametsoc.org/view/journals/mwre/115/6/1520-0493_1987_115_1083_csapol_2_0_co_2.xml.

Benedict, I., Ødemark, K., Nipen, T., Moore, R., 2019. Large-Scale Flow Patterns Associated with Extreme Precipitation and Atmospheric Rivers over Norway. Mon. Weather Rev. 147 (4), 1415–1428. http://dx.doi.org/10.1175/MWR-D-18-0362.1.

Bintanja, R., van der Wiel, K., van der Linden, E.C., Reusen, J., Bogerd, L., Krikken, F., Selten, F.M., 2020. Strong future increases in Arctic precipitation variability linked to poleward moisture transport. Sci. Adv. 6 (7), http://dx.doi.org/10.1126/sciadv.aax6869, arXiv:https://advances.sciencemag.org/content/6/7/eaax6869.full.pdf, URL https://advances.sciencemag.org/content/6/7/eaax6869.

Blackport, R., Screen, J.A., van der Wiel, K., Bintanja, R., 2019. Minimal influence of reduced Arctic sea ice on coincident cold winters in mid-latitudes. Nature Clim. Change 9, http://dx.doi.org/10.1038/s41558-019-0551-4.

Boucher, O., Randall, D., Artaxo, P., Bretherton, C., Feingold, G., Forster, P., Kerminen, V.-M., Kondo, Y., Liao, H., Lohmann, U., Rasch, P., Satheesh, S.K., Sherwood, S., Stevens, B., Zhang, X.Y., 2013. Clouds and aerosols. In: Stocker, T.F., Qin, D., Plattner, G.-K., Tignor, M., Allen, S.K., Doschung, J., Nauels, A., Xia, Y., Bex, V., Midgley, P.M. (Eds.), Climate Change 2013: The Physical Science Basis. Contribution of Working Group I To the Fifth Assessment Report of the Intergovernmental Panel on Climate Change. Cambridge University Press, Cambridge, UK, pp. 571–657. http://dx.doi.org/10.1017/CBO9781107415324.016.

Chung, C., Nigam, S., 1999. Weighting of geophysical data in Principal Component Analysis. J. Geophys. Res.: Atmos. 104, http://dx.doi.org/10.1029/1999JD900234.

Coumou, D., Petoukhov, V., Rahmstorf, S., Petri, S., Schellnhuber, H.J., 2014. Quasi-resonant circulation regimes and hemispheric synchronization of extreme weather in boreal summer. Proc. Natl. Acad. Sci. USA 111, http://dx.doi.org/10.1073/pnas.1412797111.

Dee, D.P., Uppala, S.M., Simmons, A.J., Berrisford, P., Poli, P., Kobayashi, S., Andrae, U., Balmaseda, M.A., Balsamo, G., Bauer, P., Bechtold, P., Beljaars, A.C.M., van de Berg, L., Bidlot, J., Bormann, N., Delsol, C., Dragani, R., Fuentes, M., Geer, A.J., Haimberger, L., Healy, S.B., Hersbach, H., Hólm, E.V., Isaksen, L., Kållberg, P., Köhler, M., Matricardi, M., McNally, A.P., Monge-Sanz, B.M., Morcrette, J.-J., Park, B.-K., Peubey, C., de Rosnay, P., Tavolato, C., Thépaut, J.-N., Vitart, F., 2011. The ERA-Interim reanalysis: configuration and performance of the data assimilation system. Q. J. R. Meteorol. Soc. 137, 553–597. http://dx.doi.org/10.1002/qj.828, URL https://rmets.onlinelibrary.wiley.com/doi/abs/10.1002/qj.828.

ECMWF, 2016. IFS documentation CY43R1. http://dx.doi.org/10.21957/m1u2yxwrl, URL https://www.ecmwf.int/node/17116.

Eyring, V., Bony, S., Meehl, G.A., Senior, C.A., Stevens, B., Stouffer, R.J., Taylor, K.E., 2016. Overview of the Coupled Model Intercomparison Project Phase 6 (CMIP6) experimental design and organization. Geosci. Model Dev. 9, http://dx.doi.org/10.5194/gmd-9-1937-2016.

Fichefet, T., Maqueda, M.A.M., 1997. Sensitivity of a global sea ice model to the treatment of ice thermodynamics and dynamics. J. Geophys. Res.: Oceans 102 (C6), 12609–12646. http://dx.doi.org/10.1029/97JC00480, arXiv:https://agupubs.onlinelibrary.wiley.com/doi/pdf/10.1029/97JC00480, URL https://agupubs.onlinelibrary.wiley.com/doi/abs/10.1029/97JC00480.

Fischer, E.M., Knutti, R., 2016. Observed heavy precipitation increase confirms theory and early models. Nature Clim. Change 6, http://dx.doi.org/10.1038/nclimate3110.

Francis, J.A., Vavrus, S.J., 2012. Evidence linking Arctic amplification to extreme weather in mid-latitudes. Geophys. Res. Lett. 39, http://dx.doi.org/10.1029/2012GL051000.

Gilleland, E., Katz, R., 2016. Extremes 2.0: An Extreme Value Analysis Package in R. J. Stat. Softw. Articles 72, 1–39. http://dx.doi.org/10.18637/jss.v072.i08, URL https://www.jstatsoft.org/v072/i08.

Gimeno, L., Nieto, R., Vázquez, M., Lavers, D.A., 2014. Atmospheric rivers: A mini-review. Front. Earth Sci. 2, http://dx.doi.org/10.3389/feart.2014.00002.

Grams, C.M., Beerli, R., Pfenninger, S., Staffell, I., Wernli, H., 2017. Balancing Europe's wind-power output through spatial deployment informed by weather regimes. Nature Clim. Change 7, 557–562. http://dx.doi.org/10.1038/NCLIMATE3338.

Hanssen-Bauer, I., Førland, E., Haddeland, I., Hisdal, H., Lawrence, D., Mayer, S., Nesje, A., Nilsen, J., Sandven, S., Sandø, A., Sorteberg, A., Ådlandsvik, B., 2017. Climate in Norway 2100 - a knowledge base for climate adaption.

Harvey, B., Shaffrey, L., 2021. How will climate change impact North Atlantic storms? Weather 76, http://dx.doi.org/10.1002/wea.4075.

Hersbach, H., de Rosnay, P., Bell, B., Schepers, D., Simmons, A., Soci, C., Abdalla, S., Alonso-Balmaseda, M., Balsamo, G., Bechtold, P., Berrisford, P., Bidlot, J.-R., de Boisséson, E., Bonavita, M., Browne, P., Buizza, R., Dahlgren, P., Dee, D., Dragani, R., Diamantakis, M., Flemming, J., Forbes, R., Geer, A.J., Haiden, T., Hólm, E., Haimberger, L., Hogan, R., Horányi, A., Janiskova, M., Laloyaux, P., Lopez, P., Munoz-Sabater, J., Peubey, C., Radu, R., Richardson, D., Thépaut, J.-N., Vitart, F., Yang, X., Zsótér, E., Zuo, H., 2018. Operational global reanalysis: progress, future directions and synergies with NWP. ERA Rep. Series http://dx.doi.org/10.21957/tkic6g3wm, URL https://www.ecmwf.int/node/18765.

Horton, D.E., Johnson, N.C., Singh, D., Swain, D.L., Rajaratnam, B., Diffenbaugh, N.S., 2015. Contribution of changes in atmospheric circulation patterns to extreme temperature trends. Nature 522, http://dx.doi.org/10.1038/nature14550.

Hurrell, J.W., Kushnir, Y., Visbeck, M., 2001. The North Atlantic oscillation. Science 291, http://dx.doi.org/10.1126/science.1058761.

Johnson, S.J., Stockdale, T.N., Ferranti, L., Balmaseda, M.A., Molteni, F., Magnusson, L., Tietsche, S., Decremer, D., Weisheimer, A., Balsamo, G., Keeley, S.P., Mogensen, K., Zuo, H., Monge-Sanz, B.M., 2019. SEAS5: The new ECMWF seasonal forecast system. Geosci. Model Dev. 12, http://dx.doi.org/10.5194/gmd-12-1087-2019.

Kelder, T., Müller, M., Slater, L.J., Marjoribanks, T.I., Wilby, R.L., Prudhomme, C., Bohlinger, P., Ferranti, L., Nipen, T., 2020. Using UNSEEN trends to detect decadal changes in 100-year precipitation extremes. Npj Climate Atmospheric Sci. 3, http://dx.doi.org/10.1038/s41612-020-00149-4.

Kharin, V.V., Zwiers, F.W., Zhang, X., Wehner, M., 2013. Changes in temperature and precipitation extremes in the CMIP5 ensemble. Clim. Change 119, http://dx.doi.org/10.1007/s10584-013-0705-8.

Kolstad, E.W., Screen, J.A., 2019. Nonstationary Relationship Between Autumn Arctic Sea Ice and the Winter North Atlantic Oscillation. Geophys. Res. Lett. 46, 7583–7591. http://dx.doi.org/10.1029/2019GL083059.

Kuya, E.K., Gjelten, H.M., Tveito, O.E., 2021. Homogenization of Norwegian monthly precipitation series for the period 1961–2018. URL https://www.met.no/publikasjoner/met-report.

Lavers, D.A., Villarini, G., 2015. The contribution of atmospheric rivers to precipitation in Europe and the United States. J. Hydrol. 522, http://dx.doi.org/10.1016/j.jhydrol.2014.12.010.

Lussana, C., Saloranta, T., Skaugen, T., Magnusson, J., Tveito, O.E., Andersen, J., 2018. seNorge2 daily precipitation, an observational gridded dataset over Norway from 1957 to the present day. Earth Syst. Sci. Data 10, 235–249. http://dx.doi.org/10.5194/essd-10-235-2018, URL https://www.earth-syst-sci-data.net/10/235/2018/.

Madec, G., Bourdallé-Badie, R., Bouttier, P.-A., Bricaud, C., Bruciaferri, D., Calvert, D., Chanut, J., Clementi, E., Coward, A., Delrosso, D., Ethé, C., Flavoni, S., Graham, T., Harle, J., Iovino, D., Lea, D., Lévy, C., Lovato, T., Martin, N., Masson, S., Mocavero, S., Paul, J., Rousset, C., Storkey, D., Storto, A., Vancoppenolle, M., 2017. NEMO ocean engine. URL http://hdl.handle.net/2122/13309.

Magnusdottir, G., Deser, C., Saravanan, R., 2004. The effects of North Atlantic SST and sea ice anomalies on the winter circulation in CCM3. Part I: Main features and storm track characteristics of the response. J. Clim. 17, http://dx.doi.org/10.1175/1520-0442(2004)017<0857:TEONAS>2.0.CO;2.

Michel, C., Sorteberg, A., Eckhardt, S., Weijenborg, C., Stohl, A., Cassiani, M., 2021. Characterization of the atmospheric environment during extreme precipitation events associated with atmospheric rivers in Norway - Seasonal and regional aspects. Weather Climate Extremes 34, http://dx.doi.org/10.1016/j.wace.2021.100370.

Myhre, G., Alterskjær, K., Stjern, C.W., Hodnebrog, Marelle, L., Samset, B.H., Sillmann, J., Schaller, N., Fischer, E., Schulz, M., Stohl, A., 2019. Frequency of extreme precipitation increases extensively with event rareness under global warming. Sci. Rep. 9, http://dx.doi.org/10.1038/s41598-019-52277-4.

Nakanowatari, T., Sato, K., Inoue, J., 2014. Predictability of the Barents sea ice in early winter: Remote effects of oceanic and atmospheric thermal conditions from the North Atlantic. J. Clim. 27, http://dx.doi.org/10.1175/JCLI-D-14-00125.1.

Ødemark, K., Müller, M., Tveito, O.E., 2020. Changing lateral boundary conditions for probable maximum precipitation studies: A physically consistent approach. J. Hydrometeorol. 22, http://dx.doi.org/10.1175/JHM-D-20-0070.1.

Papalexiou, S.M., Montanari, A., 2019. Global and Regional Increase of Precipitation Extremes Under Global Warming. Water Resour. Res. 55, http://dx.doi.org/10.1029/2018WR024067.

Pasquier, J.T., Pfahl, S., Grams, C.M., 2019. Modulation of Atmospheric River Occurrence and Associated Precipitation Extremes in the North Atlantic Region by European Weather Regimes. Geophys. Res. Lett. 46, http://dx.doi.org/10.1029/2018GL081194.

Pinto, J.G., Raible, C.C., 2012. Past and recent changes in the North Atlantic oscillation. Wiley Interdiscip. Rev. Clim. Change 3, 79–90. http://dx.doi.org/10.1002/wcc.150.

Rahmstorf, S., Box, J.E., Feulner, G., Mann, M.E., Robinson, A., Rutherford, S., Schaffernicht, E.J., 2015. Exceptional twentieth-century slowdown in Atlantic Ocean overturning circulation. Nature Clim. Change 5, http://dx.doi.org/10.1038/nclimate2554.

Ruggieri, P., Buizza, R., Visconti, G., 2016. On the link between Barents-Kara sea ice variability and European blocking. J. Geophys. Res. 121, 5664–5679. http://dx.doi.org/10.1002/2015JD024021.

Sato, K., Inoue, J., Watanabe, M., 2014. Influence of the Gulf Stream on the Barents Sea ice retreat and Eurasian coldness during early winter. Environ. Res. Lett. 9, http://dx.doi.org/10.1088/1748-9326/9/8/084009.

Screen, J.A., 2017. Simulated Atmospheric Response to Regional and Pan-Arctic Sea Ice Loss. J. Clim. 30, 3945–3962. http://dx.doi.org/10.1175/JCLI-D-16-0197.1.

Serreze, M.C., Barry, R.G., 2011. Processes and impacts of Arctic amplification: A research synthesis. Glob. Planet. Change 77 (1), 85–96. http://dx.doi.org/10.1016/j.gloplacha.2011.03.004, URL https://www.sciencedirect.com/science/article/pii/S0921818111000397.

Smith, D.M., Eade, R., Andrews, M.B., Ayres, H., Clark, A., Deser, C., Dunstone, N.J., García-Serrano, J., Gastineau, G., Graff, L.S., Hardiman, S.C., He, B., Hermanson, L., Jung, T., Knight, J., Levine, X., Magnusdottir, G., Manzini, E., Matei, D., Mori, M., Msadek, R., Ortega, P., Peings, Y., Scaife, A.A., Screen, J.A., Seabrook, M., Semmler, T., Sigmond, M., Streffing, J., Sun, L., Walsh, A., 2022. Robust but weak winter atmospheric circulation response to future Arctic sea ice loss. Nature Commun. 13, http://dx.doi.org/10.1038/s41467-022-28283-y.

Smith, D.M., Screen, J.A., Deser, C., Cohen, J., Fyfe, J.C., García-Serrano, J., Jung, T., Kattsov, V., Matei, D., Msadek, R., Peings, Y., Sigmond, M., Ukita, J., Zhang, X., 2019. The Polar Amplification Model Intercomparison Project (PAMIP) contribution to CMIP6: Investigating the causes and consequences of polar amplification. Geosci. Model Dev. 12, http://dx.doi.org/10.5194/gmd-12-1139-2019.

Sodemann, H., Stohl, A., 2013. Moisture Origin and Meridional Transport in Atmospheric Rivers and Their Association with Multiple Cyclones. Mon. Wea. Rev. 141 (8), 2850–2868.

Stohl, A., Forster, C., Sodemann, H., 2008. Remote sources of water vapor forming precipitation on the Norwegian west coast at 60°N–a tale of hurricanes and an atmospheric river. J. Geophys. Res.: Atmos. 113 (D5), n/a–n/a. http://dx.doi.org/10.1029/2007JD009006, D05102.

Sun, L., Deser, C., Tomas, R.A., 2015. Mechanisms of stratospheric and tropospheric circulation response to projected Arctic sea ice loss. J. Climate 28, 7824–7845.

Tamarin-Brodsky, T., Kaspi, Y., 2017. Enhanced poleward propagation of storms under climate change. Nat. Geosci. 10, http://dx.doi.org/10.1038/s41561-017-0001-8.

Tokinaga, H., Xie, S.P., Mukougawa, H., 2017. Early 20th-century Arctic warming intensified by Pacific and Atlantic multidecadal variability. Proc. Natl. Acad. Sci. USA 114, http://dx.doi.org/10.1073/pnas.1615880114.

Uvo, C.B., 2003. Analysis and regionalization of northern European winter precipitation based on its relationship with the North Atlantic Oscillation. Int. J. Climatol. 23 (10), 1185–1194.

Vihma, T., 2014. Effects of Arctic Sea Ice Decline on Weather and Climate: A review. Surv. Geophys. 35, 1175–1214. http://dx.doi.org/10.1007/s10712-014-9284-0.

Whan, K., Sillmann, J., Schaller, N., Haarsma, R., 2020. Future changes in atmospheric rivers and extreme precipitation in Norway. Clim. Dynam. 54, http://dx.doi.org/10.1007/s00382-019-05099-z.

Wickström, S., Jonassen, M.O., Vihma, T., Uotila, P., 2020. Trends in cyclones in the high-latitude North Atlantic during 1979–2016. Q. J. R. Meteorol. Soc. 146, http://dx.doi.org/10.1002/qj.3707.

Zhu, Y., Newell, R.E., 1998. A proposed algorithm for moisture fluxes from atmospheric rivers. Mon. Weather Rev. 126, http://dx.doi.org/10.1175/1520-0493(1998)126<0725:APAFMF>2.0.CO;2.

Zuo, H., Alonso-Balmaseda, M., Mogensen, K., Tietsche, S., 2018. OCEAN5: The ECMWF ocean reanalysis system and its real-time analysis component. http://dx.doi.org/10.21957/la2v0442, URL https://www.ecmwf.int/node/18519.

Supplementary Material for

Recent changes in circulation patterns and their opposing impact on extreme precipitation at the west coast of Norway

Karianne Ødemark[1,2], Malte Müller[1,2], Ole Einar Tveito[1] and Cyril Palerme[1]

1. The Norwegian Meteorological Institute

2. University of Oslo, Department of Geosciences

Contents of this file

Introduction

This Supplementary Information contains Figure S1 showing SST anomaly for positive and negative modes of the 2nd and 3rd EOF and Table S2 summarizing a sensitivity analysis done for the EOF analysis using different domains.

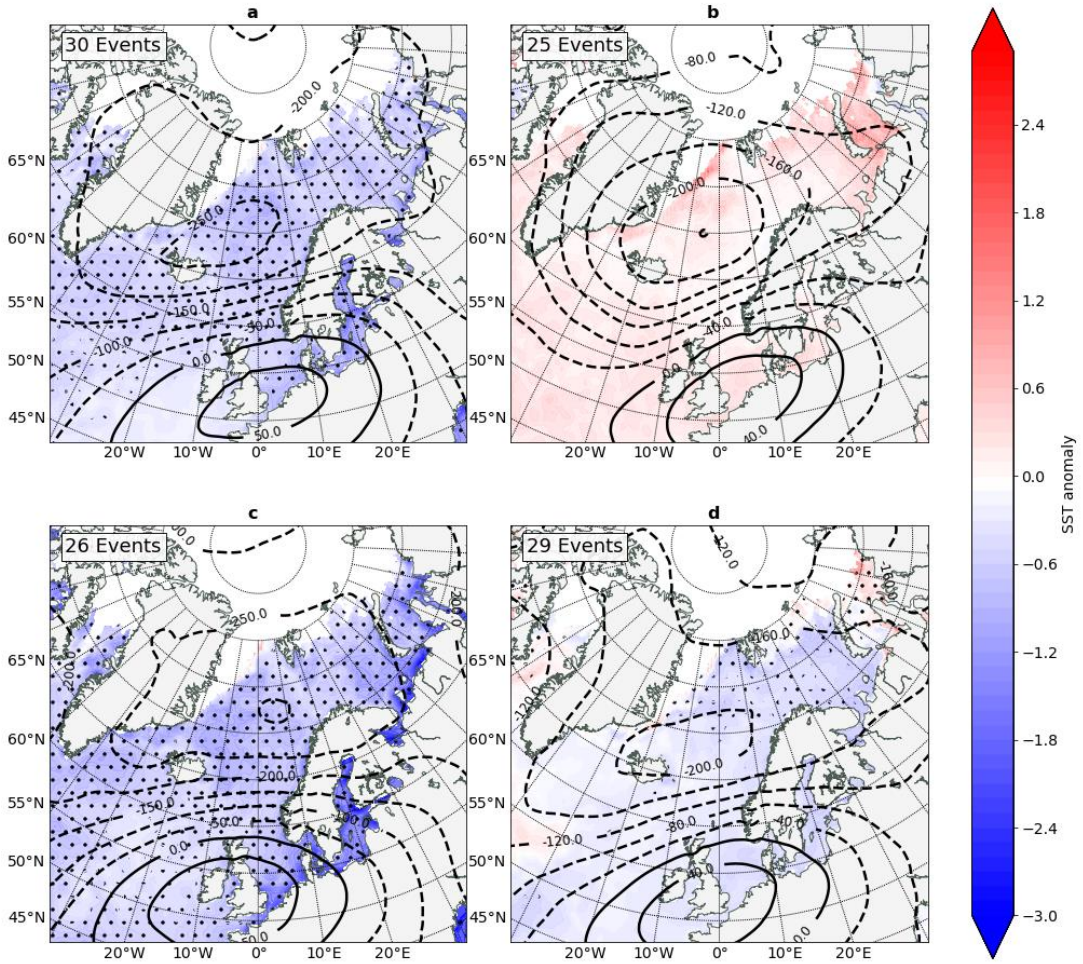

Figure S1. Composite maps showing the SST anomaly calculated relative to the season climatology. The black dots indicate where the SST anomaly is significant according to the student t-test 95 % confidence, tested with the False Discovery Rate approach. Geopotential height anomaly at the 500 hPa level is shown in black contours. Composite maps in **a** and **b** show the 2nd EOF, positive and negative mode, respectively. Correspondingly in **c** and **d** for the 3rd EOF.

Table S2. Table showing the results corresponding to Figure 4 in the main manuscript when using slightly different domains for the EOF analysis. The domains are chosen from examples found in literature. In the EOF analysis for the new domains, the two relevant EOF patterns (EOF2 and EOF3) changed order (due to similar amount of variance explained) in domain c and f, but they are listed according to their corresponding pattern found in the original EOF analysis for domain a.

Domain	EOF2		EOF3	
	Trend	Effect on precipitation	Trend	Effect on precipitation
(a) 30N – 88.5N, 80W – 40 E	p<0.01	Yes	p<0.01	Yes
(b) 10N - 80N, 100W – 40E	p<0.01	Yes	No p=0.138	Yes
(c) 20N - 80N, 90W - 30 E	p<0.01	Yes	p<0.01	Yes
(d) 20N - 80N, 90W – 40 E	p<0.01	Yes	p<0.01	Yes
(e) 20N - 90 N, 80W – 40E	p<0.01	Yes	p<0.01	Yes
(f) 30N – 90N, 90W – 30E	p<0.01	Yes*	No p=0.379	Yes

*Only for negative indexes (positive indexes has the same return values as neutral indexes)

References for the selected domains:

(a) Johnson et al., 2019, *GMD* https://doi.org/10.5194/gmd-12-1087-2019 (500 hPa geopotential height)
(b) Comas-Bru & Hernández, 2018, *Earth Syst. Sci. Data* https://doi.org/10.5194/essd-10-2329-2018 (SLP)
(c) Van der Wiel et al., 2019 *Environmental Research Letters* https://doi.org/10.1088/1748-9326/ab38d3 (500 hPa geopotential height)
(d) Hurrell, 1995, *Science DOI: 10.1126/science.269.5224.676* (SLP) and Wang et al., 2013 *Journal of Climate, DOI: 10.1175/JCLI-D-13-00230.1* (SLP)
(e) Gleeson et al., 2019 *Adv. Sci. Res.* https://doi.org/10.5194/asr-16-11-2019 (SLP)
(f) Weisheimer et al., 2017 *Quarterly Journal of the Royal Meteorological Society* DOI:10.1002/qj.2976 (500 hPa geopotential height)

Paper III

Towards a new framework for PMP estimates in Norway by combining an ensemble data set and gridded observations